Author:
Chadwick, Ailis C

Title:
Functionalised diphosphines for nuclear imaging via Pt(0)-catalysed hydrophosphination

Functionalised diphosphines for nuclear imaging via Pt(0)-catalysed hydrophosphination

Ailis Chadwick

August 2019

A thesis submitted to the University of Bristol in accordance with the requirements for award of Doctor of Philosophy in the Faculty of Science

Abstract

The use of P(III)-ligands in nuclear medicine is rare with only one clinical example called *Myoview* which is used for myocardial perfusion imaging and features two tetrofosmin ligands {$(EtOCH_2CH_2)_2PCH_2CH_2P(CH_2CH_2OEt)_2$} around a technetium-99m dioxo core. This thesis reports the synthesis of novel diphosphine ligands via a Pt(0)-catalysed hydrophosphination route for use as SPECT imaging agents. The Re(V) coordination chemistry of the ligands has been investigated as a model for Tc(V), before radiolabelling with ^{99m}Tc.

Bioconjugation is a technique used to covalently link ligands to biomolecules. The resultant bifunctional chelators allow for more selective imaging of disease and examples have been reported, though few have been used clinically. Bioconjugation of ligands described in this thesis to cyclic-RGDfk, a pentapeptide that is recognised by $\alpha_v\beta_3$ integrin receptors is detailed. $\alpha_v\beta_3$ integrin receptors play a role in the early stages of angiogenesis, an important stage in tumour development in which new blood vessels are formed which is depended on for growth. Targeting of such receptors with a bifunctional chelator would enable selective imaging of cancer.

Diphosphines with a maleic anhydride backbone have been synthesised for use as PET imaging agents. The presence of the anhydride moiety allows for efficient bioconjugation to cRGDfK peptides. A bis(dicyclohexylphosphino)maleic anhydride bioconjugate coordinates to radioactive copper-64 in high radiopurity. The biological properties of the complex including Log$D_{7.4}$ and *ex vivo* biodistribution indicated that the imaging agent mostly likely accumulates in and clears the body via the liver. This is in contrast to the diphenylphosphino analogue which is more likely to be excreted via the kidneys.

In the final chapter, a Pt(0)-catalysed hydrophosphination route to novel functionalised diphosphines is reported. A range of ligands of type $Ph_2PCH_2CH_2P(CH_2CH_2Z)_2$ where Z = CO_2Me, CO_2Et, $CO_2{}^tBu$, CN, $CONH_2$, $CONMe_2$ or $PO(OEt)_2$, have been synthesised and fully characterised. Platinum(0) chemistry and deuterium-labelling experiments as well as catalyst loading and rate investigations indicate that the mechanism of the reaction is similar to that of the previously reported Pt(0)-catalysed hydrophosphination by monophosphines. Oxidative addition is followed by a P-C bond forming Michael addition step before intramolecular C-H bond formation and then dissociation of the product.

All new compounds have been characterised by a combination of ^{31}P, ^{1}H, ^{13}C, ^{2}H and ^{195}Pt NMR spectroscopy, IR spectroscopy, mass spectrometry and X-ray crystallography.

Declaration

I declare that the work in this dissertation was carried out in accordance with the requirements of the University's Regulations and Code of Practice for Research Degree Programmes and that it has not been submitted for any other academic award. Except where indicated by specific reference in the text, the work is the candidate's own. Work done in collaboration with or with the assistance of others is indicated as such. Any views expressed in the thesis are those of the author.

Ailis Chadwick

University of Bristol

August 2019

Acknowledgements

My first thank you must go to Paul for his continued guidance, support and for the opportunity to work on this project. I will never forget his legendary stories or our annual karaoke duets at the infamous Pringle Christmas parties. I'm not sure I will have another boss like him.

The Pringle group have absolutely made my time in Bristol the best I could have hoped for and have vastly improved my lunging game. To the current Pringles – Lexy Miles-Hobbs (my weekday boyfriend, I couldn't have made it through without you!), Dan Wise, Callum Branfoot, Sarah Williams, Rachel Doyle, Rachel Nuttall, Hubert Meissel and Ashley King (snack-size Pringle), and the past Pringles - Drs Tim Shuttleworth, Adam Gorman, Louise Hazeland, Charly Faradji, and Krishna Mistry – thank you for making the lab (and the pub) such a fun place to be.

Another thank you must go to my collaborators Dr Michelle Ma and IB at King's College London for being so welcoming when I worked in in their lab, and for all the help and advice they gave me.

I would also like to thank the excellent technical staff: Tony Rogers for fixing my fumehood countless times, Paul Lawrence for help with NMR, Dr Hazel Sparkes and Natalie Pridmore for help with X-ray crystallography as well as Dr Natalie Fey for help with DFT.

Thank you to my Masters students Martin Heckenast and James Race. Some of their work is included in this thesis and I am grateful for their input and hard work on the project.

Last but not least, thank you to my family and friends who have supported me during my PhD. A special mention must go to Tim who has shared boyfriend duties with Lexy without question. Thank you for your love and support and for always managing to make me smile even when I got phosphine in my hair…

Collaborator acknowledgements and publications

The work in Chapters 2 and 3 is as yet unpublished and the radiolabelling of ligands and synthesis of bioconjugates was performed by the author in collaboration with Dr Michelle Ma at King's College London.

Chapter 5 is reproduced from '*Self-replication of chelating diphosphines via Pt(0)-catalysed hydrophosphination*', Ailis C. Chadwick, Martin A. Heckenast, James J. Race, Pauls G. Pringle, Hazel A. Sparkes, *Organometallics,* **2019**, 38, 3871-3879. Some of the ligands were synthesised by Martin Heckenast and James Race who worked under supervision of the author as Masters students.

Chapter 6 describes the experimental and supporting information for Chapters 2, 3 and 5.

Format of the thesis

This thesis is written in two distinct parts; the first details the synthesis of novel diphosphines and bioconjugates for use as radiolabelled agents for SPECT and PET imaging. The second part details Pt(0)-catalysed hydrophosphination of diphosphines including substrate scope and mechanistic investigations. Each part has a separate introduction and references are found at the end of each Chapter. All experimental details are included in Chapter 6. A removable frequently discussed compound identification chart has been included to assist the reader.

Table of Contents

Abbreviations

General			
AIBN	Azobisisobutyronitrile	**TFA**	Trifluroroacetic acid
Ar	Dichloromethane	**THF**	Tetrahydrofuran
BFC	Bifunctional Chelator	**TMS**	Trimethylsilyl
cRGDfK	(Arg-Gly-Asp-D-Phe-Lys)		
Cy	Cyclohexyl		
d	Day(s)		
DCM	Dichloromethane		
Et	Ethyl		
h	Hour(s)		
HPLC	High-performance liquid chromatography		
^{i}Bu	Isobutyl		
M	Metal		
Me	Methyl		
MeCN	Acetonitrile		
min	Minute(s)		
mmol	Millimole(s)		
NHS	N-hydroxysuccinimide		
PET	Positron emission tomography		
Ph	Phenyl		
PSMA	Prostate specific membrane antigen		
SPECT	Single photon emission computed tomography		
^{t}Bu	Tert-butyl		

Abbreviations

Spectrochemical	
{^{1}H}	Proton decoupled
br	Broad
d	Doublet
dd	Doublet of doublets
dt	Doublet of triplets
EI	Electron impact ionisation
ESI	Electronspray ionisation
J	Coupling constant
m	Multiplet
m/z	Mass/charge
NMR	Nuclear magnetic resonance
ppm	Parts per million
s	Singlet
t	Triplet
δ	Chemical shift in ppm

Part 1

Functionalised diphosphines for radioimaging

Chapter 1

Introduction

Nuclear medicine is a rapidly expanding field based on the use of radioactive isotopes for diagnosis and therapy. Radioimaging is utilised to gain information about a specific site of disease using isotopes that emit either a single gamma photon, or a positron (β^+) that annihilates with an electron to produce two gamma photons. Conversely therapeutic agents exploit radionuclides that transfer their energy to the diseased site typically using α or β^- emitters.[1] 'Dual-purpose' radiopharmaceuticals with emissions suitable for therapy and diagnosis have been named 'theranostics'. Such agents are advantageous as they have the ability to diagnose, treat and evaluate the progress of the treatment simultaneously.[2,3]

Within metal-based radiopharmaceuticals there are two sub-classes; metal-essential and metal-nonessential drugs. Metal-essential agents incorporate a radionuclide that is fundamental for biological targeting, for example in the myocardial perfusion agent ^{99m}Tc-MIBI the ligands do not accumulate in the myocardium without the metal. In contrast, metal-nonessential agents show metal-independent behaviour *in vivo* therefore tracers are easier to derivatise. This thesis will focus on specifically targeted metal-based imaging agents.

1.1 Bifunctional chelators

Most metal-nonessential drugs are made up of a radiometal, ligand/chelator, linker and target vector/biomolecule and can be classed as bifunctional chelators (BFCs). BFCs have two key functions; (1) to chelate the radionuclide and (2) to bear a functional group that can be covalently linked to a biomolecule, which serves to make the imaging agent more targeted towards a specific site of disease (Figure 1.1).

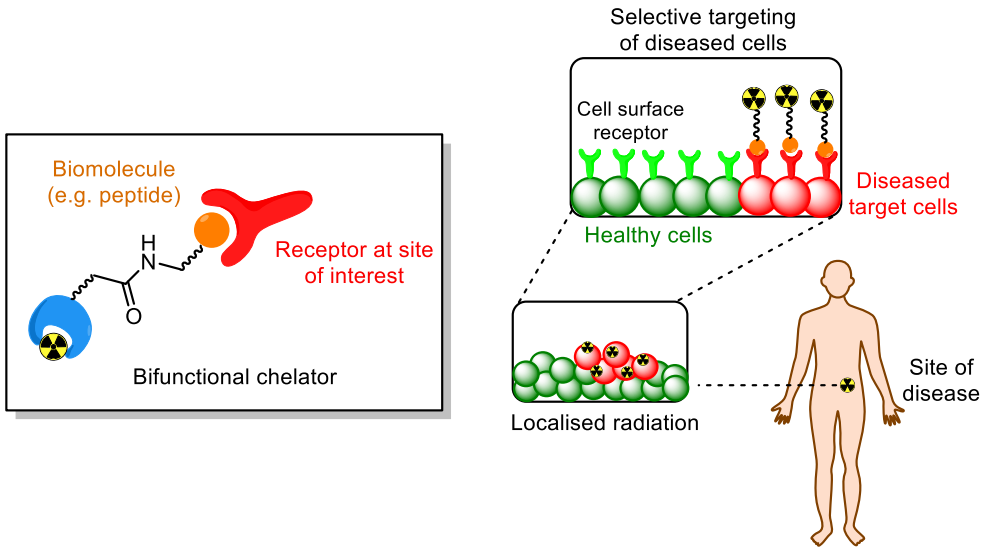

Figure 1.1 Bifunctional chelator (BFC) and mode of action.[4]

The biomolecule chosen to conjugate to the chelating ligand dictates the biodistribution of the complex. The ideal target vector will exhibit high affinity for receptors that are present on diseased cells and absent on healthy cells. Peptides are of interest due to their thermal stability which allows modifications to be made to make them less susceptible to degradation in the body.[4] Common peptide bioconjugates include RGD (Arg-Gly-Asp) which targets tumour growth, and PSMA which is specific for prostate cancer. Other biomolecules that can be conjugates includes antibodies, nanoparticles and small molecules.

1.2 SPECT imaging

Single-photon emission computed tomography (SPECT) is the most widely used nuclear imaging technique. A γ-emitting radiopharmaceutical is injected into the patient and localises at a site of disease. The γ-photons emitted from the decaying radionuclide are detected by a rotating camera and tomographically reconstructed into an image (Figure 1.2).[5] Elements that are used clinically for SPECT imaging include technetium, indium, iodine and thallium.

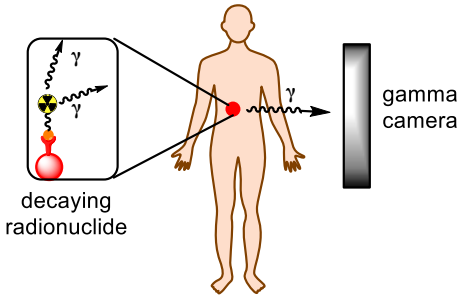

Figure 1.2 Mode of action of a SPECT scanner.

1.2.1 Indium radiopharmaceuticals

Indium-111 ($t_{1/2}$ = 67.2 h) was the first radionuclide to be used routinely in the clinic for gamma imaging.[6] The ^{111}In-based imaging agent Octreoscan (^{111}In-DTPA-octreotide) was the first FDA-approved peptide-based BFC and is used clinically to image hormone-producing tumours in the nervous and endocrine system[7]. The imaging agent incorporates the radionuclide ^{111}In with a DTPA ligand conjugated to octreotide, an analogue of the human peptide hormone somatostatin (Figure 1.3): it has a high affinity for somatostatin receptors expressed by neuroendocrine cancer cells.[8] The development of technetium-99m SPECT imaging agents means ^{111}In is less popular now, though it is still used clinically and for research purposes.[4]

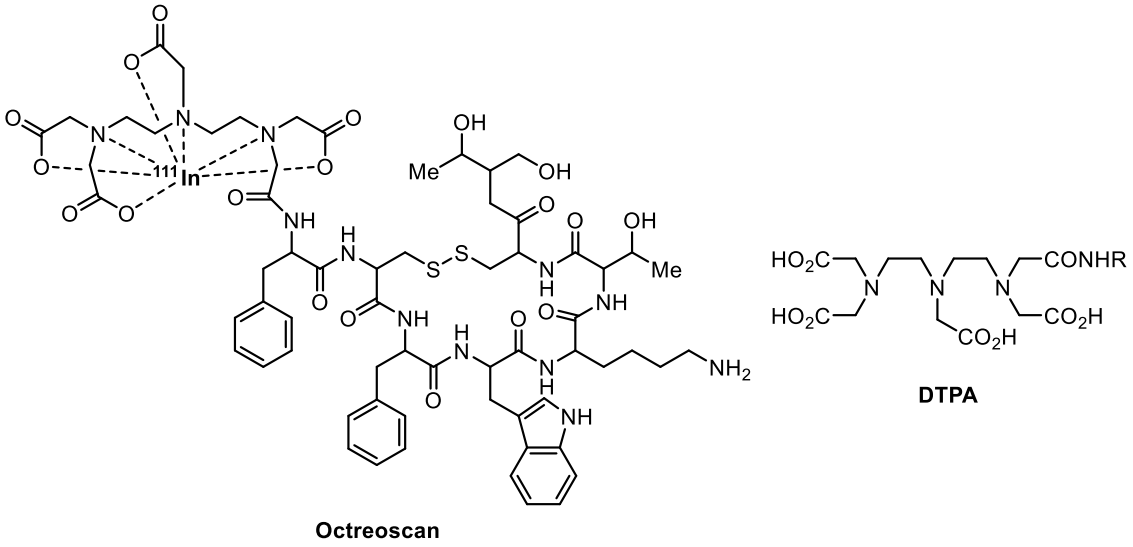

Figure 1.3 Structure of Octreoscan and DTPA ligand.

1.2.2 Iodine radiopharmaceuticals

Another FDA-approved SPECT imaging agent is Ioflupane, consisting of a cocaine-like dopamine transporter ligand that can be radiolabelled with iodine-123 and used to image Parkinson's disease (Figure 1.4).[9] A hallmark of Parkinson's disease is a reduction in dopaminergic neurons, therefore by introducing ioflupane, which binds to dopamine transporters, a quantitative assessment of the neurons can be made.

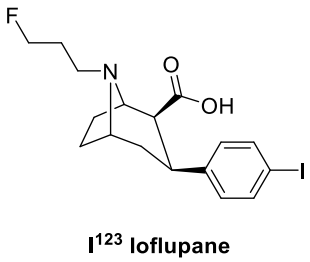

Figure 1.4 Structure of Ioflupane.

1.2.3 Thallium radiopharmaceuticals

Thallium-201 ($t_{1/2}$ = 73 h) as thallium(I) chloride has been used extensively in myocardial perfusion imaging. The $^{201}Tl^{+}$ ion is a potassium mimic so is taken up well in the myocardium by sodium/potassium ATPase.[6] However in recent years the use of ^{201}Tl has been surpassed by lipophilic complexes of technetium-99m.

1.2.4 Technetium-99m radiopharmaceuticals

Over 85% of all nuclear medicine studies use technetium-99m and it has been the 'workhorse' isotope of nuclear imaging for decades. Numerous ^{99m}Tc radiopharmaceuticals have been developed where Tc(V), Tc(III) and Tc(I) are the most commonly utilised oxidation states. ^{99m}Tc nuclei emit a single gamma photon of 140 keV which strikes a good balance between efficient detection outside the body and low attenuation by tissues as well as delivering a low dose of radioactivity to the patient.[10] The development of the ^{99m}Tc generator has enabled daily availability of the radioisotope in hospitals, overcoming the limitations of distributing an isotope with a short half-life. ^{99m}Tc ($t_{1/2}$ = 6 h) is shipped in the form of its parent isotope molybdenum-99 ($t_{1/2}$ = 60 h) as molybdate bound to an alumina column which decays to pertechnetate ($^{99m}TcO_4^-$) that is eluted from the column with saline.

Due to the relatively short half-life of ^{99m}Tc, radiosynthesis should be short (approx. 30 min), high yielding and ideally without need for purification. Instant kits, first formulated in 1971 by Eckleman and Richards, containing all components required for the imaging agent except the radionuclide have been developed to facilitate this.[11] Pertechnetate in a saline solution, eluted from the generator, is added to a vial containing a reducing agent (often stannous chloride) and a chelating ligand. The formulation often also includes a pH buffer and a weakly coordinating ligand (usually gluconate) to transiently stabilise the reduced oxidation state of Tc before coordination to the chelator.[1]

Many of the clinically approved drugs do not make use of the bifunctional chelator approach, but instead are metal-essential imaging agents.[12] In fact, the exact structures of early examples of ^{99m}Tc radiopharmaceuticals were unknown at the time of development and many were delivered as mixtures of complexes e.g. Tc-MDP (Figure 1.5, **1.1**). Tc-MDP is one of few examples of commercially used ^{99m}Tc radiopharmaceuticals with a phosphorus-containing ligand. The full structure of the ^{99m}Tc complex of the diphosphonate is not shown as it remains unknown. This type of imaging agent is widely used to diagnose metastatic bone diseases. It is believed that the presence of uncoordinated oxygen atoms allows the complex to bind exposed Ca^{2+} ions on newly formed hydroxyapatite, the main component of bone.[13]

In the early 1980s Deutsch, Davsion and Jones and others introduced well-characterised ^{99m}Tc radiopharmaceuticals.[14,15,16] This led to a range of technetium 'cores' – modifiable, stable units that could be tailored to the desired pharmacokinetics (Figure 1.5).

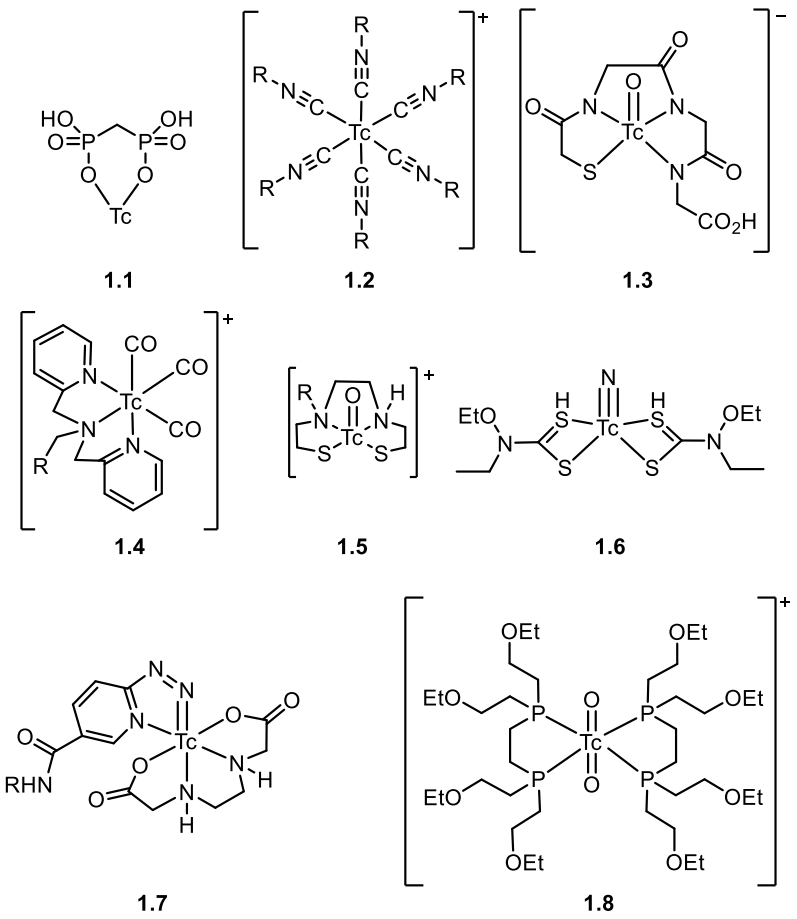

Figure 1.5 Some examples of ^{99m}Tc radiopharmaceuticals and their cores where known; Tc-MDP (**1.1**), Tc(I)-hexakis(isonitrile) (**1.2**), TcMAG3 complex (**1.3**), Tc(1)-tricarbonyl (**1.4**), Tc(V)-oxo (**1.5**), Tc(V)-nitrido(dithiocarbamate)$_2$ (**1.6**), Tc(V)-HYNIC (**1.7**), Tc(V)-dioxo, *Myoview* (**1.8**).

The homoleptic, cationic complex Tc-sestamibi (**1.2**) is based on the Tc(I) isonitrile core and is sold under the names Cardiolite and Miraluma for myocardial perfusion and breast tumour imaging respectively.[17] It is most commonly used for myocardial perfusion imaging where it accumulates in the mitochondria due to the negative charge on the inner mitochondrial matrix. The mitochondrial localisation is directly proportional to blood flow and the octahedral d^6 configuration avoids the loss or substitution of competing ligands in a biological system.[13] A SPECT scan is taken when the patient is at rest then after a period of exercise in order to diagnose any myocardial defects.[18]

The TcO^{3+} core can be bioconjugated to biomolecules by N and S containing polydentate chelators such as mercaptoacetyltriglycine (MAG3, **1.3**). MAG3 was developed by Fritzberg *et al.* in 1986 for imaging the kidneys as an alternative to ^{131}I-hippurate.[19,20] The chelator has no chiral centres decreasing the amount of products formed on complexation. However due to a lack of mirror symmetry in the complex, two

enantiomers are formed.[21] Although **1.3** is a stable complex, a mild one-step radiolabelling process is yet to be developed.[6]

1.2.5 *Myoview*

Utilised in myocardial perfusion imaging for the diagnosis of various heart conditions, the cationic complex *Myoview* ($[^{99m}TcO_2(tetrofosmin)_2]^+$, where tetrofosmin is an ethyl ether functionalised diphosphine, Figure 1.5, **1.8**) was developed in the early 1990s and marketed by GE Healthcare.[22] Many different phosphine ligands were tested during the development of *Myoview*, but tetrofosmin is the only P(III) chelator that is FDA-approved. Tetrofosmin is synthesised by the hydrophosphination of ethyl vinyl ether with bis(diphosphino)ethane, initiated by azobisisobutyronitrile (AIBN) (Scheme 1.1).[23]

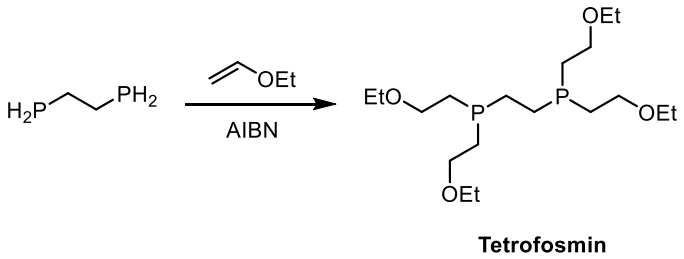

Scheme 1.1 Synthesis of Tetrofosmin; the ligand for imaging agent *Myoview*.

Myoview is formulated in an instant kit containing tetrofosmin, a stannous chloride reducing agent, pH buffer, gluconate to stabilise Tc in the +5 oxidation state and sulphosalicylic acid to enable rapid ligand exchange.[24] The kit requires 15 min at room temperature after the addition of pertechnetate to form the complex in >90% radiochemical purity. The incorporation of ether groups prevents retention of the complex in the blood and enables good clearance from the body via the liver. Importantly, the ether groups do not interfere with the complexation of the diphosphines with Tc.

This complex served as a starting point for the ligand synthesis in this project. It was hypothesised that by changing the ether functionalities to groups that could be conjugated to biomolecules we could synthesise imaging agents targeted to specific sites of disease. This will be discussed further in Chapter 2.

1.3 PET imaging

Positron-emission tomography (PET) requires β^+ emitting nuclides such as copper, fluorine, gallium, zirconium, and lanthanum. β^+ particles are emitted and meet nearby

electrons in a process called annihilation which produces two γ-rays that are detected by a PET scanner and converted into an image (Figure 1.6).[25]

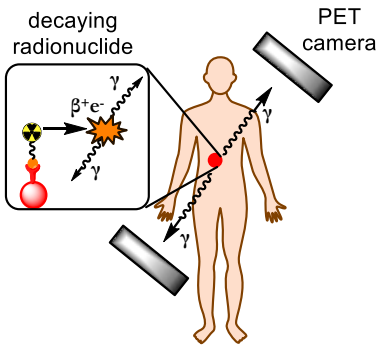

Figure 1.6 Mechanism of action of a PET scan.

1.3.1 Fluorine radiopharmaceuticals

In the 1970s PET imaging was dominated by radionuclides with short half-lives such as ^{11}C, ^{15}O and ^{18}F which limited its use to biological processes that occurred over a short period of time. Fluorine-18 ($t_{1/2}$ = 109 min) still dominates the field, most often in the form of [^{18}F]-2-fluoro-deoxyglucose (FDG), used to probe glucose metabolism which is central to many biological processes linked to cancer and inflammation (Figure 1.7).[26]

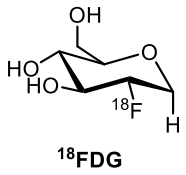

Figure 1.7 Structure of [^{18}F]-2-fluoro-deoxyglucose.

FDG is primarily used for the diagnosis of cancer as well as staging, monitoring therapeutic response and assessment of prognosis.[27] Due to its similarity to glucose, FDG is taken up by GLUT receptors which are often overexpressed in cancer cells.[28]

1.3.2 Gallium radiopharmaceuticals

The limitations of radionuclides with short half-lives have drawn focus to metallic isotopes which can be used to monitor longer biological process due to their longer half-lives. ^{64}Cu and ^{89}Zr resemble ^{18}F imaging more closely as they emit low energy positrons producing an image of comparable resolution. Conversely ^{86}Y and ^{68}Ga emit higher energy

positrons giving lower resolution images although algorithms have been developed to correct this.[26]

Gallium-67 (γ-emitter, $t_{1/2}$ = 3.26 days) is used clinically to image lymphoma and other types of tumours[29] as well as infection[30] based on its ability to mimic the role of iron in biological systems.

Gallium-68 (β^+-emitter, $t_{1/2}$ = 68 min) is to PET what ^{99m}Tc is to SPECT imaging since its half-life is long enough for radiolabelling and biodistribution but short enough to keep the dose of radiation to the patient low.[6] Ga^{3+} is the most common oxidation state in aqueous solution but a major challenge of Ga^{3+} coordination chemistry is that at low pH there is a strong tendency for hydrolysis to occur. Therefore, radiolabelling often needs to occur in acidic conditions or in the presence of a stabilising ligand. Ga also tends to demetalate at neutral and high pH to form $Ga(OH)_4^-$ and hence there is a need for high complex stability and inertness over a wide pH range.[4,31]

^{68}Ga has been widely used with the DOTA chelator bioconjugated to somatostatin receptor-targeting peptides such as DOTATOC and DOTATATE (Figure 1.8).[31] Despite the size mis-match between the 12-membered ring of the DOTA chelator and the Ga^{3+} ion, resulting in a distorted octahedral coordination geometry, the thermodynamic stability of this family of complexes is high enough to use in the clinic.[17] Moreover, labelling of DOTA and its analogues with ^{68}Ga can require high temperature (100 °C) and low pH (<6) which may be incompatible with biomolecules.[4] Incorporation of a pyridine ring into the macrocycle to form DOTA derivative PCTA (Figure 1.8) greatly improved the class of chelator allowing them to be labelled at room temperature as well as displaying good tumour accumulation *in vivo*. NOTA is a better size match for Ga^{3+} with its 9-membered macrocycle (Figure 1.8), which is reflected in its higher stability compared to DOTA. Bifunctional analogues of NOTA have achieved radiolabelling at room temperature within 10 min and phosphonate and phosphinate containing derivatives have shown excellent tumour uptake.[32]

A more detailed discussion of ^{68}Ga chelators is beyond the scope of this thesis as the complexes have been reviewed many times in the literature.[4,6,31,33]

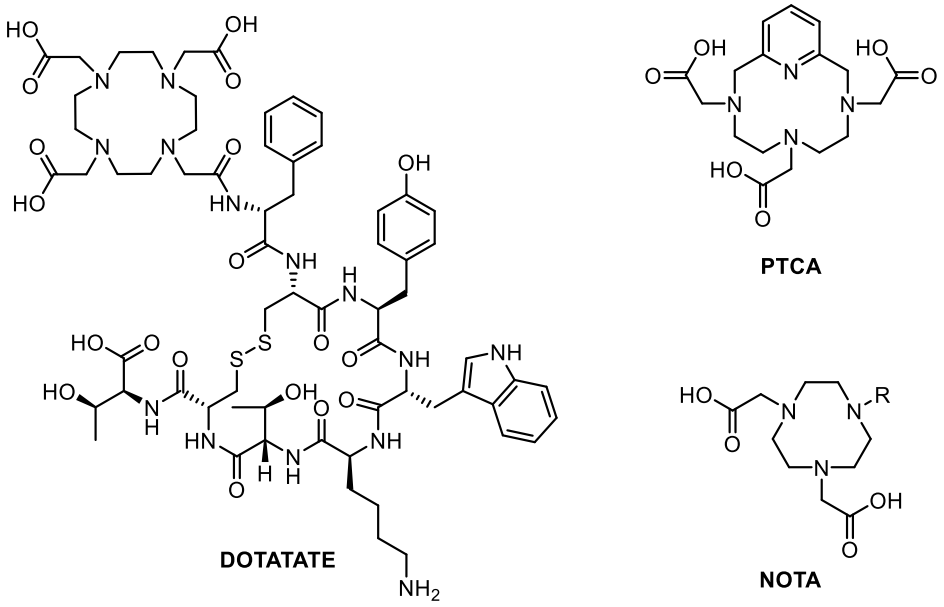

Figure 1.8 Structures of Ga chelators DOTATATE, PTCA and NOTA.

1.3.3 Zirconium radiopharmaceuticals

Zirconium-89 ($t_{1/2}$ = 78.4 h) is often used for labelling target vectors with slow pharmacokinetics (e.g. antibodies), with the chelator desferrioxamine (DFO) (Figure 1.9). Monoclonal antibodies clear slowly from blood and accumulate in targeted tumours so imaging is conducted over a period of 24-72 h; hence the relatively long half-life of ^{89}Zr makes it suitable for labelling such biomolecules.[6,10]

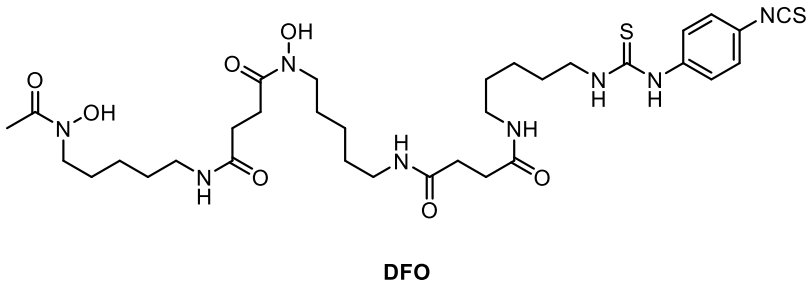

Figure 1.9 Structure of ^{89}Zr chelator desferrioxamine (DFO).

^{89}Zr most often exists as Zr^{4+}, an acidic cation with hard character suited to anionic oxygen-donor ligands, such as DFO in high coordination number.[34] Studies have shown that DFO is stable in human serum as a ^{89}Zr chelator, and many derivatives have been developed for bioconjugation to antibodies for specific cancer PET imaging.[35]

1.3.4 Copper-64 radiopharmaceuticals

Copper has multiple radioisotopes of which the most useful for imaging is copper-64 ($t_{1/2}$ = 12.7 h). Cu(II) (d^9) dominates the coordination chemistry with copper complexes of coordination numbers 4-6 most common. The bis(thiosemicarbazone) ligands in particular have shown great promise for tumour imaging (Figure 1.10). It is thought that when complexed to Cu(II) they diffuse into cells wherein they are reduced to Cu(I) by intracellular reducing agents.[6,36] The ligands then dissociate and the copper is incorporated into proteins or effluxed from the cell depending on the cell type. The complexes that dissociate more slowly can be re-oxidised by oxygen in the cell and diffuse out. This is the hypothesised basis for selectivity of bis(thiosemicarbazone) complexes for hypoxic cells such as tumour cells. Complexes with rapidly dissociating ligands, facilitated by labile axial ligands due to strong Jahn-Teller distortion, show no selectivity for hypoxic cells.[1]

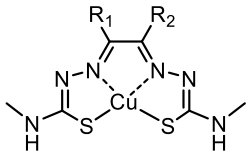

Cu(II)-**ptsm**: R_1 = H, R_2 = Me
Cu(II)-**atsm**: R_1 = Me, R_2 = Me
Cu(II)-**gtsm**: R_1 = H, R_2 = H

Figure 1.10 Structures of bis(thiosemicarbazonato)copper(II) complexes.

In 1998, a study by Dearling *et al.* evaluated the hypoxia selectivity of 13 different bis(thiosemicarbazone) ^{64}Cu complexes. They concluded that ^{64}Cu-ATSM exhibited a 3-fold higher retention in oxygen-deficient cells compared to healthy cells, the greatest *in vitro* selectivity of the group. Subsequent *in vivo* studies showed high uptake of ^{64}Cu-ATSM by tumour cells and the imaging agent was used clinically for the first time in 2000 for imaging lung cancer.[18]

Diphosphine ligands **1.9**-**1.13** have been used to form Cu(diphosphine)$_2^+$ lipophilic cationic complexes for multidrug resistant tumours (Figure 1.11).[37] *In vitro* studies showed that this series of ligands when complexed to ^{64}Cu showed good stability in human serum and rapid uptake by cells.

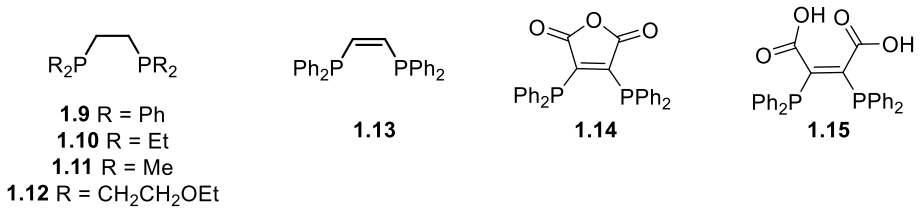

Figure 1.11 Structure of diphosphines ligands developed for 64Cu PET imaging.

Anhydride and carboxylate derivatives (**1.14** and **1.15**) of the diphosphine ligands offer potential as ^{64}Cu(I) BFCs but have not been applied clinically to date.[38,39] Ligands with an anhydride backbone such as **1.14** and in the ring opened form **1.15** will be discussed further in Chapter 3.

1.4 Objectives

The aims of the projects described in this thesis were to:

- Synthesise analogues of tetrofosmin with functional groups available for bioconjugation to biomolecules for specific imaging of sites of disease

- Investigate the coordination chemistry of the 'tetrofosmin-like' ligands to rhenium and technetium-99m

- Formulate 'tetrofosmin-like' ligands into instant kits and explore their use as ^{99m}Tc SPECT imaging agents

- Synthesise a diphosphine ligand with an anhydride backbone analogous to previous work by Blower *et al.*[39] for use as a PET BFC

- Investigate the coordination chemistry for the anhydride ligand focussing on copper for ^{64}Cu imaging

- Evaluate the stability and biodistribution of the new ^{64}Cu-anhydride complex *in vitro*

1.5 References

1 E. Boros and A. B. Packard, *Chem. Rev.*, 2018, **119**, 870–901.

2 S. C. Srivastava, *Semin Nucl Med*, 2012, **42**, 151–163.

3 S. S. Kelkar and T. M. Reineke, *Bioconjug. Chem.*, 2011, **22**, 1879–1903.

4 T. I. Kostelnik and C. Orvig, *Chem. Rev.*, 2018, **119**, 902–956.

5 R. Chakravarty, H. Hong and W. Ca, *Curr Drug Targets*, 2015, **16**, 592–609.

6 P. J. Blower, *Dalton Trans.*, 2015, **44**, 4819–4844.

7 J. B. Bomanji and N. D. Papathanasiou, *Eur. J. Nucl. Med. Mol. Imaging*, , DOI:10.1007/s00259-011-2013-8.

8 B. Wängberg, O. Nilsson, A. Wigander, V. Johansson, E. Forssell-Aronsson, P. Andersson, M. Fjälling, L. E. Tisell and H. Ahlman, *Oncologist*, 1997, **94**, 50–58.

9 N. A. Gharibkandi and S. J. Hosseinimehr, *Eur. J. Med. Chem.*, 2019, **166**, 75–89.

10 R. Southworth, R. Torres Martin de Rosales, L. K. Meszaros, M. T. Ma, G. E. D. Mullen, G. Fruhwirth, J. D. Young, C. Imberti, J. Bagunya-Torres, E. Andreozzi and P. J. Blower, *Insights from Imaging in Bioinorganic Chemistry*, Elsevier Inc., 1st edn., 2016, vol. 68.

11 S. Chakraborty and L. Liu, *Dalt. Trans.*, 2011, **40**, 6077.

12 V. Carroll, D. W. Demoin, T. J. Hoffman and S. S. Jurisson, *Radiochim Acta*, 2012, **100**, 653–667.

13 U. Abram and R. Alberto, *J. Braz. Chem. Soc.*, 2006, **17**, 1486–1500.

14 A. G. Jones and A. Davison, *J. Nucl. Med.*, 1982, **23**, 1041–1044.

15 A. G. Jones, H. S. Trop, A. Davison and M. A. Davis, *J. Nucl. Med.*, 1980, **21**, 279–282.

16 K. Libson, J. Vanderheyden, A. R. Ketring and H. R. Maxon, *Nucl. Med. Biol.*, 1986, **13**, 465–477.

17 M. D. Bartholomä, A. S. Louie, J. F. Valliant and J. Zubieta, *Chem. Rev.*, 2010, **110**, 2903–2920.

18 B. M. Zeglis, J. L. Houghton, M. J. Evans, Nerissa Viola-Villegas and J. S. Lewis, *Inorg. Chem.*, 2014, **53**, 1880–1899.

19 A. R. Fritzberg, S. Kasina, D. Eshima and D. L. Johnson, *J. Nucl. Med.*, 1986, **27**, 111–116.

20 K. Itoh, *Ann. Nucl. Med.*, 2001, **15**, 179–190.

21 S. R. Banerjee, K. P. Maresca, L. Francesconi, J. Valliant, J. W. Babich and J. Zubieta, *Nucl. Med. Biol.*, 2005, **32**, 1–20.

22 J. D. Kelly, A. M. Forster, B. Higley, C. M. Archer, F. S. Booker, L. R. Canning, K. W. Chiu, B. Edwards, H. K. Gill and M. McPartlin, *J. Nucl. Med.*, 1993, **34**, 222–227.

23 GE Healthcare Ltd., US5045302, *US Pat.*, 1989.

24 K. Schomacker and H. Schicha, *Eur. J. Nucl. Med.*, 2000, **27**, 1845–1863.

25 L. Mansi, S. Kitson, V. Cuccurullo and A. Ciarmiello, *J. Diagnostic Imaging Ther.*, 2014, **1**, 137–156.

26 G. E. Smith, H. L. Sladen, S. C. G. Biagini and P. J. Blower, *Dalton Trans.*, 2011, **40**, 6196–6205.

27 H. Feng, X. Wang, J. Chen, J. Cui, T. Gao, Y. Gao and W. Zeng, *Contrast Media Mol. Imaging*, 2019, **2019**, 1–12.

28 M. L. Bowen and C. Orvig, *Chem. Commun.*, 2008, 5077.

29 E. Even-Sapir and O. Israel, *Eur. J. Nucl. Med. Mol. Imaging*, 2003, **30**, S65–S81.

30 S. Basu, H. Zhuang, D. A. Torigian, J. Rosenbaum, W. Chen and A. Alavi, *Semin. Nucl. Med.*, 2009, **39**, 124–145.

31 T. J. Wadas, E. H. Wong, G. R. Weisman and C. J. Anderson, *Chem. Rev.*, 2010, **110**, 2858–2902.

32 K. D. Mjos and C. Orvig, *Chem. Rev.*, 2014, **114**, 4540–4563.

33 I. Velikyan, *Theranostics*, 2014, 4, 47–80.

34 C. F. Ramogida and C. Orvig, *Chem. Commun.*, 2013, **49**, 4720–39.

35 N. B. Bhatt, D. N. Pandya and T. J. Wadas, *Molecules*, 2018, **23**, 1–24.

36 P. S. Donnelly, *Dalton Trans.*, 2011, **40**, 999.

37 J. S. Lewis, J. L. J. Dearling, J. K. Sosabowski, J. Zweit, P. Camochan, L. R. Kelland, H. M. Coley and P. J. Blower, *Eur. J. Nucl. Med.*, 2000, **27**, 638–646.

38 J. S. Lewis, J. Zweit, J. L. J. Dearling, B. C. Rooneya and P. J. Blower, *Chem. Commun.*, 1996, 1093–1094.

39 J. S. Lewis, S. L. Heath, A. K. Powell and P. J. Blower, *J. Chem. Soc., Dalton Trans.*, 1997, 855–861.

Chapter 2

Synthesis, coordination and ^{99m}Tc radiolabelling of tetrofosmin-like ligands

2.1 Introduction

Since the 1970s ^{99m}Tc-labelled radiopharmaceuticals have been routinely used clinically. The first generation complexes were used without detailed knowledge of their structure and coordination chemistry. However in the 1980s and 1990s kit-based Tc(I), Tc(III) and Tc(V) complexes with well-defined structures and cores that could be functionalised were developed (Figure 2.1).[1,2]

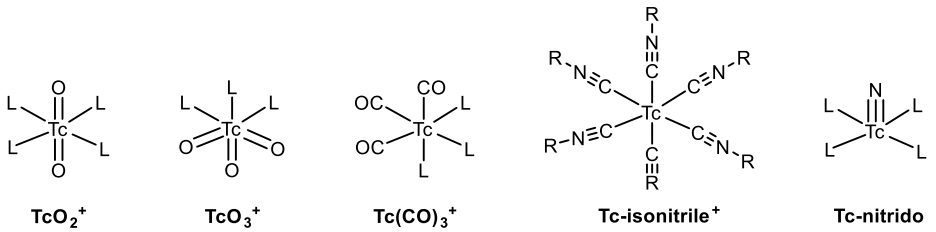

Figure 2.1 Examples of Tc cores used to develop ^{99m}Tc radiopharmaceuticals.

Radiopharmaceutical kits are comprised of a lyophilised formulation of all the ingredients except the radiometal allowing for rapid radiolabelling. When ready to use, the radioisotope is added to the kit, often as a saline solution, left to stand and then administered to the patient.[3] Tc is added as pertechnetate and reduced using a reducing agent such as tin chloride, contained in the kit.

Many nitrogen-based and some P(V)-based ^{99m}Tc imaging agents have been developed but there is only one example of a P(III)-based radiopharmaceutical that is used clinically. *Myoview* was developed in the 1990s and is based on a TcO_2^+ core with two bidentate tetrofosmin ligands (Figure 2.2).[4]

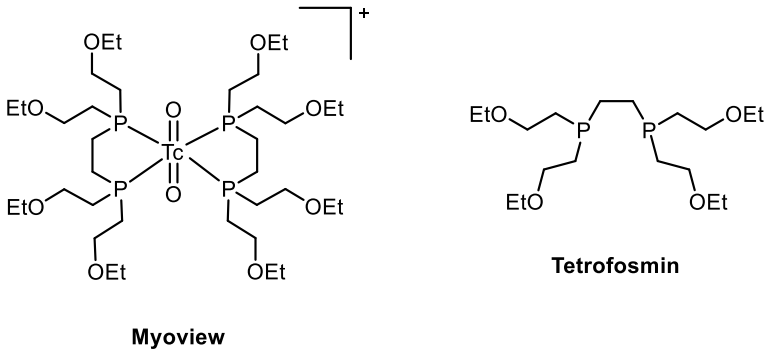

Figure 2.2 Structure of ^{99m}Tc radiopharmaceutical *Myoview* and tetrofosmin ligand.

Myoview is a lipophilic cationic Tc complex that is used in myocardial perfusion imaging for the diagnosis of coronary artery disease. Derivatives of tetrofosmin have been synthesised as part of this project and their rhenium coordination chemistry investigated. Kit preparation and radiolabelling with ^{99m}Tc has also been explored.

For a more in-depth review of Tc-based imaging agents, including *Myoview*, see Chapter 1.

2.1.1 Bioconjugation

The incorporation of biomolecules to afford imaging agents targeted towards specific receptors has become a focus for current radiopharmaceutical research.[5,6,7] The idea centres on the synthesis of bifunctional chelators (BFCs) that bear a reactive functional group to conjugate to a specific biomolecule (e.g. a peptide) and can also chelate the chosen radiometal (Scheme 2.1).

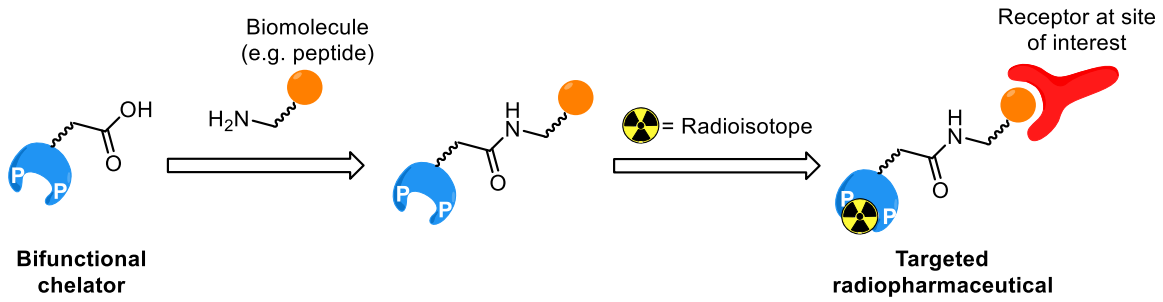

Scheme 2.1 Schematic of a bioconjuagted imaging agent.

Certain limitations still need to be overcome before a ^{99m}Tc bioconjugate kit reaches the clinic:

- Fast reduction of pertechnetate and coordination of BFCs
- The process needs to occur under mild aqueous conditions with non-toxic reagents
- Almost quantitative yield must be achieved in order to avoid further purification

In this project we aimed to synthesise P(III) ligands related to tetrofosmin bearing functional groups (e.g. carboxylates) that could be bioconjugated to biomolecules (e.g. peptides) that would be recognised at specific sites of disease.

2.2 Ligand synthesis

2.2.1 Synthesis of dicarboxylate diphosphine ligands

Amide linkages are commonly used to conjugate carboxylic acids or activated esters to the *N*-terminus of a specific peptide.[7] Tsvetkov *et al.* previously reported the synthesis of phosphinocarboxylic acids by addition of chloro-substituted carboxylic acids to secondary phosphines with base (Scheme 2.2).[8]

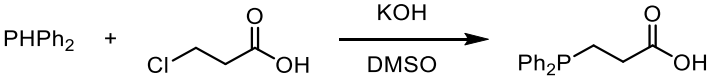

Scheme 2.2 Synthesis of ω-diphenylphosphinopropionic acid.

The same reaction conditions were applied to a diphosphine precursor $Ph_2PCH_2CH_2PH_2$ (**P-PH$_2$**) to synthesise di-acid **2.1** (Scheme 2.3).

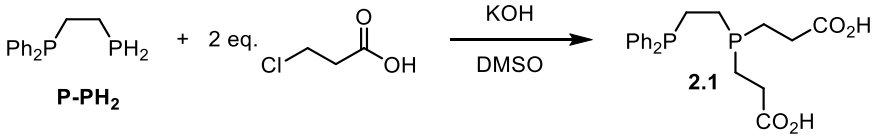

Scheme 2.3 Synthesis of di-acid ligand **2.1**.

After stirring the reaction mixture at ambient temperature overnight the starting material was still the major species in solution according to $^{31}P\{^1H\}$ NMR spectroscopy. The reaction mixture was then heated to 50 °C for a further 16 h to give multiple P-containing species, including starting material (Figure 2.3).

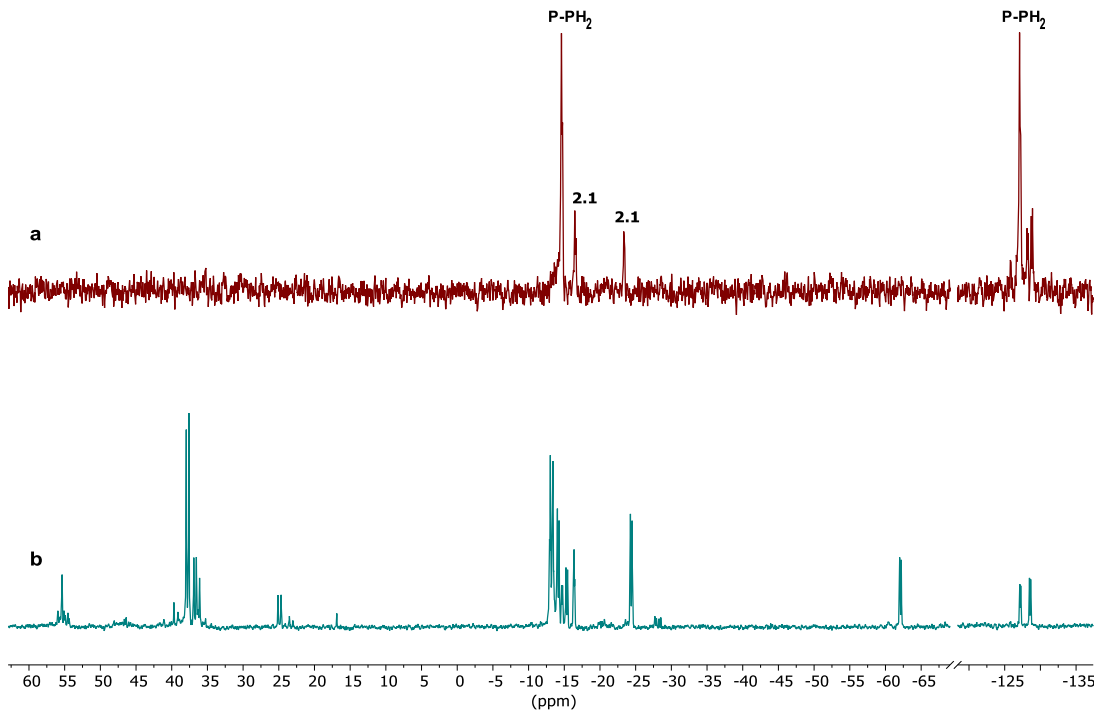

Figure 2.3 ^{31}P{^{1}H} NMR (121 Hz, DMSO) spectra showing (a) synthesis of **2.1** at room temperature overnight; (b) reaction after stirring at 50°C for a further 16 h.

The production of multiple by-products indicates that **2.1** may be more sensitive to decomposition or oxidation than the monophosphine product synthesised by Tsvetkov.

An alternative route to **2.1** is via the hydrolysis of a parent diester. The synthesis of diester ligand **2.2** begins with the hydrophosphination by diphenylphosphine of diethyl vinylphosphonate, initiated by azoisobutylnitrile (AIBN) (Scheme 2.4). This is followed by a reduction with lithium aluminium hydride to give the precursor, $Ph_2PCH_2CH_2PH_2$ (**P-PH$_2$**) and then another hydrophosphination, this time catalysed by a Pt(0) catalyst (Pt(0)-catalysed hydrophosphination is discussed in Chapter 5).

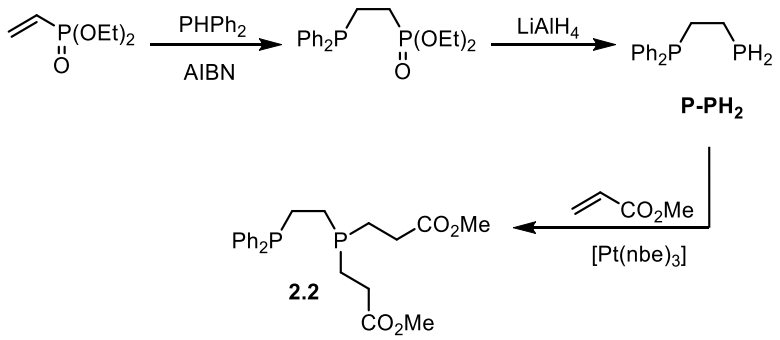

Scheme 2.4 Synthesis of diester ligand **2.2**.

In order to hydrolyse **2.2**, the ligand was stirred at ambient temperature overnight in a mixture of water and methanol with sodium hydroxide (Scheme 2.5). Attempts to isolate the diacid without oxidation were unsuccessful; however the sodium salt (**2.3**) was obtained and fully characterised after neutralising the reaction mixture.

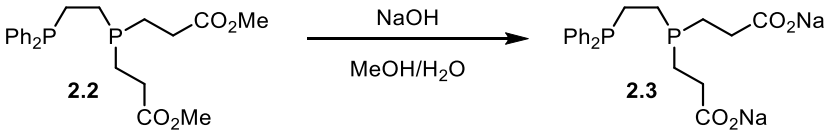

Scheme 2.5 Hydrolysis of **2.2** to sodium salt **2.3**.

2.2.2 Synthesis of monocarboxylate diphosphine ligand 2.5

It was hoped that increasing the length of the carbon chain between phosphorus and the carboxylic acid group may improve the isolation of a diphos bearing an acid functional group.

Hydrophosphination by phenylphosphine of hex-5-enoic acid gave the mono-substituted product **2.4** in 50% yield. The crude mixture of **2.4** and the di-substituted by-product was used without purification in the next hydrophosphination step with diphenylvinylphosphine (Scheme 2.6).

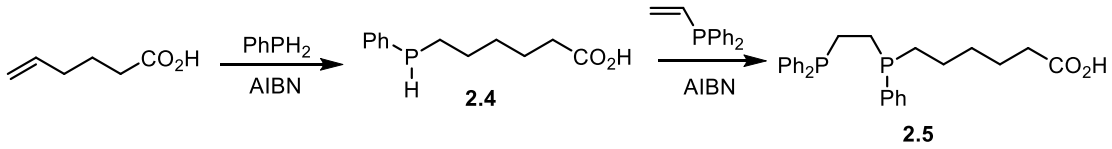

Scheme 2.6 Synthesis of **2.5**.

The moderately air stable product **2.5** was isolated by column chromatography in 65% yield and fully characterised (see Chapter 6).

2.2.3 Synthesis of tetracarboxylate diphosphine ligand 2.6

A symmetrical diphosphine with four groups that could be bioconjugated would be a more targeted analogue of tetrofosmin. Pt(0)-catalysed hydrophosphination was employed as before (see Section 2.3.1) to synthesise tetracarboxylate **2.6** from precursor $PH_2CH_2CH_2PH_2$ (Scheme 2.7).

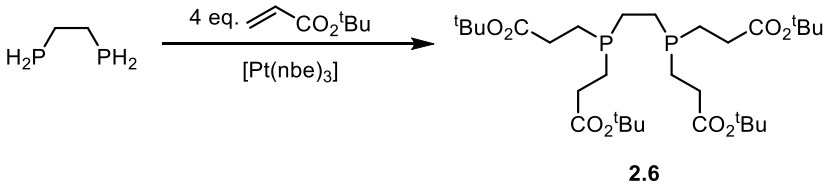

Scheme 2.7 Synthesis of **2.6**.

A high yield of **2.6** could not be obtained as it is believed that the four ^{t}Bu groups render the ligand more volatile than expected hence even in low boiling solvents the ligand co-evaporated.

The Pt(II) complex was obtained by stirring **2.6** with $[Pt(cod)Cl_2]$ in DCM for 1 h (Scheme 2.8).

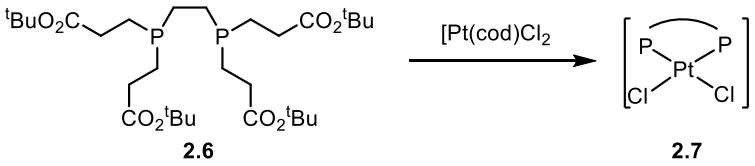

Scheme 2.8 Synthesis of Pt(II) complex **2.x**.

Crystals of complex **2.7** suitable for X-ray crystallography were grown by slow diffusion of hexane into a DCM solution (Figure 2.4)

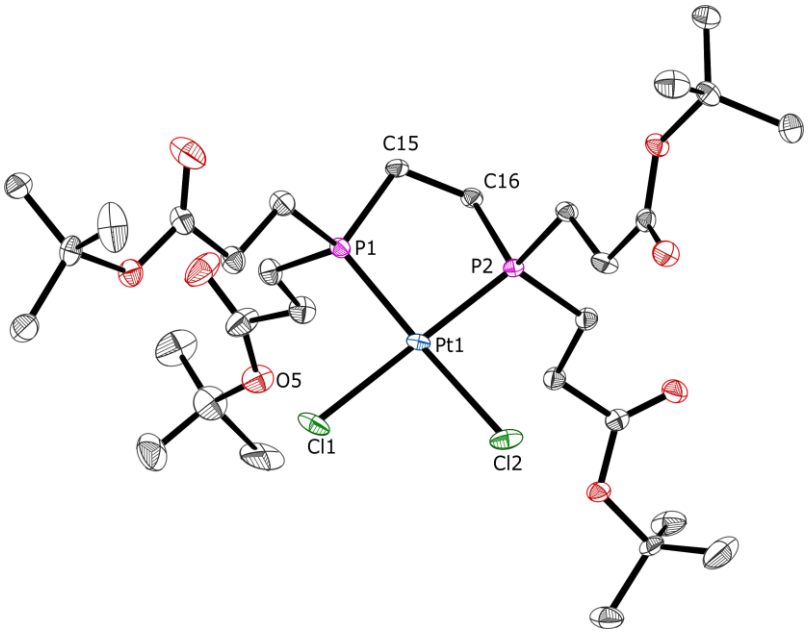

Figure 2.4 Crystal structure of **2.7**. Hydrogen atoms omitted for clarity. Selected bond lengths (Å) and bond angles (°): Pt(1)-P(1) 2.2121(6), Pt(1)-P(2) 2.2185(6), Pt(1)-Cl(1) 2.3547(6), Pt(1)-Cl(2) 2.3617(6), P(1)-C(15) 1.836(2), P(2)-C(16) 1.827(2), C(15)-C(16) 1.535(3), Cl(1)-Pt(1)-P(1) 91.90(2), Pt(1)-P(1)-C(15) 109.08(8), P(1)-C(15)-C(16) 110.41(16).

The bond lengths and angles reported above are comparable (within standard deviation) to [Pt(dppe)Cl$_2$].[9]

Preliminary work to isolate the sodium salt (**2.8**) by reaction with either aqueous NaOH or acid has been performed (Scheme 2.9).

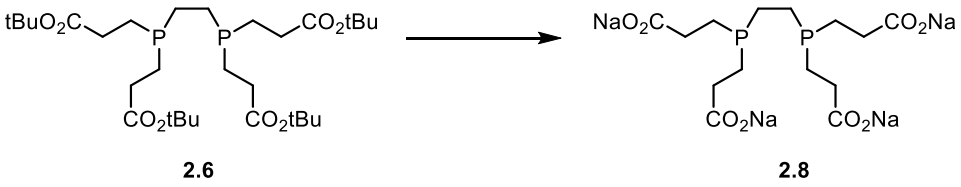

2.6 **2.8**

Scheme 2.9 Attempted synthesis of hydrolysis product **2.8**.

Studies indicate that the precursor **2.6** is unstable to acid following the addition of 11 equiv. TFA in DCM. Complete conversion to a mixture of P-containing species was observed by ^{31}P{^{1}H} NMR spectroscopy which are tentatively assigned to either oxide or protonated species (Figure 2.5).

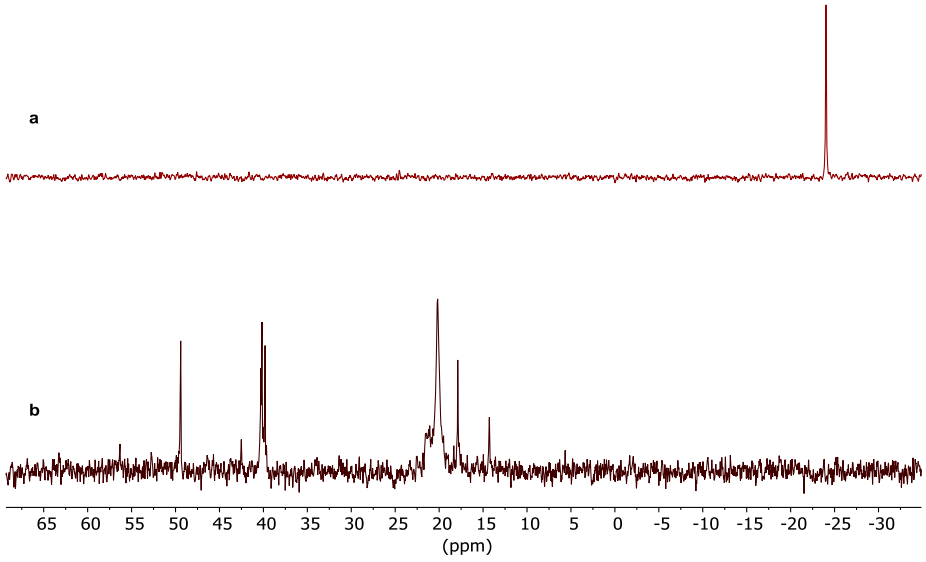

Figure 2.5 $^{31}P\{^{1}H\}$ NMR (121 MHz, CH_2Cl_2) spectra of (a) tetraester ligand **2.6**; (b) P-containing species after reaction of **2.6** with 11 equiv. TFA.

When **2.6** is stirred overnight with aqueous NaOH there is no significant change by $^{31}P\{^{1}H\}$ NMR spectroscopy but the signal corresponding to the ^{t}Bu groups by ^{1}H NMR spectroscopy is no longer observed, therefore indicating hydrolysis of the ester. The apparent sensitivity to air of the hydrolysis product means that further work needs to be carried out to isolate a pure product.

2.3 Rhenium coordination chemistry

Rhenium has similar chemistry to its lighter congener technetium, in part due to the lanthanide contraction, but has the advantage of having a stable non-radioactive isotope. This makes Re an ideal coordination model for Tc as complexes for a given oxidation state are often isostructural.[10] The similar physical characteristics of Re and Tc makes it hard for biological systems to tell them apart, but their differing redox properties may explain their dissimilar behaviour *in vivo*. Re is generally more stable than Tc in a higher oxidation state and so is more readily re-oxidised to perrhenate *in vivo,* and thus Re radiopharmaceuticals (used for therapy rather than imaging) require stronger reducing agents than Tc-based drugs. Re also has a larger ligand field splitting than Tc causing slower ligand substitution.[11] Discussion of Re radiopharmaceuticals is beyond the scope of this thesis as Re was used only as a coordination model in this work.

2.3.1 Re(V) Chemistry

Re(V) was first explored as a model for the TcO_2^+ core that *Myoview* is based on.

The Re(V) complex of **2.2** was prepared by stirring the ligand with precursor $[ReI(O)_2(PPh_3)_2]$ to give a mixture of the *cis* and *trans* species (Scheme 2.10). The $^{31}P\{^1H\}$ NMR spectrum showed two multiplets at δ 8.6 and 9.0 ppm with a coordination shift of Δδ 25 ppm (Figure 2.6).

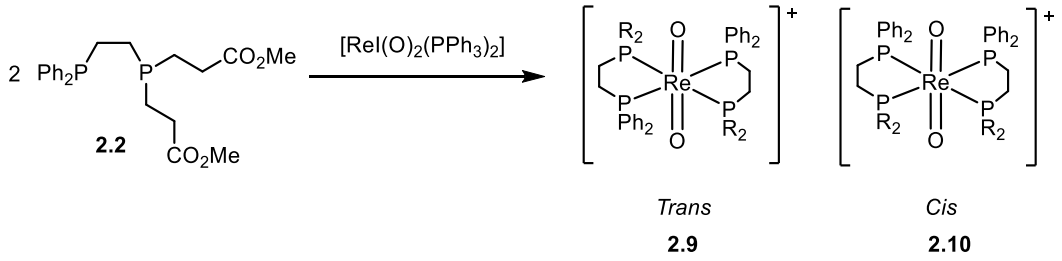

Scheme 2.10 Synthesis of Re(V) complex 2.2

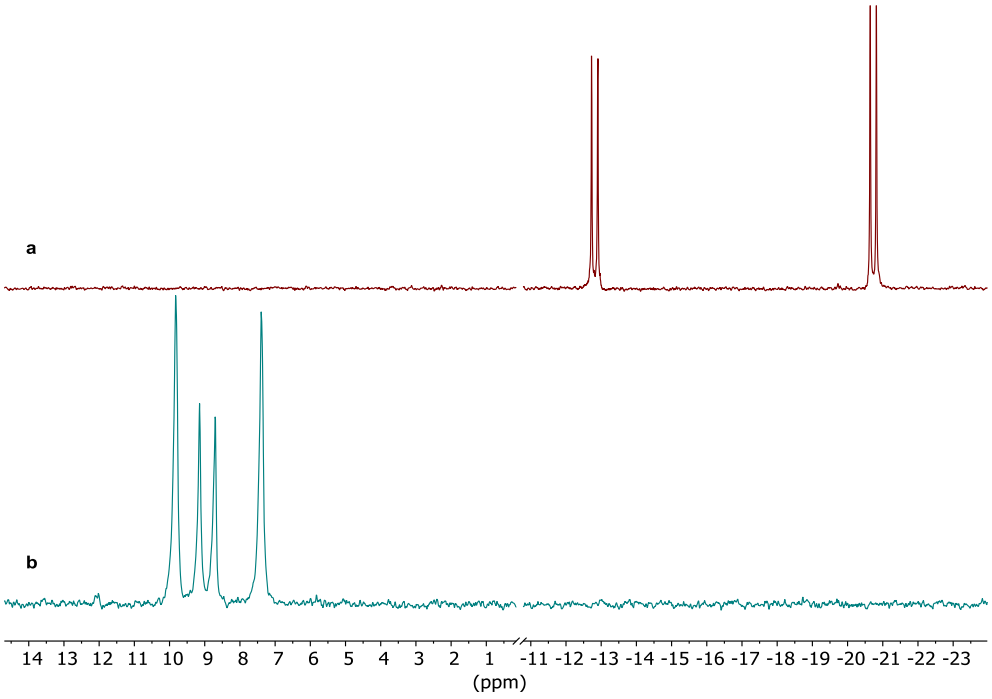

Figure 2.6 $^{31}P\{^1H\}$ NMR (122 MHz, CD_2Cl_2) spectra of (a) diester ligand **2.2**; (b) Re complexes **2.9** and **2.10**.

Crystals of the *trans* complex **2.9** suitable for X-ray diffraction were grown by slow diffusion of pentane into a methanol solution (Figure 2.7).

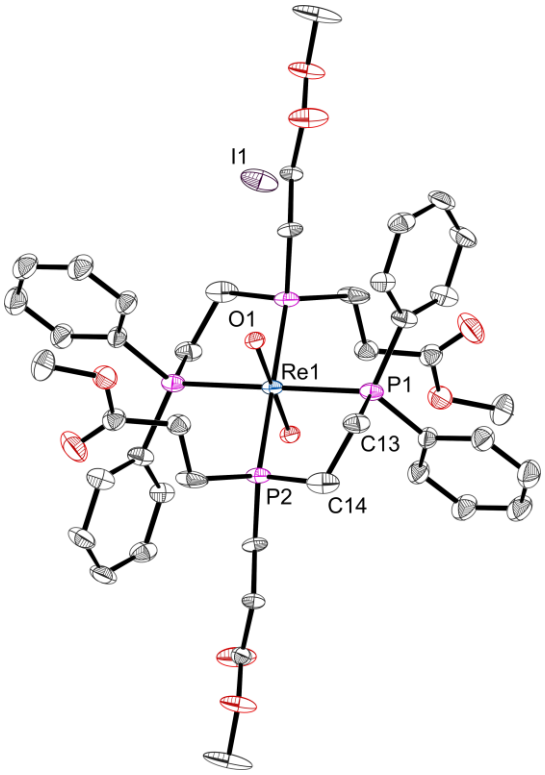

Figure 2.7 Crystal structure of **2.9**. Hydrogen atoms omitted for clarity. Selected bond lengths (Å) and bond angles (°): Re(1)-P(1) 2.465, Re(1)-P(2) 2.462, Re(1)-O(1) 1.778, P(1)-C(1) 1.808, P(1)-C(7) 1.768, P(1)-C(13) 1.824, P(2)-C(14) 1.837, P(2)-C(15) 1.812, P(2)-C(19) 1.807, C(13)-C(14) 1.538(8), P(1)-Re(1)-P(2) 180.00, P(1)-Re(1)-P(2) 80.29, P(1)-Re(1)-O(1) 96.6, P(2)-Re(1)-O(1) 89.5.

The Re=O bond length (1.778 Å) is slightly longer (within standard deviation) than the average reported for Re dioxo complexes but the average Re-P bond length (2.464 Å) matches closely that of the Re dioxo complex of dmpe (Re-P average bond length 2.461 Å) reported by Roodt et al.[11]

The Re(V) complex of dicarboxylate ligand **2.3** was prepared in a similar fashion to give a mixture of the *trans* and *cis* isomers (Scheme 2.11).

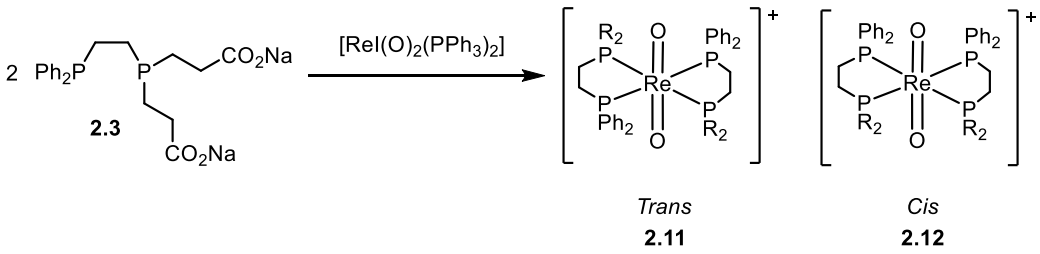

Scheme 2.11 Synthesis of Re(V) complexes of **2.3**.

The *cis* and *trans* isomers were separated by reverse phase HPLC and fully characterised (Figure 2.8) (see Chapter 6).

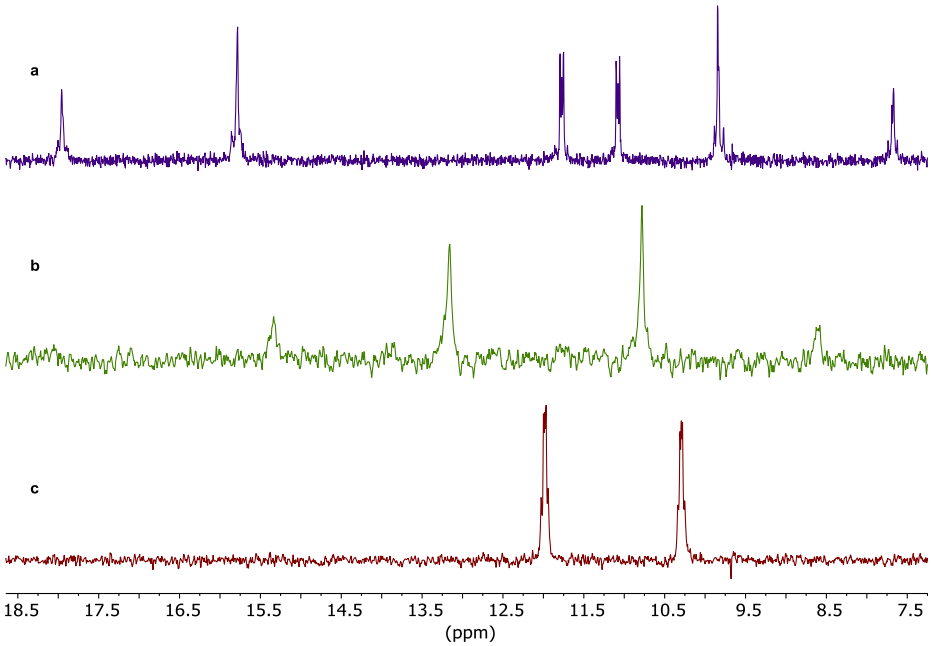

Figure 2.8 $^{31}P\{^{1}H\}$ NMR (121 MHz CD_3OD) spectra of (a) mixture of cis and trans isomers **2.11** and **2.12**; (b) trans complex **2.11** ($^{3}J_{PP}$ = 351 Hz); (c) cis complex **2.12** ($^{3}J_{PP}$ = 231 Hz)

The Re(V) complex of **2.5** was prepared using the same procedure described above (Scheme 2.12). However the $^{31}P\{^{1}H\}$ NMR spectrum of the product showed a complicated mixture of P-containing species most likely due to the diastereoisomers that are formed and their *cis* and *trans* isomers (Figure 2.9).

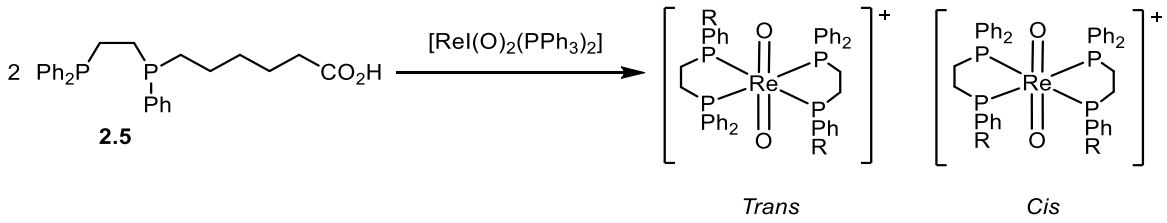

Scheme 2.12 Synthesis of Re(V) complexes of **2.5**.

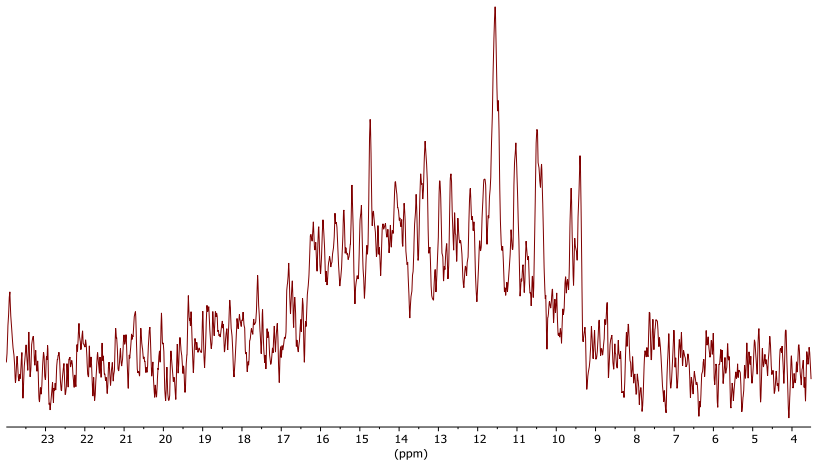

Figure 2.9 $^{31}P\{^{1}H\}$ NMR spectrum of Re(V) complex of **2.5**.

The mixture of Re complexes formed indicates that a similar number of compounds would be formed when complexing **2.5** to ^{99m}Tc and thus is not ideal as single compounds would be much preferred to be administered to patients.

2.3.2 Re(I) Chemistry

Mono-chelate complex **2.13** was prepared from dicarboxylate **2.3** and $[Re(H_2O)_3(CO)_3]$ (Scheme 2.13).

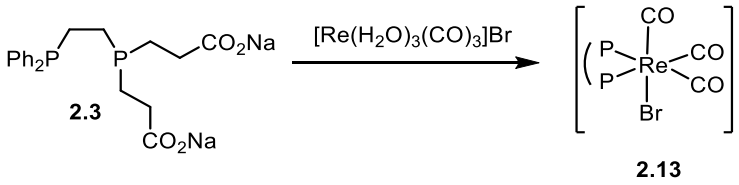

Scheme 2.13 Synthesis of Re complex **2.13**.

The $^{31}P\{^{1}H\}$ NMR spectrum showed two doublets with a coordination shift of $\Delta\delta$ 55 ppm (Figure 2.10). The same complex could also be prepared from $[Re(CO)_5Br]$ although the reaction time was much longer (2 days vs. 30 min).

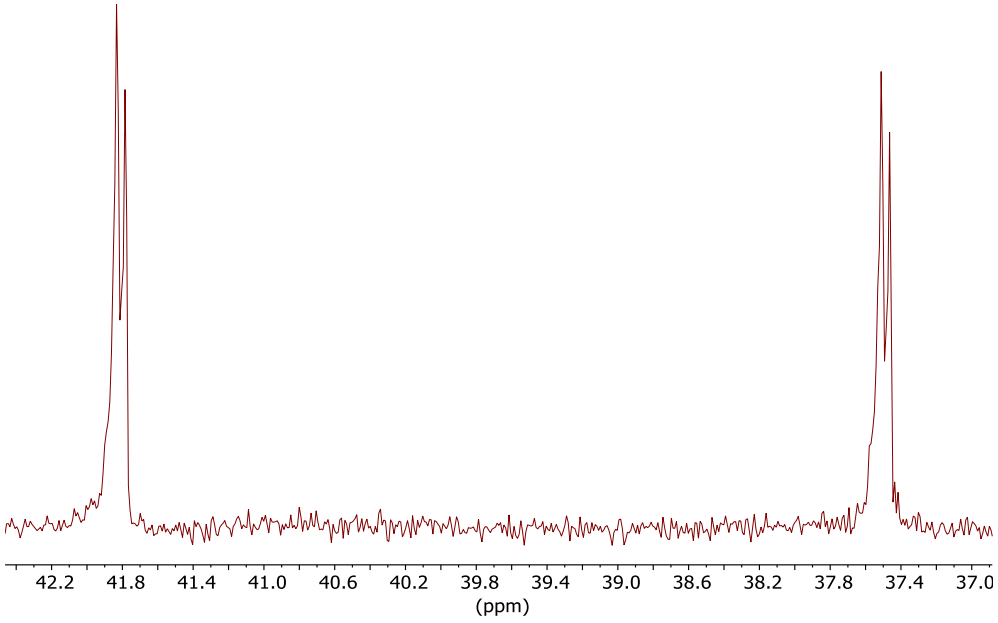

Figure 2.10 $^{31}P\{^{1}H\}$ NMR spectrum (MeOH, 122 MHz) of Re(I) complex **2.13**.

2.4 Bioconjugation

Before conjugating to a peptide, carboxylates are often activated using a succinimidyl ester to avoid the need for additional coupling agents.[12] The carboxylate groups of diphos **2.3** were substituted with N-hydroxysuccinimide (NHS) ester groups in the presence of base and a dehydrating agent (Scheme 2.14). The product (**2.14**) was characterised by mass spectrometry (ESI+ m/z calcd. for $C_{28}H_{30}N_2O_8P_2$ ($[M + H]^+$) = 585.1; obs. = 584.9) (Scheme 2.14).

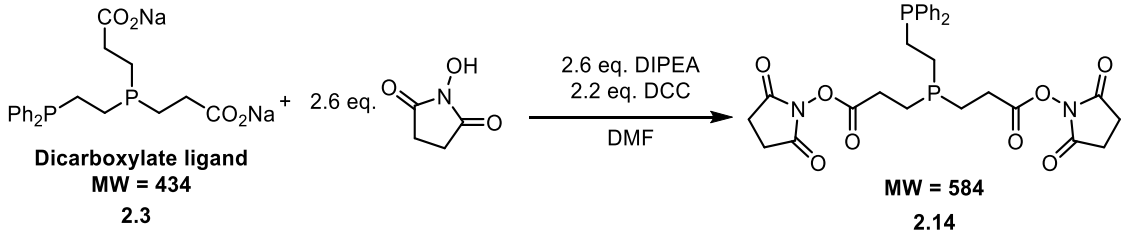

Scheme 2.14 synthesis of NHS ester **2.14**.

Following the formation of the NHS ester, **2.14** was coupled to two cyclic-RGDfK (cRGDfK) peptides to give bioconjugate **2.15**, which was fully characterised (Scheme 2.15).

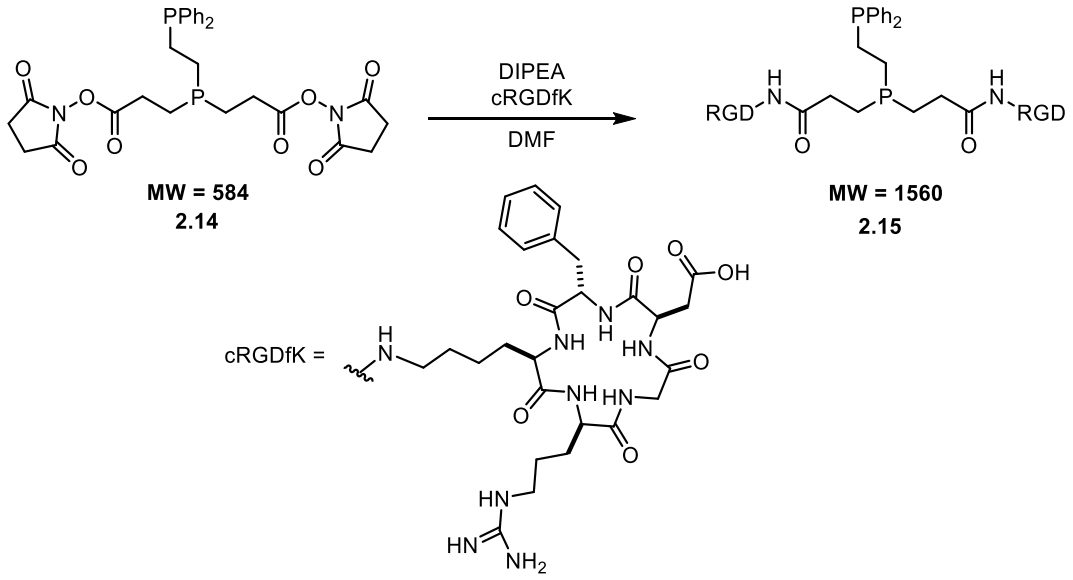

Scheme 2.15 Synthesis of bioconjugate **2.15**.

cRGDfK peptides bind with high affinity to the $\alpha_v\beta_3$ integrin receptor which is overexpressed in some cancer tumours.[13] Integrin $\alpha_v\beta_3$ plays a role in the early stages of angiogenesis, an important stage in tumour development in which new blood vessels are formed which is depended on for growth. An imaging agent with an attached cRGDfK peptide can carry the radiotracer to a tumour so that it can be selectively imaged.[14]

2.5 Radiolabelling

2.5.1 Kit preparation

^{99m}Tc based radiopharmaceuticals are often formulated from kits which contain the ligand that will complex to ^{99m}Tc, reducing agent (stannous chloride), buffer to adjust the pH (sodium hydrogen carbonate) and a stabilising agent (gluconate or tartrate). The kit is freeze-dried so that it can be kept for several months and when ready to use, pertechnetate is added before injecting into a patient. The initial ratios of the components of the kits produced in this work were based on *Myoview* kits. Tetrofosmin was substituted for the ligands discussed in this Chapter (Tables 2.1, 2.2 and 2.3).

Table 2.1 Kit preparation for diester ligand **2.2**.

Kit	Ligand (μmol)	Disodium sulphosalicylate (μmol)	Weak chelator (μmol)	Sodium hydrogen carbonate (μmol)	Stannous chloride dihydrate (μmol)	Final volume
EAC1	0.65	1.30	A - 4.60	20.7	0.26	1.0 mL
EAC2	0.65	0	A - 4.60	20.7	0.26	1.0 mL
EAC3	0.65	0	B - 3.60	20.7	0.26	1.0 mL
EAC4	0.27	0	A - 4.60	20.7	0.13	1.0 mL
EAC5	0.27	0	B - 3.60	20.7	0.13	1.0 mL

A = sodium d-gluconate, B = tartrate

Table 2.2 Kit preparation for dicarboxylate ligand **2.3**.

Kit	Ligand (μmol)	Disodium sulphosalicylate (μmol)	Weak chelator (μmol)	Sodium hydrogen carbonate (μmol)	Stannous chloride dihydrate (μmol)	Final volume
SAC1	0.65	1.30	A - 4.60	20.7	0.26	1.0 mL
SAC2	0.65	0	A - 4.60	20.7	0.26	1.0 mL
SAC3	0.65	0	B - 3.60	20.7	0.26	1.0 mL
SAC4	0.27	0	A - 4.60	20.7	0.13	1.0 mL
SAC5	0.27	0	B - 3.60	20.7	0.13	1.0 mL

A = sodium d-gluconate, B = tartrate

Table 2.3 Kit preparation for monocarboxylate ligand **2.5**.

Kit	Ligand (μmol)	Disodium sulphosalicylate (μmol)	Weak chelator (μmol)	Sodium hydrogen carbonate (μmol)	Stannous chloride dihydrate (μmol)	Final volume
LAC1	0.65	1.30	A - 4.60	20.7	0.26	1.0 mL
LAC2	0.65	1.30	B - 3.60	20.7	0.26	1.0 mL

A = sodium d-gluconate, B = tartrate

2.5.2 ^{99m}Tc radiolabelling of diester ligand 2.2

The kit formulation for diester ligand **2.2** that gave the fewest number of peaks by radio-HPLC was EAC3. When $[TcO_4]^-$ was added to the kit containing the reducing agent stannous chloride dihydrate, two complexes were expected to form: *trans* **2.16** and *cis* **2.17** (Scheme 2.16).

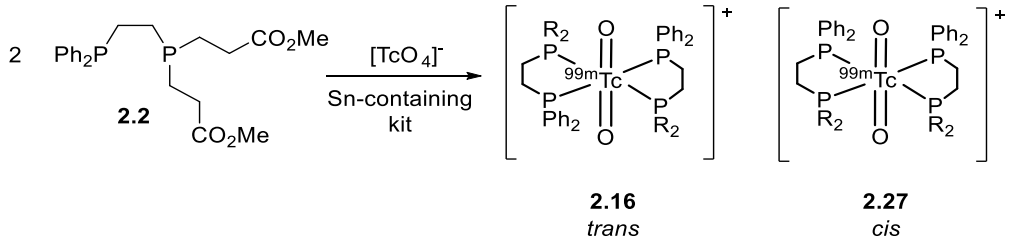

Scheme 2.16 Radiolabelling of diester **2.2**.

After 30 min at 60 °C the mixture was analysed by radio-HPLC (Figure 2.11). The small peak at approx. 4 min corresponds to free $[TcO_4]^-$ that has not complexed. It is hypothesised that the mixture of peaks between 9 – 14 min correspond to the mixture of isomers of the desired ^{99m}Tc complex.

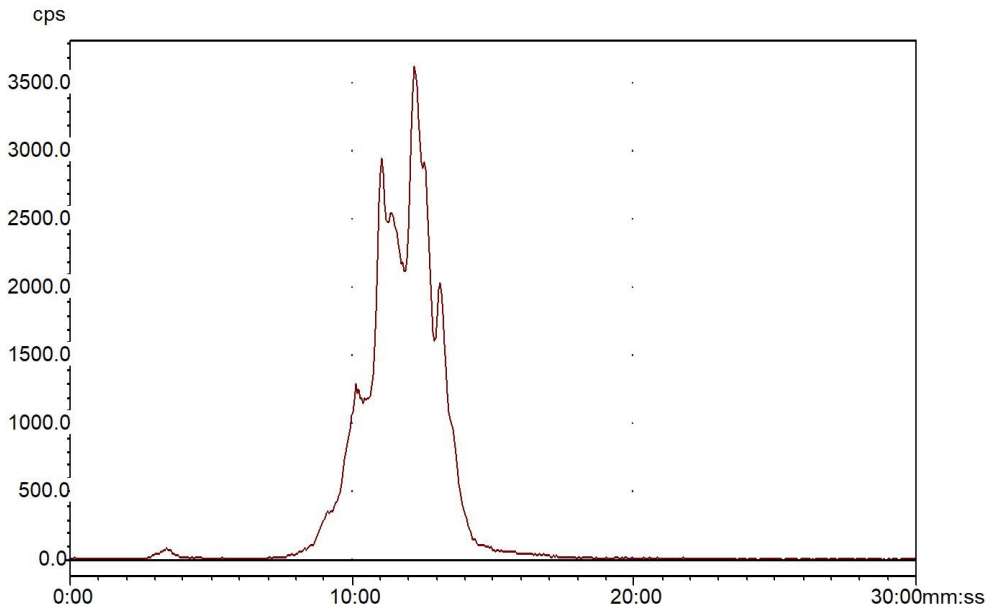

Figure 2.11 Radio-HPLC chromatogram for radiolabelled kit EAC3.

A similar radio-HPLC trace was observed when the same conditions were applied to kit EAC2 containing gluconate.

No further analysis was performed to identify the composition of the mixture of the complexes.

2.5.3 ^{99m}Tc radiolabelling of dicarboxylate ligand 2.3

When $[TcO_4]^-$ was added to the kit SAC2 containing the reducing agent stannous chloride dihydrate, two complexes were expected to form: *trans* **2.18** and *cis* **2.19** (Scheme 2.17).

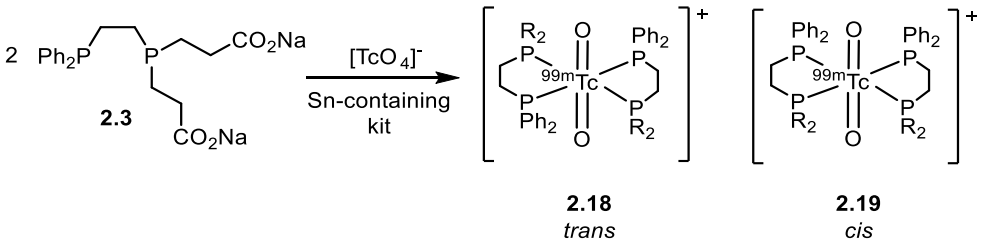

Scheme 2.17 Radiolabelling of dicarboxylate **2.3**.

After 30 min at room temperature, the mixture was analysed by HPLC (Figure 2.12). The chromatogram shows a small peak at approx. 2 min corresponding to free $[TcO_4]^-$ and two more peaks at 10 min and 12 min hypothesised to be the *cis* and *trans* complexes **2.19** and **2.18**. The trace observed for kit SAC1 under the same conditions gave the same peaks indicating that the presence of disodium sulphosalicylate (present to aid the exchange between the stabilising ligand gluconate and **2.3**) does not make a difference in the formation of the ^{99m}Tc complex. No degradation of the complexes was observed for either kit after 1 h at room temperature or at 60 °C after 1 h.

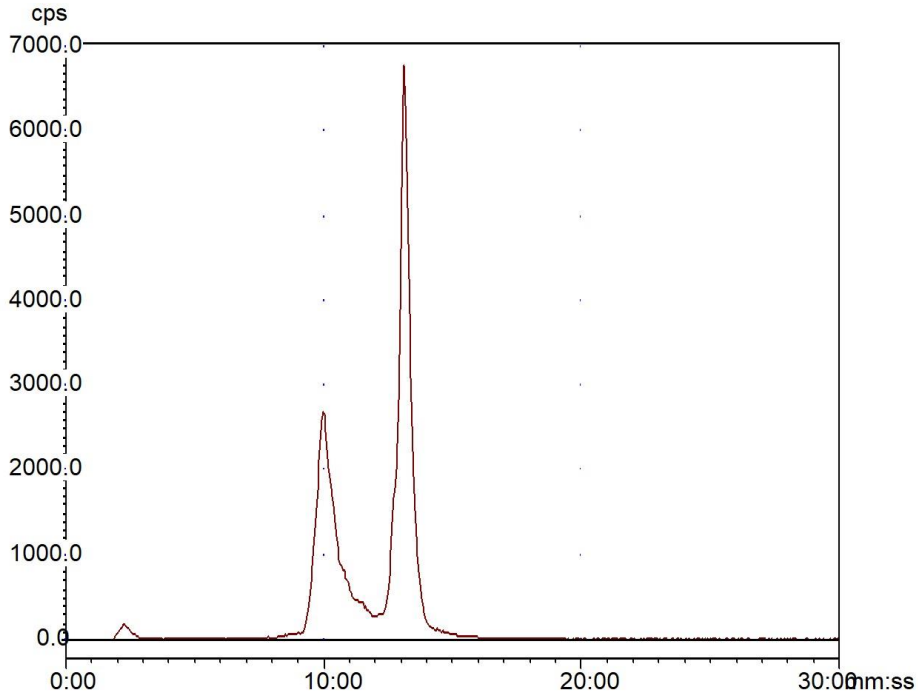

Figure 2.12 HPLC chromatogram for radiolabelled kit SAC2.

When kit SAC3 containing tartrate instead of gluconate was assessed, more peaks were observed in the HPLC chromatogram. This indicates that under these conditions, gluconate dissociates from the metal centre more rapidly than tartrate. The increased number of species detected by HPLC could be due to a mixture of the product complexes as well as intermediate ^{99m}Tc species comprising tartrate bound to ^{99m}Tc.

The ^{99m}Tc radiolabelling experiment using kit SAC2 was repeated but the mixture was spiked with ^{99}Tc so that samples could be analysed further, due to the longer half-life of ^{99}Tc ($t_{1/2}$ = 2 x 10^5 years). The products were separated by preparative HPLC, freeze-dried and submitted for mass spectrometry analysis. The masses of the complexes contained in the fractions were the same indicating that the two peaks observed by HPLC corresponded to the *cis* and *trans* isomers; MALDI *m/z* calcd. for $C_{40}H_{46}O_{10}P_4Tc$ ([*M* - 4 Na,+ 2 H]$^{2-}$) 909.60; obs. = 909.25.

2.5.4 ^{99m}Tc radiolabelling of monocarboxylate ligand 2.5

When $[TcO_4]^-$ was added to the kit LAC1 containing the reducing agent stannous chloride dihydrate, multiple complexes were expected to form including *trans* **2.20** and *cis* **2.21** (Scheme 2.18) as well as diastereoisomers, due a chiral centre at one of the phosphorus atoms in the ligand.

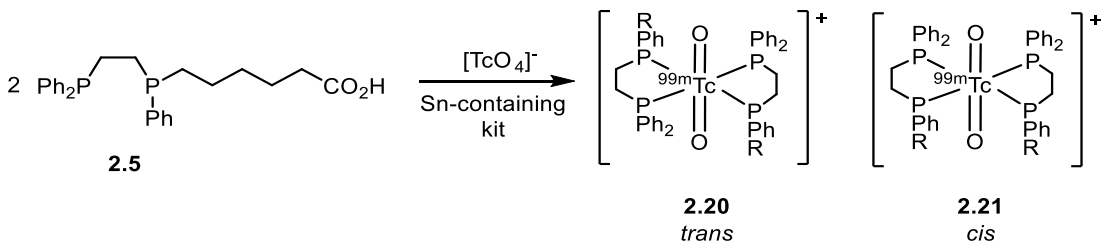

Scheme 2.18 Expected *cis* and *trans* products of the complexation of **2.5** to ^{99m}Tc.

After 30 min at 60 ºC, the mixture was analysed by HPLC (Figure 2.13). The chromatogram shows a small peak at approx. 3 min corresponding to free $[TcO_4]^-$ and multiple peaks between 10 min - 15 min.

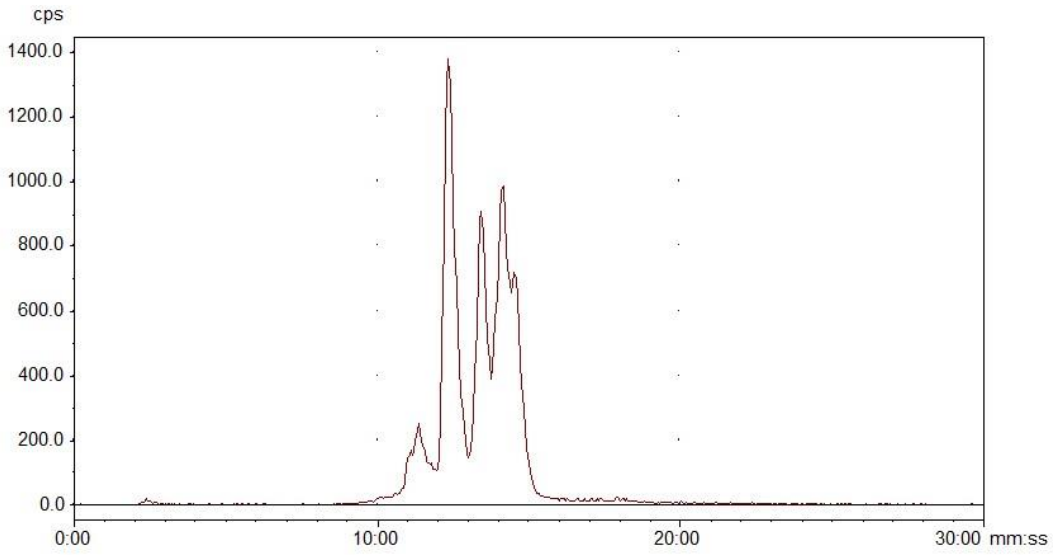

Figure 2.13 HPLC chromatogram for radiolabelled kit LAC2.

No further analysis was performed to identify the identity of the complexes.

2.6 Conclusions and future work

The synthesis of ligands analogous to tetrofosmin with groups available for bioconjugation has been demonstrated and their coordination to Re(I) and Re(V) centres investigated. ^{99m}Tc radiolabelling was carried out, with dicarboxylate ligand **2.3** giving the most promising result by labelling with the least number of isomers as observed by HPLC. A bioconjugate of **2.3** was synthesised with cRGDfK peptide for the targeting of $\alpha_v\beta_3$ integrin receptors. It would be of interest in further work to isolate this bioconjugate on a larger scale in order to formulate it into a Tc kit. Following this radiolabelling with ^{99m}Tc should be assessed and then biological testing can follow including serum stability evaluation, biodistribution studies using mouse models and SPECT imaging.

2.7 References

1 R. Southworth, R. Torres Martin de Rosales, L. K. Meszaros, M. T. Ma, G. E. D. Mullen, G. Fruhwirth, J. D. Young, C. Imberti, J. Bagunya-Torres, E. Andreozzi and P. J. Blower, *Insights from Imaging in Bioinorganic Chemistry*, Elsevier Inc., 1st edn., 2016, vol. 68.

2 W. C. Eckelman, *JACC Cardiovasc. Imaging*, 2009, **2**, 364–368.

3 V. Carroll, D. W. Demoin, T. J. Hoffman and S. S. Jurisson, *Radiochim Acta*, 2012, **100**, 653–667.

4 S. Jones and R. C. Hendel, *J. Nucl. Med. Technol.*, 1993, **21**, 191–196.

5 L. Genc, *Asian J. Chem.*, 2014, **26**, 7887.

6 G. B. Giovenzana, C. Guanci, S. Demattio, L. Lattuada and V. Vincenzi, *Tetrahedron*, 2014, **70**, 4809–4813.

7 E. W. Price and C. Orvig, *Chem. Soc. Rev.*, 2014, **43**, 260–290.

8 E. N. Tsvetkov, N. A. Bondarenko, I. G. Malakhova and M. I. Kabachinik, *Synthesis*, 1986, **3**, 198.

9 D. H. Farrar and G. Ferguson, *J. Crystallogr. Spectrosc. Res.*, 1982, **12**, 465–471.

10 J. D. G. Correia, A. Paulo, P. D. Raposinho and I. Santos, *Dalt. Trans.*, 2011, **40**, 6144–6167.

11 H. P. Engelbrecht, S. S. Jurisson, C. S. Cutler, L. Den Drijver and A. Roodt, *Synth. React. Inorganic, Met. Nano-Metal Chem.*, 2005, **35**, 83–99.

12 C. F. Ramogida and C. Orvig, *Chem. Commun.*, 2013, **49**, 4720–39.

13 M. T. Ma, O. C. Neels, D. Denoyer, P. Roselt, J. A. Karas, D. B. Scanlon, J. M. White, R. J. Hicks and P. S. Donnelly, *Bioconjug. Chem.*, 2011, **22**, 2093–2103.

14 F. Wang, Y. Li, Y. Shen, A. Wang and S. Wang, *In. J. Mol. Sci*, 2013, **14**, 13447–13462.

Chapter 3

Synthesis, coordination chemistry and ^{64}Cu radiolabelling of anhydride diphos ligands

3.1 Introduction

The coordination chemistry of 5-membered copper-diphosphine chelates has been studied extensively.[1–7] In particular, we are interested in tertiary diphos ligands with an anhydride backbone and their application in radioimaging, a topic that has been little explored.[8,9] In this Chapter, we report a new preparation of 2,3-dichloromaleic anhydride-derived diphosphine **3.1** and the synthesis of the novel dicyclohexyl analogue **3.2**. The coordination chemistry with group 11 metals is explored as well as an investigation of their biological properties.

3.1.1 Previous investigations of diphos anhydride 3.1

Copper(I) bis(diphosphine) complexes including the diphenylphosphino anhydride ligand **3.1** and ring-opened derivatives **3.3** and **3.4** have been investigated as potential PET imaging agents by Blower *et al.* (Figure 3.1).[9,8]

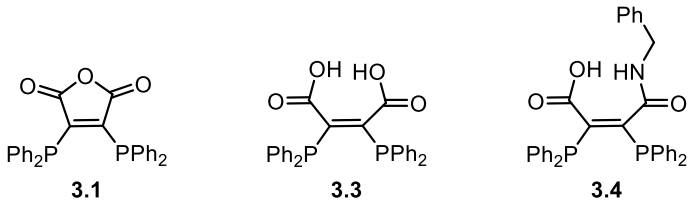

Figure 3.1 Structure of 2,3-bis(diphenylphosphino)maleic anhydride **3.1** and ring-opened derivatives **3.3** and **3.4**.

Mass spectrometry and X-ray crystallography suggested that **3.1** forms monomeric, approximately tetrahedral, intensely coloured complexes with copper(I); [CuCl(**3.1**)$_2$] when diphos **3.1** was added to CuCl, and [Cu(**3.1**)$_2$]$^+$ when it was added to Cu(MeCN)$_4^+$. The reported Cu-P bond lengths of both complexes are significantly longer than in [Cu_2Cl_2(μ–dppe)$_3$] (2.321(3) Å and 2.3048(2) Å compared to 2.291(5) Å) which may in part be due to the electron-withdrawing anhydride group. Ligands bearing an anhydride backbone offer the potential to bioconjugate small molecules for specific targeting of disease. It is also possible to modify their biodistribution due to the tunability of the substituents on phosphorus, though this has not been widely reported.[8]

3.1.2 Coordination chemistry of 3.1

The coordination chemistry of **3.1** has been widely reported with Group 6,[10–12] Group 10[13–17] and Group 11[18] metals as well as Re,[19,20] Mn, Fe[21,22] and Co[23–29].

Shollhammer *et al.* studied **3.1** as a potentially redox-active ligand as part of a synthetic mimic of the [FeFe] hydrogenase active site: an enzyme that catalyses reversible oxidation of H_2 (Figure 3.2).[30]

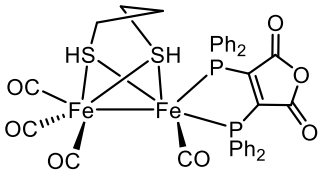

Figure 3.2 Structure of a [FeFe] hydrogenase active site mimic incorporating **3.1**.

With respect to electron transfer between the ligand and metal, it was concluded that there was a lack of electronic communication between **3.1** and the diiron site. As the diphosphine has a low-lying π* orbital delocalised over the anhydride backbone it is reduced at a fairly low potential and the electron added is predominantly ligand-based. They showed that the synthetic mimic including **3.1** did not reduce protons to H_2, which was attributed to the gap between redox potentials of the anhydride ligand and the [FeFe] site being too large for coupling of proton and electron transfers to occur.

A number of stable 17- and 19-electron complexes with Co, Mo and W have also been investigated using diphos **3.1**.[10–12] EPR studies have concluded that the odd electron is likely to be ligand-centred.

3.1.3 Anhydride diphos ligands in catalysis

Borner *et al.*[31,32] have used the anhydride ligand MalPHOS, synthesised via a silyl elimination reaction (Scheme 3.1), for Rh(I)-catalysed enantioselective hydrogenation of pharmaceutically relevant unsaturated amino acid precursors.

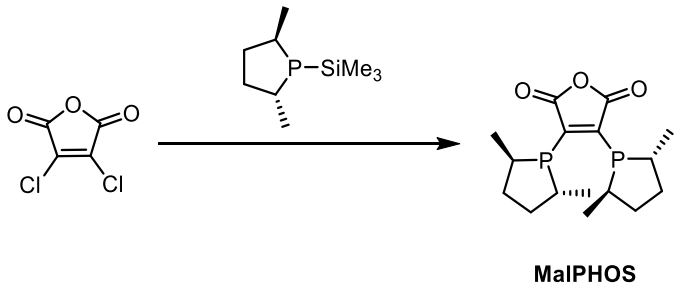

Scheme 3.1 Synthesis of MalPHOS.

The MalPHOS-Rh(I) complex, with its wider bite angle, proved to be a superior hydrogenation catalyst in terms of enantioselectivity to a related MeDuPHOS complex.

In subsequent work, Borner *et al.* synthesised a series of chiral bisphosphine ligands by varying the ligand backbone and tested them in enantioselective hydrogenation.[33] They showed that ligands with maleic anhydride or maleimide bridges gave consistently higher enantioselectivities when the reaction was performed in methanol, compared to ligands with three-, four-, five- and six-membered heterocyclic or alicyclic backbones.

3.2 Synthesis of anhydride diphos ligands

The synthesis of anhydride ligand **3.1** has been reported *via* a silyl elimination reaction.[34] We applied the same conditions in order to prepare dicyclohexyl analogue **3.2**; dicyclohexyl(trimethylsilyl)phosphine and 2,3-dichloromaleic anhydride were heated to 60 °C in THF for 18 h to give a mixture of products. The major product gave a singlet at δ –13.5 ppm in the *in situ* ^{31}P{^{1}H} NMR spectrum (Scheme 3.2, Figure 3.3).

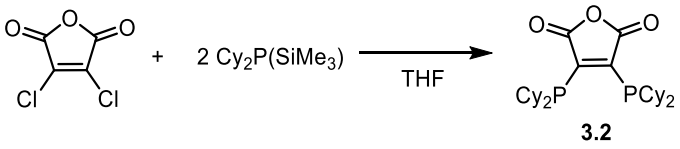

Scheme 3.2. Different syntheses of dicyclohexyl anhydride ligand **3.2**.

Alternatively, when 2 equiv. of dicyclohexylphosphine was added to 2,3-dichloromaleic anhydride in THF and heated at 60 °C for 18 h, a singlet at δ 127.9 ppm was observed by *in situ* ^{31}P{^{1}H} NMR spectroscopy (Figure 3.3).

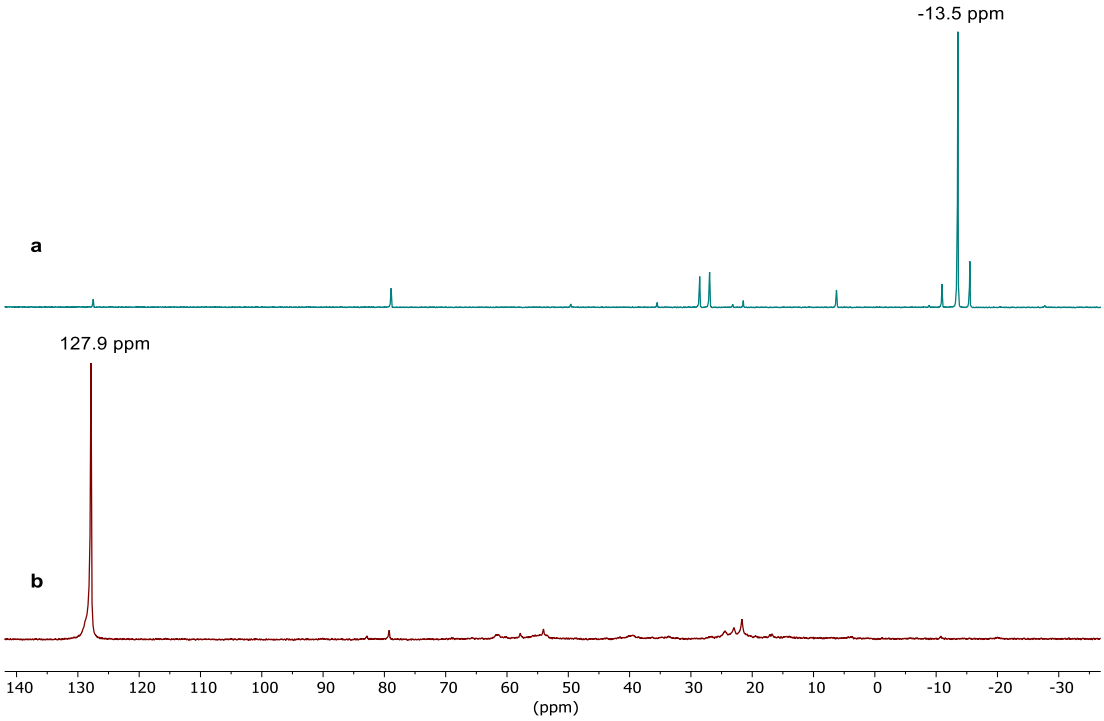

Figure 3.3 $^{31}P\{^{1}H\}$ NMR (121 MHz, THF) spectra (a) synthesis of **3.2** from $PCy_2(SiMe_3)$; (b) attempted synthesis of **3.2** from PCy_2H.

Subsequent addition of $[Pt(cod)Cl_2]$ to both reaction mixtures gave the same platinum complex, **3.5** (Figure 3.4) according to the $^{31}P\{^{1}H\}$ NMR spectra obtained (δ 110.6 ppm, $^{1}J_{PPt}$ = 3958 Hz).

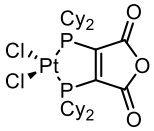

Figure 3.4 Platinum complex **3.5.**

Furthermore, addition of HCl to the reaction mixture with the singlet at δ –13.5 ppm produced a new peak at δ 127.9 ppm. This led to the hypothesis that the signal at δ -13.5 ppm corresponded to the desired product **3.2**, whereas the peak at δ 127.9 ppm corresponded to a protonated or bis-protonated derivative due to HCl produced in the reaction (Figure 3.5).

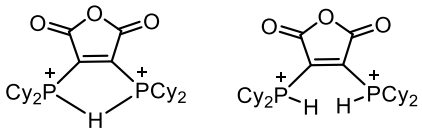

Figure 3.5 Hypothesised protonated analogues of **3.2**.

In an attempt to remove the acidic by-product from the reaction mixture, 4 Å molecular sieves were added. This proved unsuccessful and so varying equivalents of sodium carbonate were introduced. Finally, it was found that the addition of 2.2 equiv. of triethylamine and a small excess of dicyclohexylphosphine were the optimum reaction conditions for the synthesis of **3.2** (Scheme 3.3). The only by-products are an ammonium salt which is filtered away and Cy_2PH which can removed *in vacuo*.

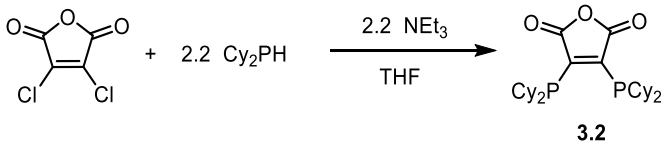

Scheme 3.3 Optimised synthetic route towards 3.2.

Red crystals suitable for X-ray crystallography were obtained by slow evaporation of a THF solution and the structure is shown in Figure 3.6.

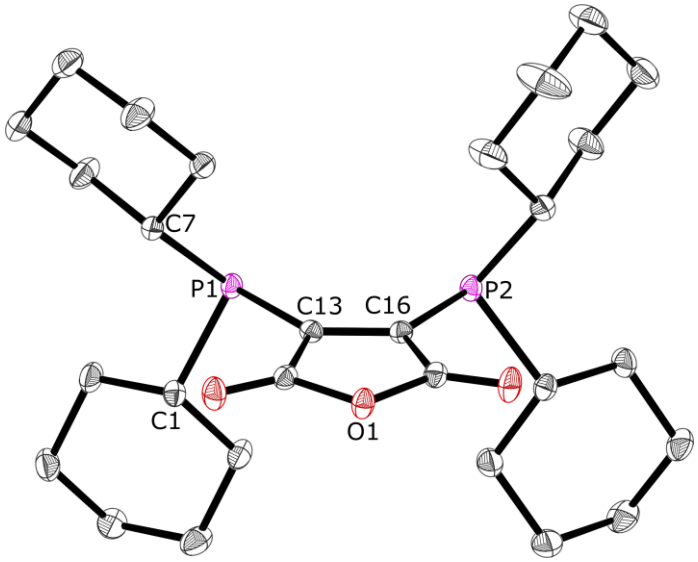

Figure 3.6 Crystal structure of **3.2**. Selected bond lengths (Å) and bond angles (°): P(1)-C(1) 1.8702(14), P(1)-C(13) 1.8388(13), C(13)-C(16) 1.3480(17), C(1)-P(1)-C(13) 96.95(6), P(1)-C(13)-C(16) 127.76(10).

The optimised conditions were applied to analogues with Ph and ^{i}Bu substituents on the phosphorus (Figure 3.7). Diphenyl derivative **3.1** was isolated and fully characterised but the attempted synthesis of **3.6** gave a mixture of P-containing species and requires further optimisation (Figure 3.7).

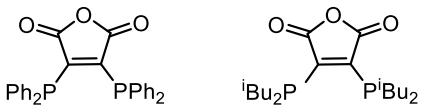

3.1 **3.6**

Figure 3.7 Structures of anhydride analogues **3.1** and **3.6**.

In the *in situ* $^{31}P\{^{1}H\}$ NMR spectrum for the synthesis of **3.6 t**he major peak at δ -43.4 ppm accounts for 63% of the product mixture Figure 3.8). Mass spectrometry shows that the desired product **3.6** is present (ESI+ *m*/*z* calcd. for $C_{20}H_{37}O_3P_2$ ($[M+H]^+$) = 387.1; obs. = 387.0). The minor species are assigned to oxides and protonated compounds.

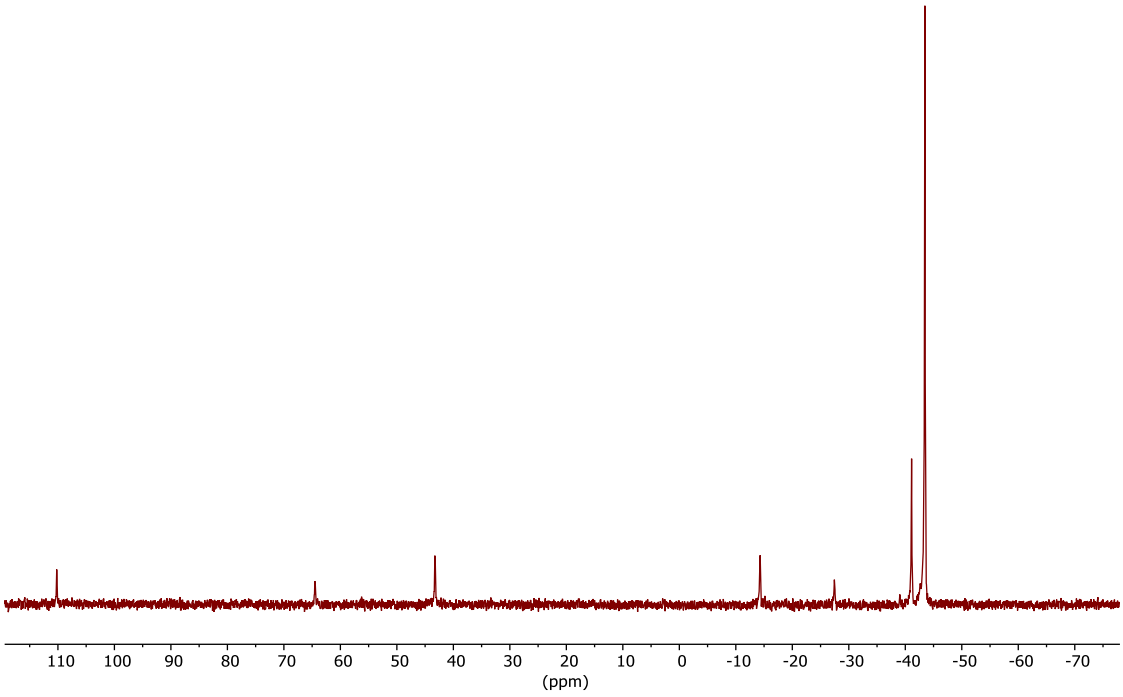

Figure 3.8 *In situ* $^{31}P\{^{1}H\}$ NMR (122 MHz, THF) spectrum of the synthesis of **3.6**.

3.3 Coordination chemistry

3.3.1 Copper coordination

Previous work by Blower[8,9] and others[35,18] has shown that diphos anhydride ligand **3.1** can be coordinated to copper(I), silver(I) and gold(I) to give complexes useful for imaging and potential anticancer applications.

The analogous dicyclohexylphosphine anhydride **3.2** was complexed to Cu(I) *via* the precursor [CuI] to give a broad signal in its $^{31}P\{^{1}H\}$ NMR spectrum with a small coordination shift compared to **3.2** (Δδ approx. 4 ppm) (Figure 3.9). The signal has been tentatively assigned to a rapidly equilibrating mixture of **3.7, 3.8** and **3.9** based on mass spectrometry data (Scheme 3.4).

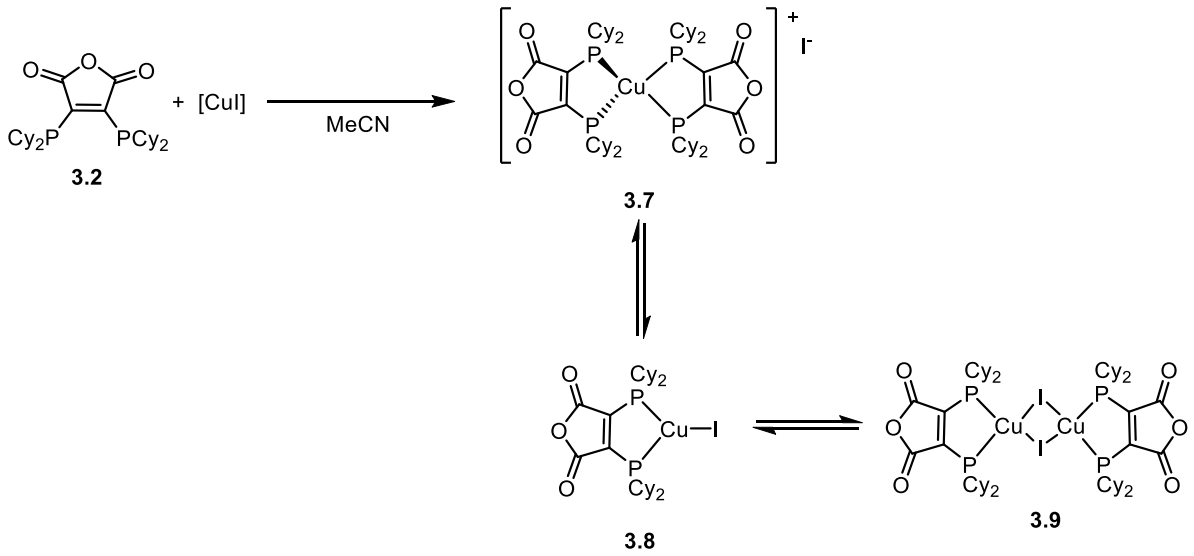

Scheme 3.4 Synthesis of Cu complexes **3.7**, **3.8** and **3.9**.

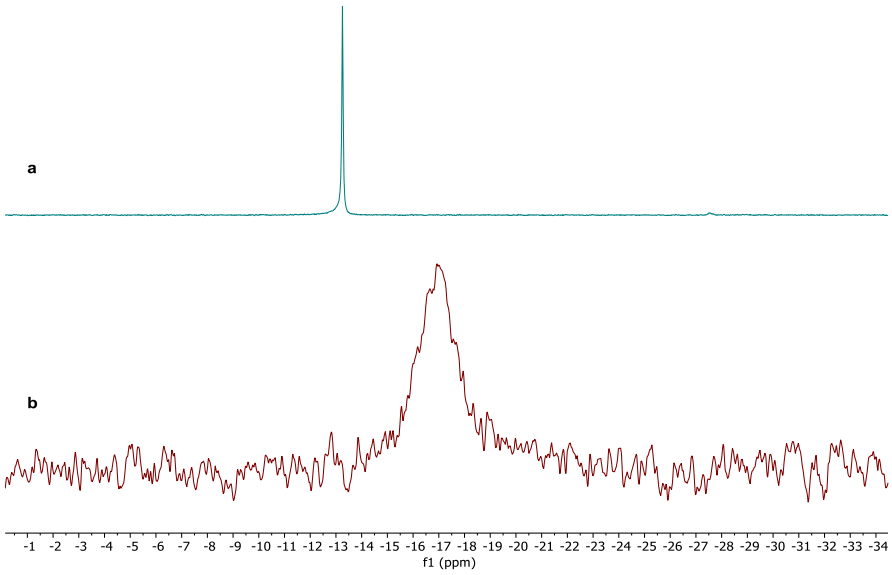

Figure 3.9 $^{31}P\{^{1}H\}$ NMR (CH_2Cl_2, 121 MHz) spectra of (a) ligand **3.2**; (b) complex mixture **3.7, 3.8,** and **3.9**.

Blue crystals of complex **3.9** suitable for X-ray crystallography were grown by slow evaporation of a methanol solution (Figure 3.10).

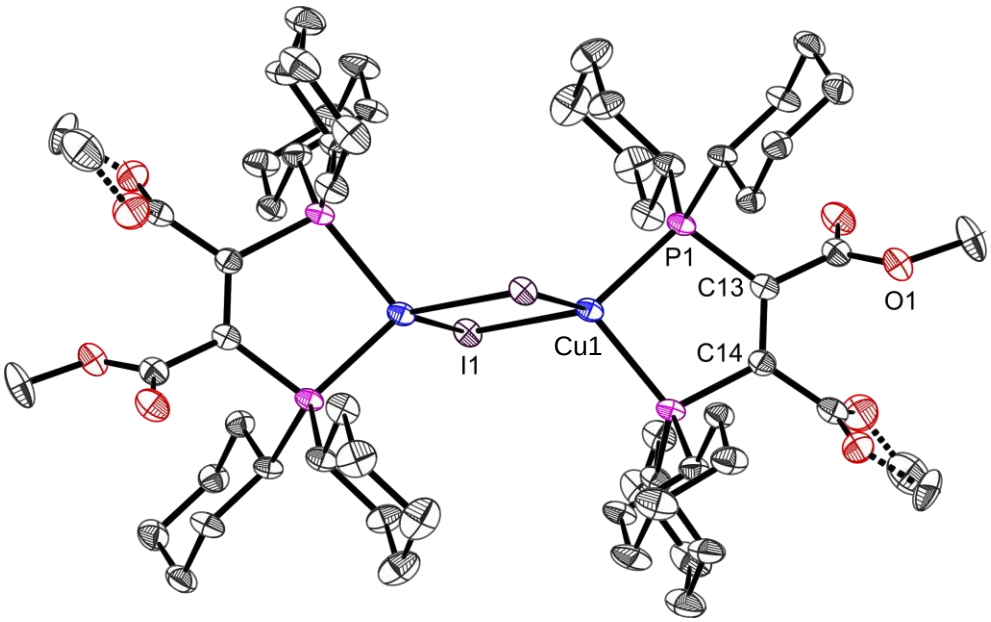

Figure 3.10 Crystal structure of **3.9**. Hydrogen atoms omitted for clarity. Selected bond lengths (Å) and bond angles (°): Cu(1)-P(1) 2.2672(9), P(1)-C(13) 1.848(4), Cu(1)-I(1) 2.6352(5), C(13)-C(14) 1.345(5), I(1)-Cu(1)-P(1) 117.23(3), Cu(1)-P(1)-C(13) 105.49(16), P(1)-C(13)-C(14) 121.5(3).

The crystal structure shows that the anhydride backbone has been opened following weeks dissolved in methanol. Blower reported that ring opening of the anhydride backbone of the diphenylphosphino ligand **3.1** can be achieved when the ligand is coordinated to the metal by treatment of the complex with aqueous NaOH or by the addition of aqueous methanol.[9] They showed that both **3.1** and the ring opened product when complexed to Cu(I) form mononuclear species $[Cu(L)_2]^+$. The blue crystals of the dinuclear complex **3.9** precipitated from an orange solution suggesting that the structure obtained in the solid state was not the only species present; this may be due to a mixture of ring-opened and ring-closed ligands as well as mono- and dinuclear complexes.

Further work including low temperature NMR studies are required to characterise the species present in solution.

3.3.2 Silver and gold coordination

Berners-Price *et al.* have studied the structure and anti-tumour activity of the ring-opened 2.3-bis(diphenylphosphinomaleic) acid **3.10** with silver(I) and gold(I) (Figure 3.11).[18] 2:1

and 1:2 adducts were prepared and characterised by X-ray crystallography. No significant *in vitro* cytotoxic activity was found for gold complex **3.12** following testing against 8 cell lines.

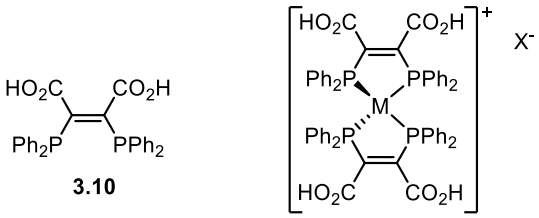

Figure 3.11 Structure of 2.3-bis(diphenylphosphinomaleic) acid **3.10** and silver and gold complexes **3.11** and **3.12** studied by Berners-Price.

In the studies performed by the author, dicyclohexylphosphino anhydride **3.2** was stirred with [AgBr] in MeCN for 2 h to form a complex that corresponds to a doublet {(^{1}J(^{109}AgP) = 249.3 Hz, ^{1}J(^{107}AgP) = 218.0)} in the ^{31}P{^{1}H} NMR spectrum with a coordination shift Δδ of 18 ppm (Figure 3.12). The species has been tentatively assigned to the cationic mononuclear complex **3.13** (Scheme 3.5).

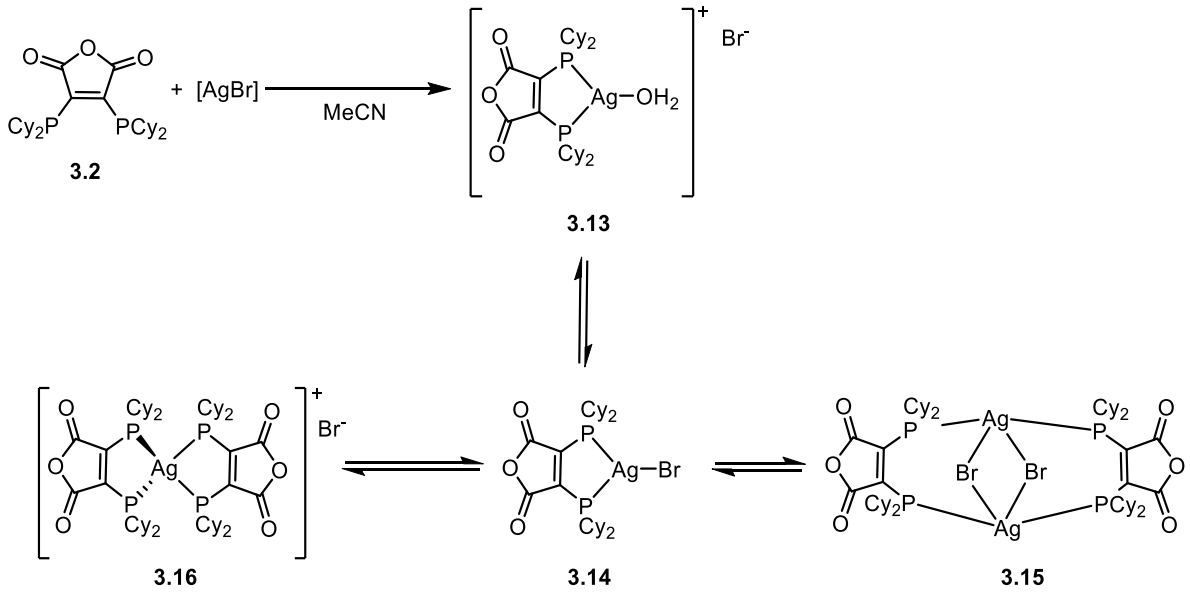

Scheme 3.5 Synthesis of silver(I) complexes **3.13**, **3.14**, **3.15** and **3.16**.

The Ag(I) complex of **3.13** was synthesised in MeCN that had not been dried over molecular sieves. When this solvent was removed and the complex redissolved in dry MeCN that had been kept over molecular sieves, the ^{31}P{^{1}H} NMR spectrum became more complicated (Figure 3.12). It is clear that there are multiple species present in the

product mixture. The new doublets at δ 10.7 and 9.22 ppm have been tentatively assigned to complex **3.14** as water is removed from the solution. This mononuclear species may have the tendency to dimerise to give dinuclear species **3.15** with bridging bromide atoms. Alternatively, it could form the $[Ag(L)_2]^+$ cationic species **3.16**, similar to the structure of the Ag complex synthesised by Berners-Price *et al.* (Figure 3.11).[18] The orientation of the anhydride rings can make the phosphorus atoms of **3.16** inequivalent to give an A_2X_2 spin system indicated by the doublets of triplets ($^1J_{AX}$ = 30.7 Hz).

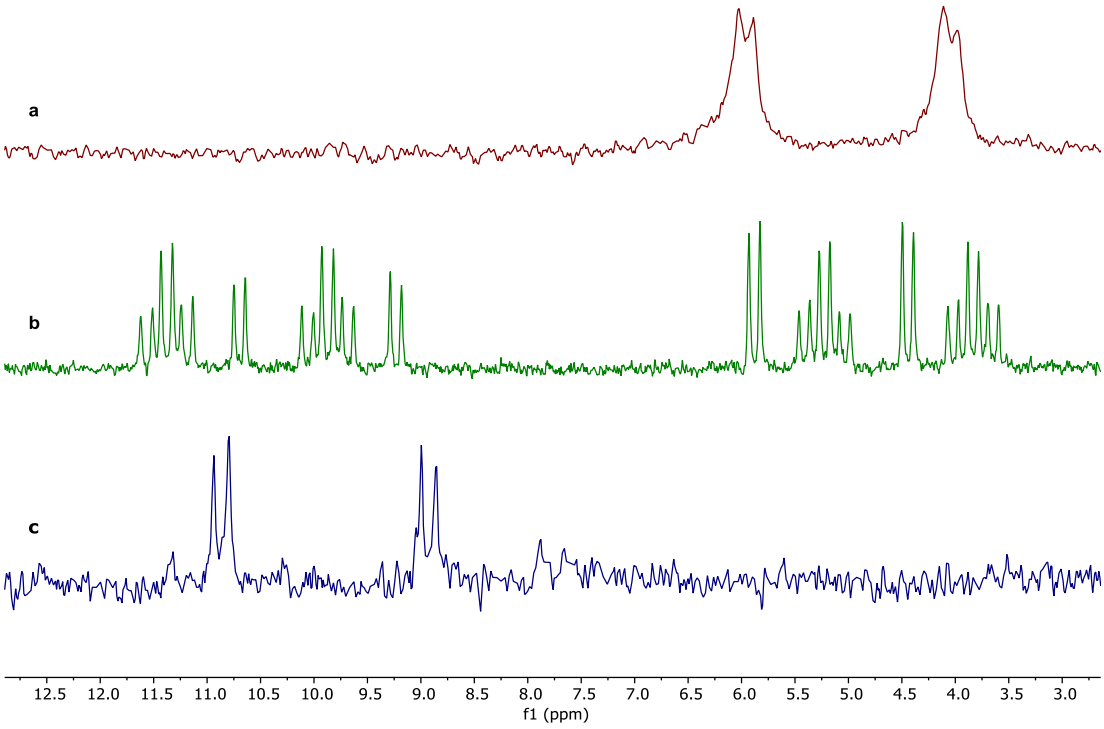

Figure 3.12 ^{31}P{^{1}H} NMR (121 MHz, MeCN) spectra of: (a) *in situ* reaction mixture of silver complexes of **3.14** in wet MeCN; (b) reaction mixture using dry MeCN; (c) solid precipitate in dry MeCN.

Crystals of **3.15** suitable for X-ray crystallography were grown from slow diffusion of diethyl ether into its DCM solution (Figure 3.13).

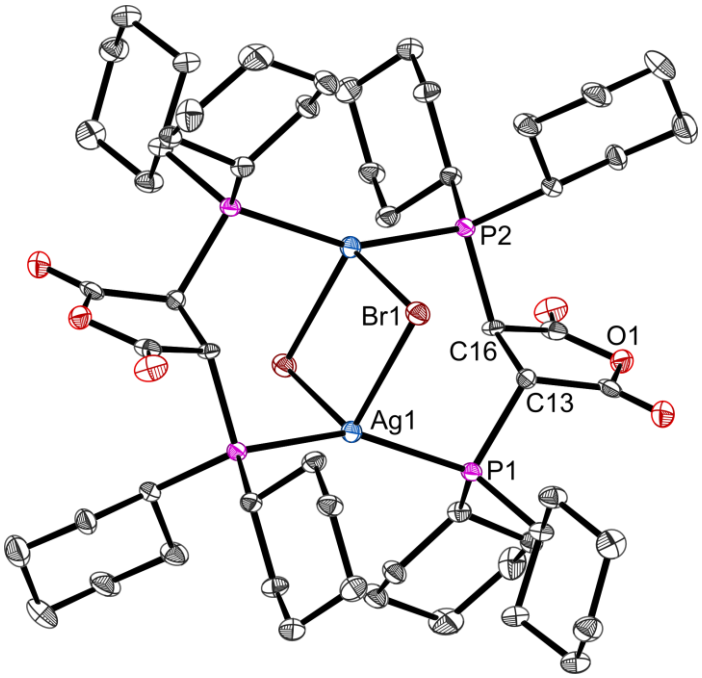

Figure 3.13 Structure of **3.15**. Hydrogen atoms omitted for clarity. Selected bond lengths (Å) and bond angles (°): Ag(1)-P(1) 2.4160(10), Ag(1)-Br(1) 2.7668(5), P(1)-C(13) 1.886(2), C(13)-C(16) 1.541(5), Br(1)-Ag(1)-P(1) 98.07(2), Ag(1)-P(1)-C(13) 104.16(11), P(1)-C(13)-C(16) 113.5(2).

The P(1)-C(13) bond in **3.15** is longer than in the free ligand (1.8388(13) Å in the free ligand) and the P(1)-C(13)-C(16) bond angle decreases form 127.76(10)° to 113.5(2)°). The C(13)-C-(16) bond is also elongated when the ligand is complexed to Ag (1.3480(17) Å when free ligand). (See Section 3.2 for crystal structure of free ligand **3.2**).

When 1 equiv. **3.2** was stirred with [AuCl(tht)] for 30 min (Scheme 3.6), the ^{31}P{^{1}H} NMR spectrum of the product displayed a singlet at δ 18 ppm and an additional broad signal at around δ 21 ppm (coordination shift Δδ of 31 ppm) (Figure 3.14). Mass spectrometry data supported the presence of a mononuclear species with two ligands attached (ESI+ *m*/*z* calcd. for $C_{56}H_{88}AuO_6P_4$ ([*M*+H]$^+$) = 1177.5; obs. = 1177.7). This is analogous to the type of complex prepared by Berners-Price *et al.* who showed that when the ratio of Au to ligand is 1:1 or less the bis-chelate [Au(P-P)$_2$]$^+$ is formed; the bis-chelate **3.17** is assigned to a ^{31}P{^{1}H} NMR signal at δ 18.1 ppm.[18]

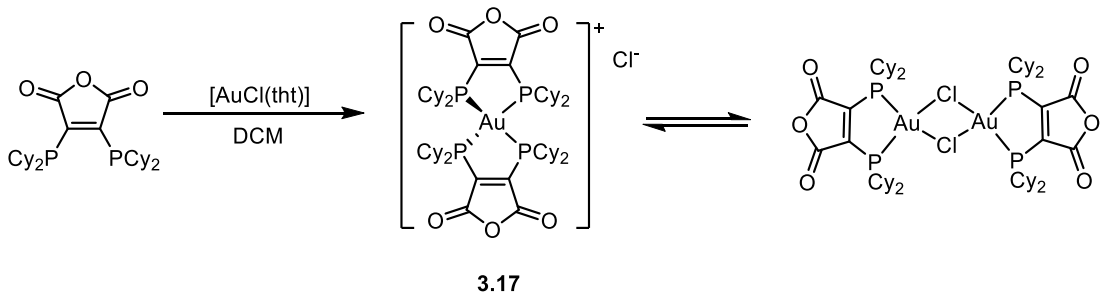

3.17

Scheme 3.6 Synthesis of Au complex **3.17**.

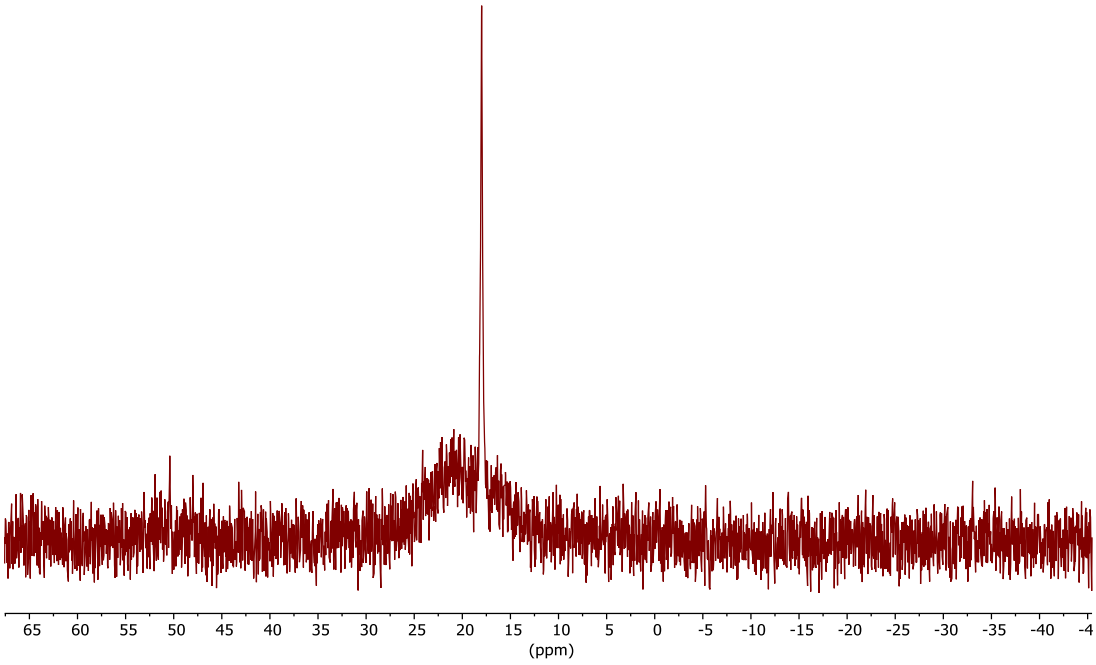

Figure 3.14 $^{31}P\{^{1}H\}$ NMR (121 MHz, CH_2Cl_2) spectrum of a mixture of P-containing Au complexes including **3.17**.

The broad signal observed in the $^{31}P\{^{1}H\}$ NMR is tentatively assigned to a dinuclear species with bridging chlorides which may be in equilibrium with **3.17**.

3.4 Anhydride ring-opening and bioconjugation

As discussed in Chapter 1, the use of bifunctional chelators is a common strategy to form imaging agents specifically targeted to certain sites of disease.

The anhydride backbone of **3.2** can be easily opened by stirring the ligand with a peptide and base (Scheme 3.7). Peptides containing the sequence RGD (arginine-glycine-aspartic acid) such as cyclic-RGDfK pentapeptide (cRGDfK, where f = D-Phe) bind to $\alpha_v\beta_3$ integrin receptors which are often overexpressed in the tumours of different cancers.[36]

Imaging of such receptors allows the characterisation of tumour angiogenesis, the proliferation of blood vessels essential for tumour growth.[37]

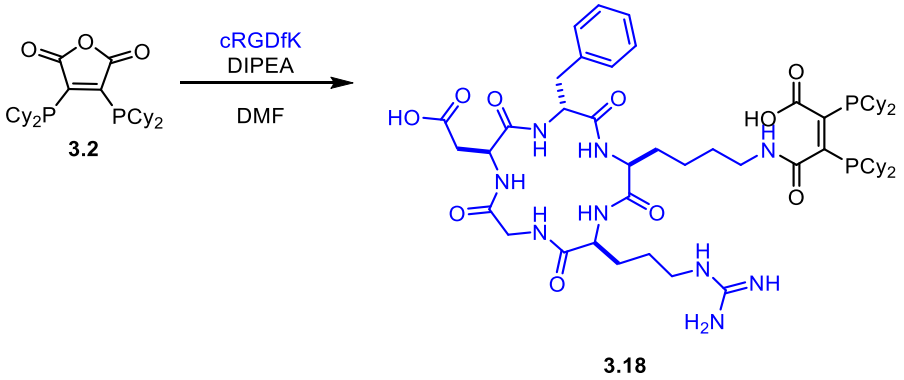

Scheme 3.7 Synthesis of bioconjugate **3.18**.

The ^{31}P{^{1}H} NMR spectrum of the moderately air-stable bioconjugate **3.18** shows an AB splitting pattern due to the inequivalent phosphorus atoms (Figure 3.15). For full characterisation see Chapter 6.

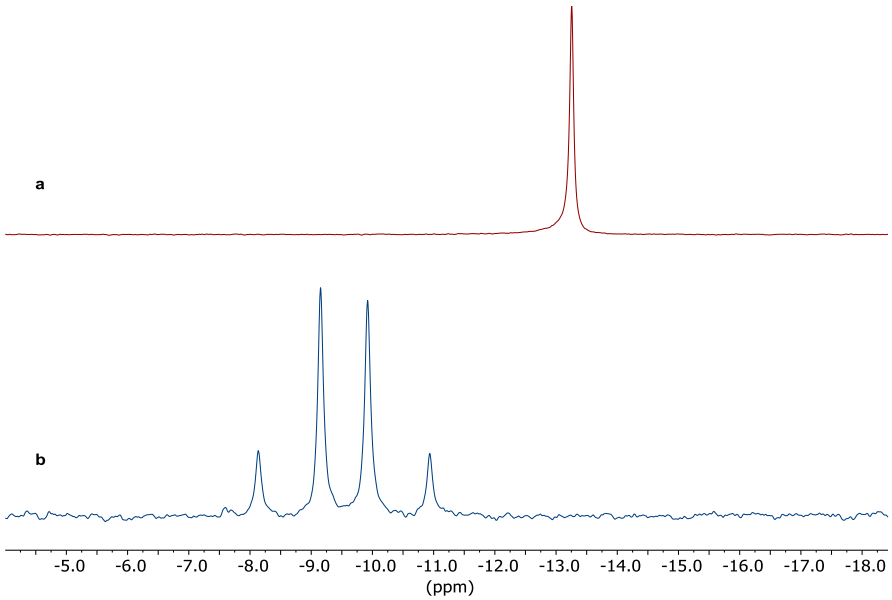

Figure 3.15 ^{31}P{^{1}H} NMR (161 MHz, MeCN) spectra of (a) anhydride ligand **3.2** (δ -13.3); (b) bioconjugate **3.18** (δ -8.8, -10.28; $^{3}J_{PP}$ = 163.8 Hz).

3.5 Radiolabelling with copper-64

Following the addition of anhydride bioconjugate **3.18** to [^{64}CuCl$_2$] under mild conditions (room temperature, pH 5-6) (Scheme 3.8), one species with a retention time of 19 min was detected by analytical reverse-phase HPLC (Figure 3.17).

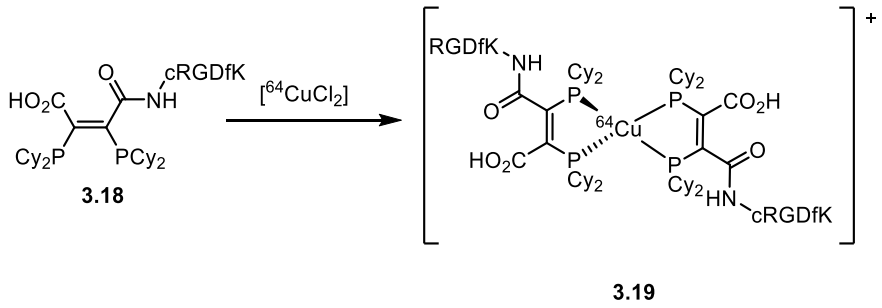

3.18 **3.19**

Scheme 3.8 Radiolabelling of **3.18** with ^{64}Cu.

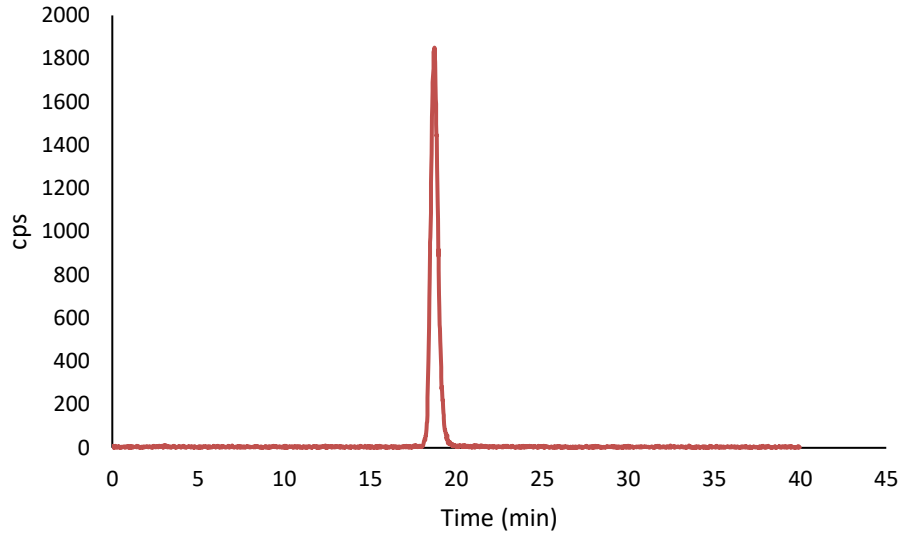

Figure 3.17 HPLC chromatogram of [^{64}Cu(**3.19**)$_2$]$^+$.

Instant thin layer chromatography showed efficient radiolabelling (>90%) was achieved at concentrations as low as 0.01 mgmL^{-1} with no need for post-labelling purification giving a radiochemically pure complex without colloidal or unbound ^{64}Cu. Mass spectrometry supported the 2:1 stoichiometry of the complex (ESI+ *m*/*z* calcd. for $C_{110}H_{170}CuN_{18}O_{20}P_4$ ([*M*+H]$^{3+}$) = 750.3; obs. = 751.1).

3.6 Biological studies

3.6.1 Distribution coefficient determination

A distribution coefficient (Log$D_{7.4}$) describes the pH-dependant concentration ratio of a compound in a mixture of immiscible phases at equilibrium; in this case octanol and water at pH 7.4. Log$D_{7.4}$ was calculated as shown in the equation below (aliquots of octanol and

water containing the tracer were taken and counts were measured using a gamma counter):[38]

$$LogD_{7.4} = \frac{counts\ in\ octanol}{counts\ in\ water}$$

Determination of Log$D_{7.4}$ for **3.19** revealed low hydrophilicity (Log$D_{7.4}$ = +2.13 ± 0.18) indicating it would most likely clear the body via the liver. In contrast the phenyl analogue **3.20** showed higher hydrophilicity (Log$D_{7.4}$ = -0.62 ± 0.04) representative of compounds that are likely to be excreted via the kidneys (Figure 3.17).[39] Damage to the bladder following radiotherapy is a common side-effect of prostate cancer treatment.[40] The tendency of **3.19** to clear via the liver would make the compound an attractive potential prostate cancer imaging agent if a prostate-directing peptide could be conjugated instead of cRGDfK.

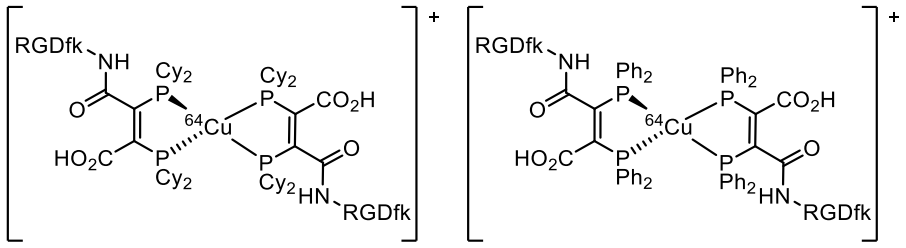

3.19
Log$D_{7.4}$ = +2.13 (± 0.18)

3.20
Log$D_{7.4}$ = -0.62 (± 0.04)

Figure 3.17 Structures and distribution coefficient values for bioconjugates **3.19** and **3.20**.

3.6.2 Serum stability and *in vivo* studies

The stability of radiotracers in biological media is vital for their utility in the clinic.[41] The stability of **3.19** incubated in human serum over 24 h was investigated by reverse-phase and size exclusion HPLC and compared to the elution profile of unchelated ^{64}Cu in serum at 1 h. [^{64}Cu(**3.18**)$_2$]$^+$ was stable in serum at 37 °C for up to 4 h with no detected changes in retention time.

The *ex vivo* biodistribution of [^{64}Cu(**3.18**)$_2$]$^+$ was assessed in albino, laboratory-bred mice of strain BALB/c (n = 4, where n is the number of mice used in the group, group A) and compared to BALB/c mice (n=4, group B) with [^{64}Cu(**3.18**)$_2$]$^+$ and an additional blocking

dose of cRGDfK peptide dissolved in saline ($[^{64}Cu(\mathbf{3.18})_2]^+$ + RGD). Mice were anaesthetised, injected with the radiotracer and culled after 1 h, after which organs were harvested and the radioactivity counted (Figure 3.18).

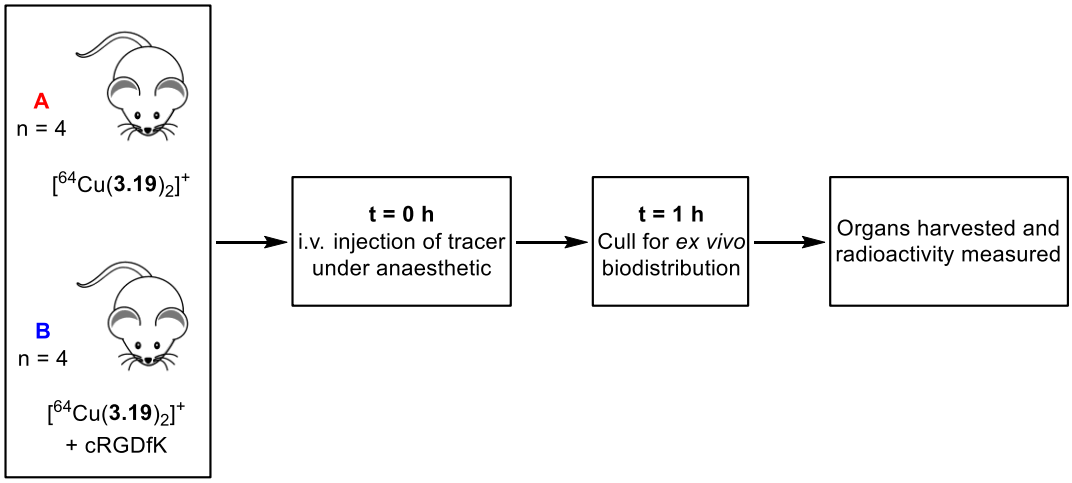

Figure 3.18 Procedure for *ex vivo* biodistribution study.

The blocking dose of cRGDfK peptide in group B was injected in order to block the receptor sites that recognise cRGDfK peptide. By comparing to the mice in group A, injected with the radiotracer only, the selectivity of the tracer can be assessed.

Ex vivo biodistribution data indicate that after 1 h the distribution of activity of group A mirrored that of group B (Figure 3.19); this is most likely due to injection of a low amount of activity per animal (0.1-0.4 MBq); therefore, conclusions about selectivity cannot be drawn from the data collected.

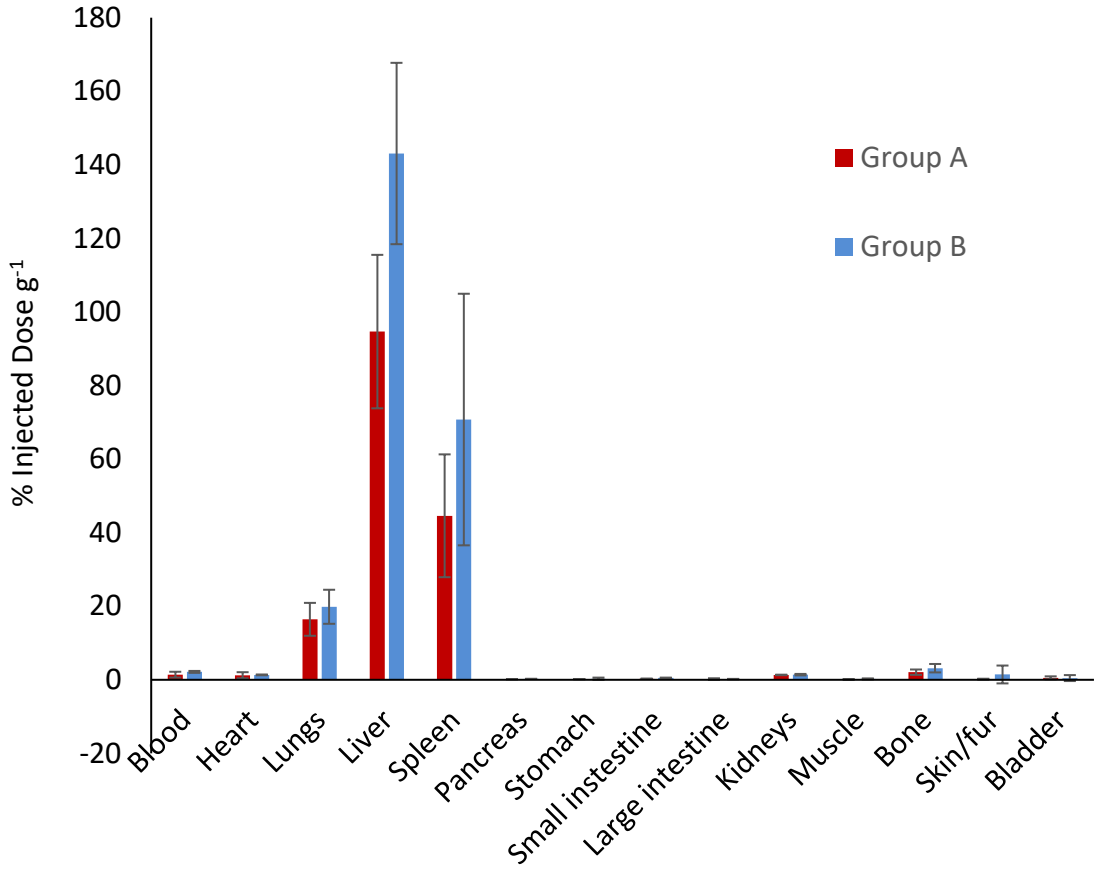

Figure 3.19 Average biodistribution of normal female BALB/c mice injected with $[^{64}Cu(\mathbf{3.18})_2]^+$ (group A, red) and ($[^{64}Cu(\mathbf{3.18})_2]^+$ + cRGDfK (group B, blue) after 1 h; error bars correspond to standard error of the mean, (n = 4 for each group).

For both groups the majority of activity was contained in the lungs (A = 16.4 ± 4.5% ID g^{-1}, B = 19.8 ± 4.6% ID g^{-1}), liver (A = 94.7 ± 20.9%ID g^{-1}, B = 143.1 ± 24.7% ID g^{-1}) and spleen (A = 44.6 ± 16.7% ID g^{-1}, B = 70.8 ± 34.2% ID g^{-1}). The absence of a significant amount of activity in the kidneys and bladder suggests that the compound is cleared *via* the liver and most likely within the first hour of biodistribution. This is supported by the $LogD_{7.4}$ data shown in Section 3.6.1.

PET scans acquired at 0.5 h, 1 h, 2 h, 3 h and 20 h were consistent with the biodistribution data; PET images of a mouse imaged with $[^{64}Cu(\mathbf{3.18})_2]^+$ exhibited predominantly liver associated activity even at the 0.5 h time point and remains unchanged over the scans (Figure 3.20).

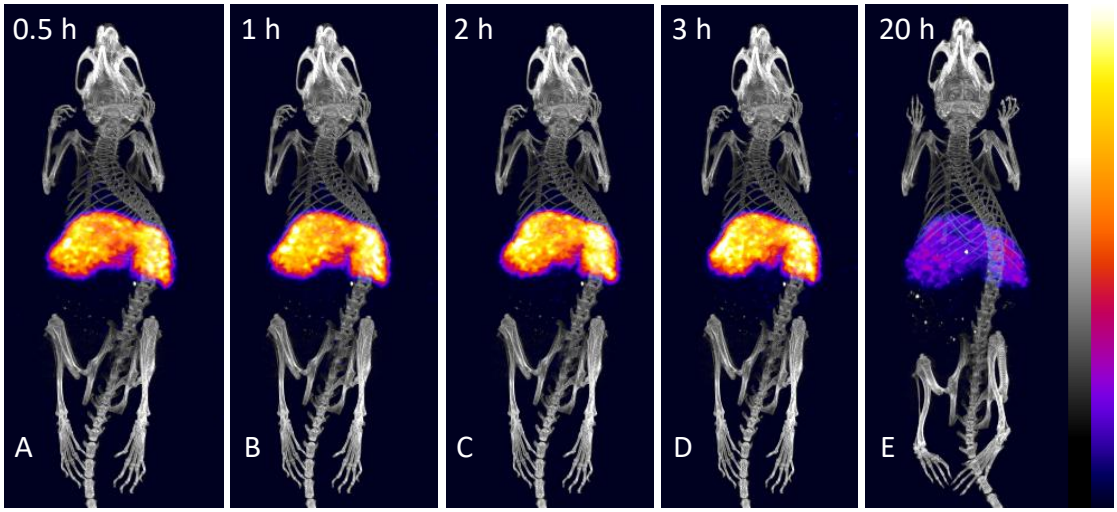

Figure 3.20 PET scans of a BALB/c mouse administered with 1-2 MBq $[^{64}Cu(\mathbf{3.18})_2]^+$.

When a mouse was injected with unbound ^{64}Cu, a high proportion of activity is associated with the liver; however, there is also a significant amount in the kidneys, bladder and intestines, the distribution of which varies between timepoints 1 and 20 h. If tracer $[^{64}Cu(\mathbf{3.18})_2]^+$ were to degrade over time *in vivo,* it would be expected that the distribution of activity on the PET images would look similar to those of free ^{64}Cu. As shown in Figure 3.21-3.23, the activity for the mouse imaged with tracer $[^{64}Cu(\mathbf{3.18})_2]^+$ stays associated with the liver suggesting it maintains good serum stability over time.

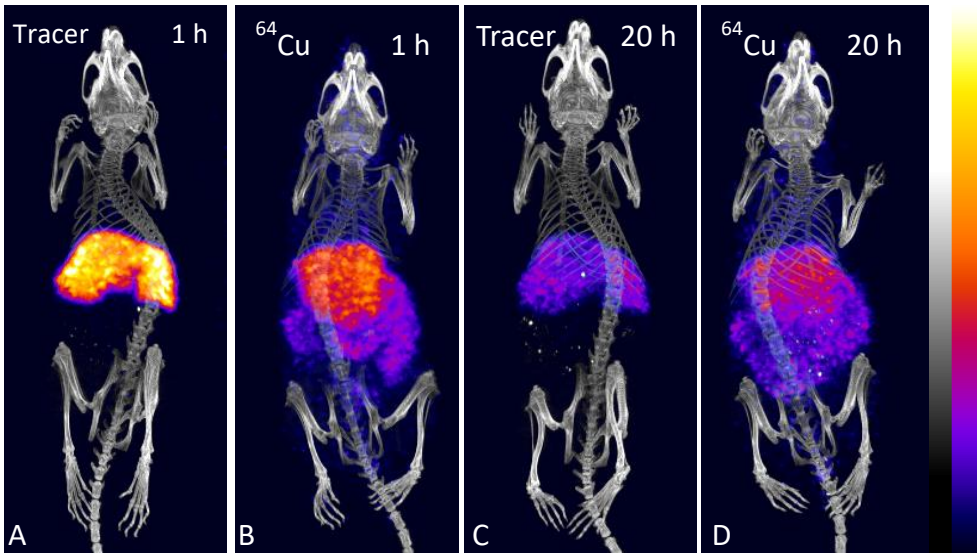

Figure 3.21 PET scans of BALB/c mice administered with tracer ([^{64}Cu(**3.18**)$_2$]$^+$) at 1 h (A) and 20 h (C) and unbound ^{64}Cu at 1 h (B) and 20 h (D).

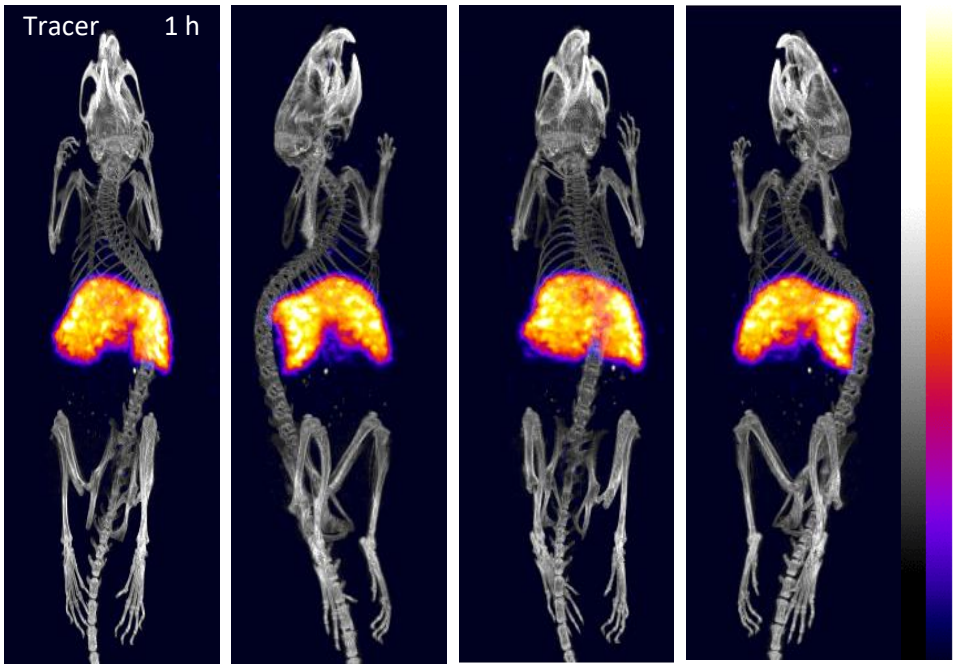

Figure 3.22 PET scans of BALB/c mice administered with tracer ([^{64}Cu(**3.18**)$_2$]$^+$) at 1 h (rotated image).

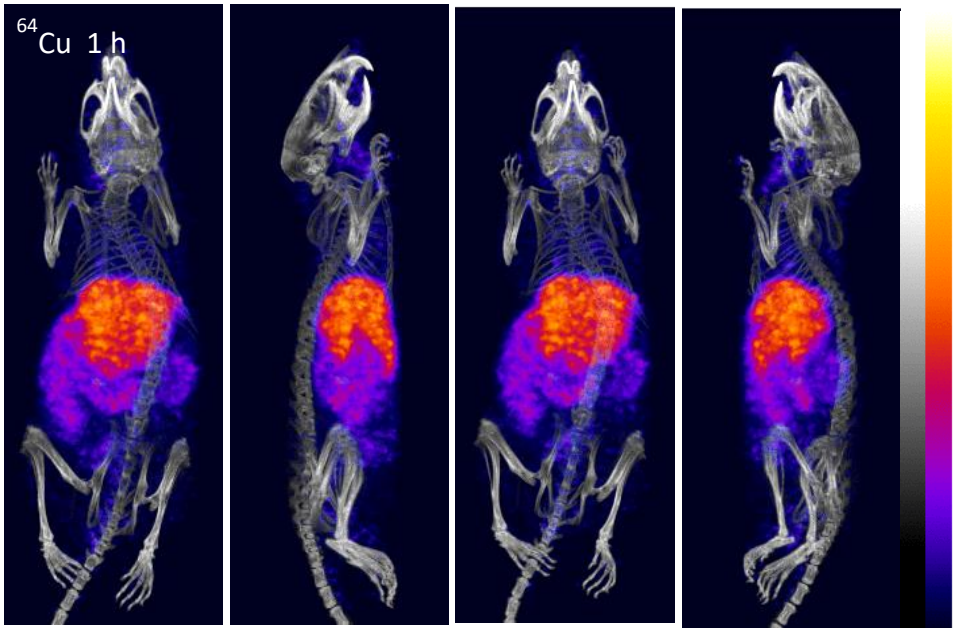

Figure 3.23 PET scans of BALB/c mice administered with free ^{64}Cu at 1 h (rotated image).

3.7 Conclusions and future work

It has been shown that the base-mediated route developed to synthesise dicyclohexylphosphino anhydride ligand **3.2** can be applied to the preparation of the analogous diphenylphosphino ligand **3.1** but the synthesis of **3.6** needs further optimisation. The synthesis of a derivative with ether chains attached at phosphorus has been attempted (Scheme 3.9).

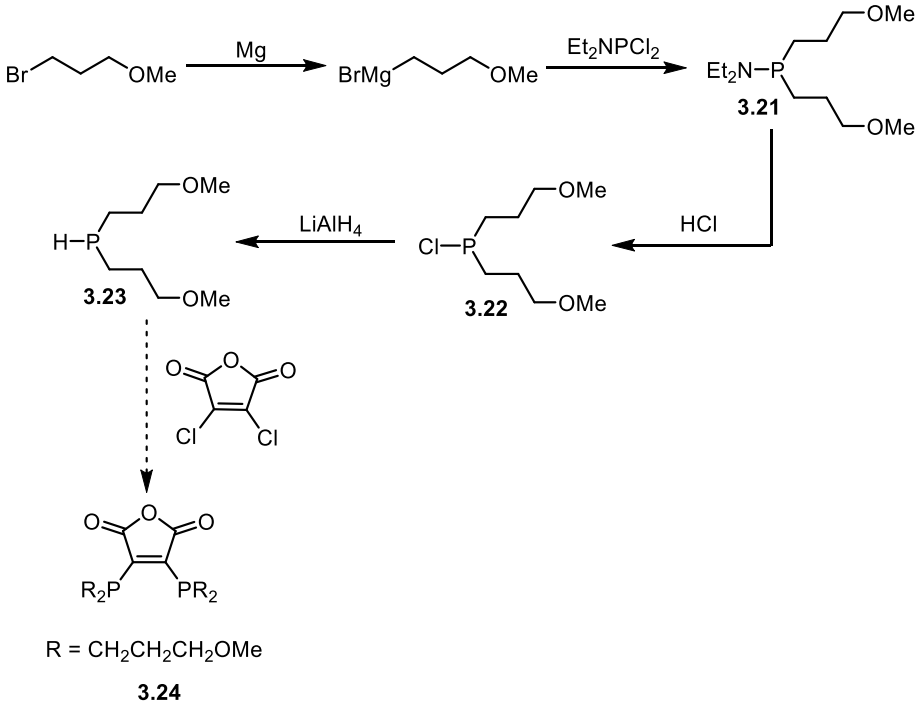

Scheme 3.9 Synthesis of **3.24**.

The novel secondary phosphine **3.23** has been fully characterised (see Chapter 6) but **3.24** has been synthesised with some impurities on a small scale only and therefore needs further work (Figure 3.24).

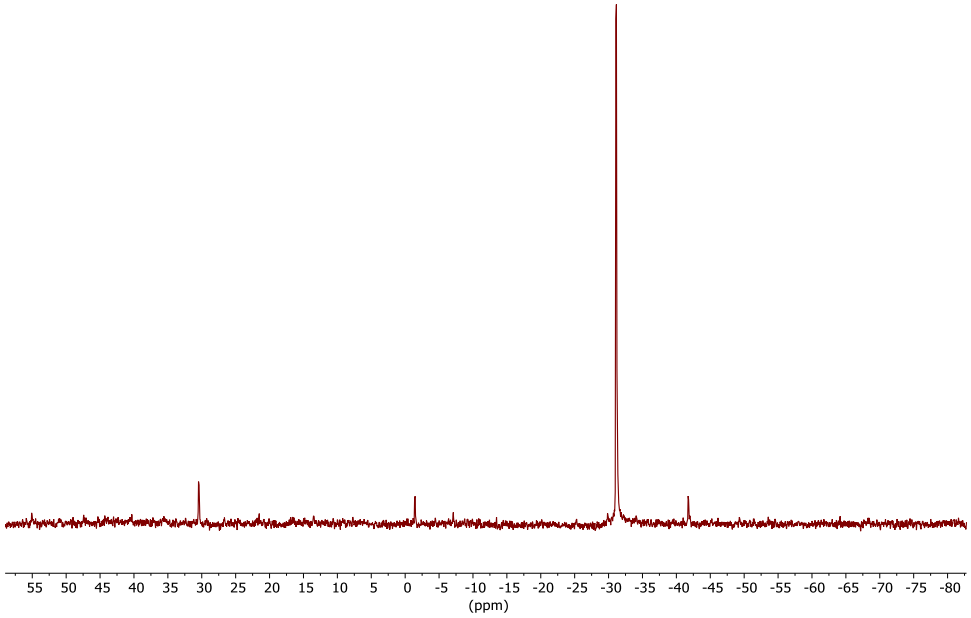

Figure 3.24 *In situ* ^{31}P{^{1}H} NMR (162 MHz, THF) spectrum of the synthesis of **3.24**. The major peak is assigned to **3.24**.

Complexes of **3.2** with Cu, Ag and Au have been prepared with **3.9** and **3.15** and characterised by X-ray crystallography. From mass spectrometry and NMR spectroscopy data it is concluded that multiple species for both Cu and Ag complexes are formed which are likely in equilibrium with each other. Low temperature NMR spectroscopy would be useful to decipher the product mixture.

The bioconjugation and subsequent radiolabelling of **3.2** with ^{64}Cu was performed to give tracer $[^{64}Cu(\mathbf{3.18})_2]^+$. Log$D_{7.4}$ data, supported by biodistribution studies and PET images, indicated that the tracer is cleared via the liver within 1 h. This contrasts with Log$D_{7.4}$ data for radiolabelled **3.20** which was shown to be more hydrophilic and therefore likely to clear via the kidneys and bladder.

Based on the differences observed between diphenylphosphino ligand **3.1** and dicyclohexylphosphino ligand **3.2**, it would be of interest to modify the substituents at phosphorus to evaluate variations in biodistribution. In addition, changing the bioconjugated peptide on tracer $[^{64}Cu(\mathbf{3.18})_2]^+$ from cRGDfK to PSMA (prostate-specific membrane antigen) would modify the target from $\alpha_v\beta_3$ integrin receptors, often overexpressed in the tumours, to receptors found on the prostate.[41,42]

3.8 References

1 M. S. Balakrishna, Ed., *Copper(I) Chemistry of Phosphines, Functionalised Phosphines and Phosphorus Heterocycles*, Elsevier Inc., 2019.

2 X. Yu, W. Fan, G. Wang, S. Lin, Z. Li, M. Liu, Y. Yang, X. Xin and Q. Jin, *Polyhedron*, 2019, **157**, 301–309.

3 T. H. Huang, M. H. Zhang, J. Yan, H. Yang, S. X. Hao and C. L. Zhang, *Inorg. Chim. Acta*, 2015, **437**, 47–53.

4 S. Roy, T. K. Mondal, P. Mitra and C. Sinha, *Polyhedron*, 2013, **51**, 27–40.

5 B. P. Nell, C. D. Swor, E. A. Henle, L. N. Zakharov, N. I. Rinehart, A. Nathan and D. R. Tyler, *Dalton Trans.*, 2016, **45**, 8253–8264.

6 A. Kaeser, O. Moudam, G. Accorsi, I. Séguy, J. Navarro, A. Belbakra, C. Duhayon, N. Armaroli, B. Delavaux-Nicot and J. F. Nierengarten, *Eur. J. Inorg. Chem.*, 2014, 1345–1355.

7 C. Di Nicola, C. Pettinari, M. Ricciutelli, B. W. Skelton, N. Somers and A. H. White, *Inorg. Chim. Acta*, 2005, **358**, 4003–4008.

8 J. S. Lewis, S. L. Heath, A. K. Powell and P. J. Blower, *J. Chem. Soc., Dalton Trans.*, 1997, 855–861.

9 J. S. Lewis, J. Zweit, J. L. J. Dearling, B. C. Rooneya and P. J. Blower, *Chem. Commun.*, 1996, 1093–1094.

10 F. Mao, S. K. Sur and D. R. Tyler, *J. Am. Chem. Soc.*, 1989, **111**, 7627–7628.

11 F. Mao, C. E. Philbin, T. J. R. Weakley and D. R. Tyler, *Organometallics*, 1990, **9**, 1510–1516.

12 N. W. Duffy, R. R. Nelson, M. G. Richmond, A. L. Rieger, P. H. Rieger, B. H. Robinson, D. R. Tyler, J. C. Wang and K. Yang, *Inorg. Chem.*, 1998, **37**, 4849–4856.

13 S. G. Bott, K. Yang, K. A. Talafuse and M. G. Richmond, *Organometallics*, 2003, **22**, 1383–1390.

14 D. Fenske and W. Bensmann, *Z. Naturforsch., B,* 1985, **40**, 1093–1096.

15 A. Kinting and C. Döbler, *J. Organomet. Chem.*, 1989, **370**, 351–356.

16 D. Fenske and W. Bensmann, *Z. Naturforsch., B,*, 1984, **39**, 1819–1822.

17 V. J. W. Gilje, W. S. Sheldrick, N. Weferling and R. Schmutzler, *Angew. Chemie*, 1982, **94**, 393–394.

18 S. J. Berners-Price, R. J. Bowen, M. A. Fernandes, M. Layh, W. J. Lesueur, S. Mahepal, M. M. Mtotywa, R. E. Sue and C. E. J. Van Rensburg, *Inorg. Chim. Acta*, 2005, **358**, 4237–4246.

19 K. Yang, S. G. Bott and M. G. Richmond, *Organometallics*, 1995, **14**, 2387–2394.

20 S. G. Bott, K. Yang and M. G. Richmond, *J. Organomet. Chem.*, 2004, **689**, 791–800.

21 S. Ghosh, N. Hollingsworth, M. Warren, D. A. Hrovat, M. G. Richmond and G. Hogarth, *Dalton Trans.*, 2019, **48**, 6051–6060.

22 R. Meyer, D. M. Schut, K. J. Keana and D. R. Tyler, *Inorg. Chim. Acta*, 1995, **240**, 405–412.

23 D. R. Tyler, *Acc. Chem. Res.*, 1991, **24**, 325–331.

24 K. Yang, J. M. Smith, S. G. Bott and M. G. Richmond, *Organometallics*, 1993, **12**, 4779–4787.

25 K. Yang, J. A. Martin, S. G. Bott and M. G. Richmond, *Organometallics*, 1996, **15**, 2227–2236.

26 J. Smith, S. Bott and M. Richmond, *Inorg. Chim. Acta*, 1993, **212**, 1–3.

27 S. G. Bott, K. Yang and M. G. Richmond, *Polyhedron*, 2007, **26**, 3737–3742.

28 F. Mao, D. R. Tyler and D. Keszler, *J. Am. Chem. Soc.*, 1989, **111**, 130–134.

29 S. G. Bott, K. Yang, J. C. Wang and M. G. Richmond, *Inorg. Chem.*, 2000, **39**, 6051–6055.

30 Y. Si, K. Charreteur, J. F. Capon, F. Gloaguen, F. Y. Pétillon, P. Schollhammer and J. Talarmin, *J. Inorg. Biochem.*, 2010, **104**, 1038–1042.

31 WO 2005/049629 A1, 2005.

32 J. Holz, A. Monsees, H. Jiao, J. You, I. V. Komarov, C. Fischer, K. Drauz and A. Borner, *J. Org. Chem.*, 2003, **68**, 1701–1707.

33 J. Holz, O. Zayas, H. Jiao, W. Baumann, A. Spannenberg, A. Monsees, T. H. Riermeier, J. Almena, R. Kadyrov and A. Börner, *Chem. Eur. J.*, 2006, **12**, 5001–5013.

34 F. Mae, D. R. Tyler and D. A. Keszler, *J. Am. Chem. Soc.*, 1989, **11**, 4434–4436.

35 Y. Wang, A. Eichhöfer, F. Weigend, D. Fenske and O. Fuhr, *Dalton Trans.*, 2019, **48**, 6863–6871.

36 A. J. North, J. A. Karas, M. T. Ma, P. J. Blower, U. Ackermann, J. M. White and P. S. Donnelly, *Inorg. Chem.*, 2017, **56**, 9725–9741.

37 M. T. Ma, O. C. Neels, D. Denoyer, P. Roselt, J. A. Karas, D. B. Scanlon, J. M. White, R. J. Hicks and P. S. Donnelly, *Bioconjug. Chem.*, 2011, **22**, 2093–2103.

38 Y. Kwon, *Handbook of Essential Pharmacokinetics, Pharmacodynamics and Drug Metabolism for Industrial Scientists*, Springer, 2002.

39 D. Kapusta, in *xPharm: The Comprehensive Pharmacology Reference*, Elsevier Inc., 2007, pp. 1–2.

40 S. P. Elliott and B. S. Maleab, *World J Urol.*, 2011, **29**, 35–41.

41 C. Imberti, Y. L. Chen, C. A. Foley, M. T. Ma, B. M. Paterson, Y. Wang, J. D. Young, R. C. Hider and P. J. Blower, *Dalton Trans.*, 2019, **48**, 4299–4313.

42 S. S. Chang, *Rev. Urol.*, 2004, **6**, 13–18.

Part 2

Pt(0)-catalysed hydrophosphination of activated alkenes to produce diphosphines

Chapter 4

Introduction

This thesis has been written in two main parts. The work detailed in this second half focusses on Pt(0)-catalysed hydrophosphination and this introduction will review various examples of transition metal catalysed hydrophosphination pertinent to our study. For comprehensive reviews of the topic see reports by Rosenberg,[1] Glueck[2] and Waterman.[3]

The hydrophosphination of terminal alkenes by R_nPH_{3-n} is an atom-efficient route to tertiary phosphines (Scheme 4.1).

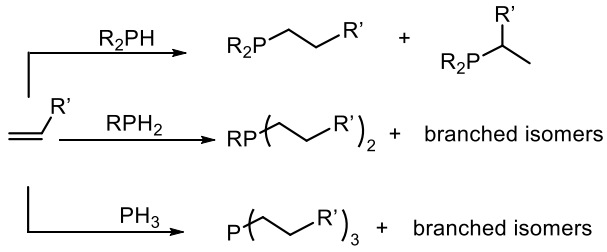

Scheme 4.1 Anti-Markovnikov and Markovnikov hydrophosphination of alkenes (R, R' = alkyl or aryl).

Radically-initiated hydrophosphination generally proceeds with high regioselectivity and has been widely applied,[4,5] including in large scale commercial production of alkyl phosphines such as trioctylphosphine[6] and in the synthesis of tetrofosmin, the ligand for the imaging agent, *Myoview* (Scheme 4.2).[7] The reaction may also be catalysed by alkyl lithium reagents[8–10] or base[11,12] though these methods often have low selectivity, efficiency and produce by-products. Routes catalysed by transition metals, first reported by Pringle *et al.*[13], offer greater regio- and stereoselectivity and have been the focus of global research for over 20 years.[1,3,14]

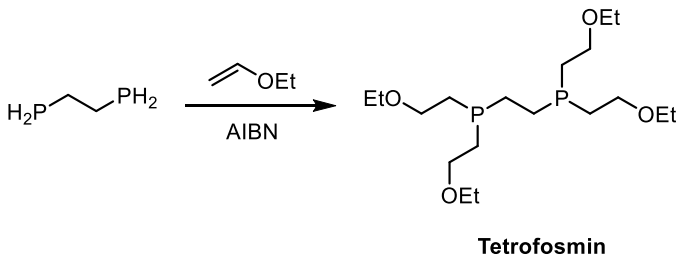

Scheme 4.2 Synthesis of Tetrofosmin; the ligand for imaging agent *Myoview*.

Depending on the metal catalyst and the substrate, hydrophosphination may occur via different mechanisms.[2] In hydrophosphination reactions catalysed by electron-deficient metals, the insertion of the alkene into the metal-P bond is generally critical to P-C bond formation. Conversely, for many electron-rich catalysts, a Michael-type addition of the

highly nucleophilic coordinated phosphido to the activated alkene is important. Therefore there is a dichotomy between inner-sphere and outer-sphere reactivity for such P-C bond forming reactions (Scheme 4.3).[1]

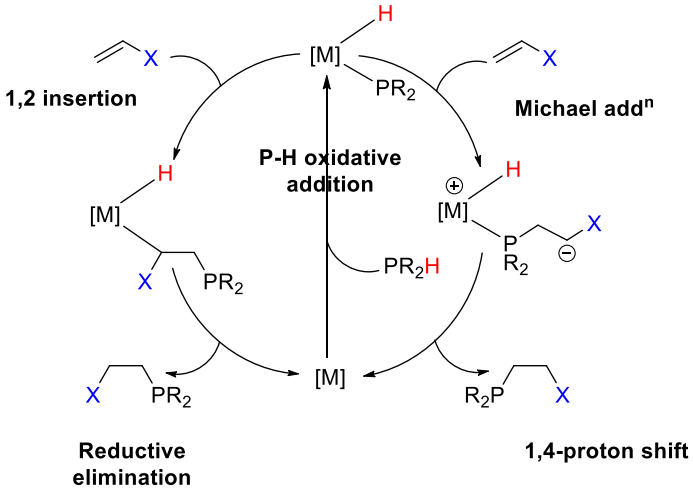

Scheme 4.3 Inner sphere hydrophosphination mechanism (left) and outer-sphere mechanism (right).

1.1 Electron-rich metal catalysts

1.1.1 Platinum(0) catalysts

Alkene hydrophosphination catalysed by transition metal complexes was first reported in the 1990s by Pringle *et al.* who showed that Michael addition reactions were catalysed with high chemoselectivity by Pt(0) complexes (Scheme 4.4).[13,15] One intriguing aspect of this catalysis is that the phosphines coordinated to the Pt(0) are also the product phosphines, i.e. this is an example of an abiological, catalytic, self-replicating system.[16–19]

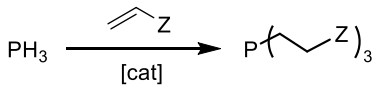

[cat] = $Pt(PCH_2CH_2Z)_3$, Z = CN or CO_2Et

Scheme 4.4 Pt(0)-catalysed hydrophosphination by PH_3.

Studies by Glueck *et al.* focussed on the mechanism of Pt(0)-catalysed alkene hydrophosphination by monophosphines.[20–23] This topic is discussed further in Chapter 5.

Glueck *et al.* also showed that asymmetric hydrophosphination can be achieved using a Pt(0)-Duphos complex to synthesise chiral monophosphines with control of stereochemistry at phosphorus or carbon centres (Scheme 4.5).[24]

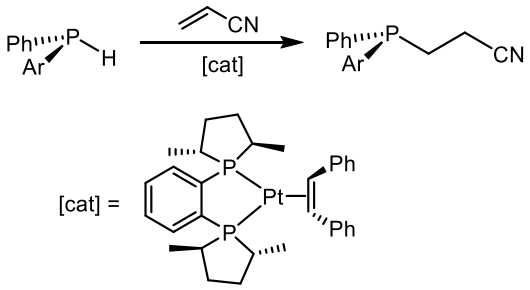

Scheme 4.5 Asymmetric Pt(0)-catalysed hydrophosphination with Pt(0)-Duphos.

1.1.2 Ruthenium catalysts

The role of ruthenium phosphido complexes in inner-sphere vs. outer-sphere mechanisms for the hydrophosphination of alkenes has been investigated by Morris *et al.*[25] and Rosenberg *et al.* (Scheme 4.6).[26]

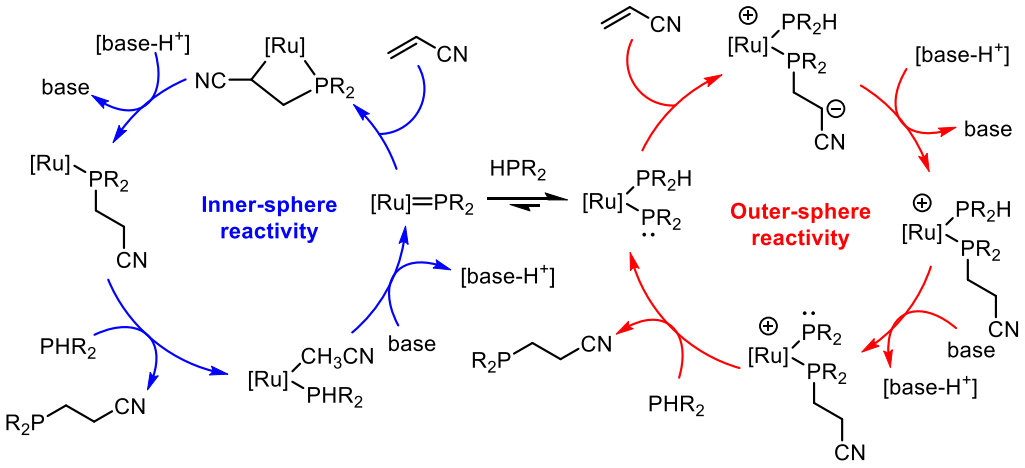

Scheme 4.6 Hypothesised mechanisms for Ru-catalysed hydrophosphination.

Rosenberg *et al.* investigated the involvement of inner-sphere reactivity when a cycloaddition of an alkene occurs to a Ru=P bond, following a deprotonation of a coordinated secondary phosphine by an external base. The conjugate acid then protonates the metallacycle to complete the hydrophosphination cycle. In an assessment of a series of ruthenium indenyl complexes, an alternative outer-sphere cycle was suggested which involves a zwitterionic intermediate due to nucleophilic attack of the phosphide ligand on the alkene. In this scenario the proton source acts to quench the carbanion rather than

acting as a proton shuttle as in the inner-sphere mechanism. In Pt(0)-catalysed hydrophosphination Glueck showed that added ^{t}BuOH or H_2O could transfer a proton to a similar carbanion intermediate,[22] while Morris suggested free secondary phosphine can play this role in the hydrophosphination of acrylonitriles with a [Cp*Ru] phosphide complex (Scheme 4.7).[25]

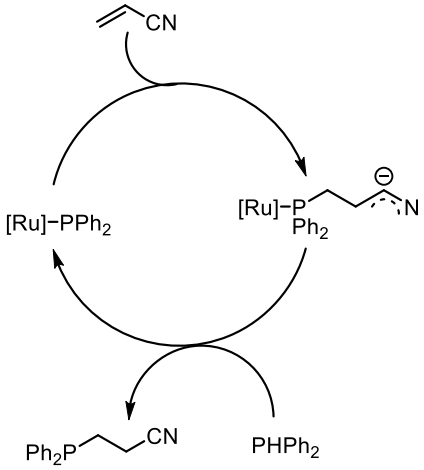

Scheme 4.7 Ru-catalysed hydrophosphination mechanism proposed by Morris.[25]

1.1.3 Rhodium catalysts

A crucial intermediate in late transition metal-catalysed hydrophosphination is the terminal phosphide (M-PR_2). In 2015 Tejel *et al.* isolated phosphido rhodium complexes that result from the oxidative addition of a secondary phosphine to a Rh metal centre (Scheme 4.8).[27] The structures were supported by DFT calculations and X-ray crystallography.

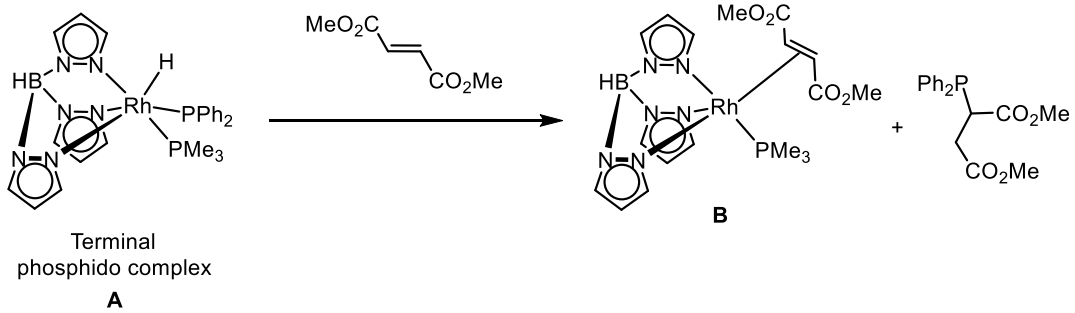

Scheme 4.8 Rh-catalysed hydrophosphination of dimethyl fumarate.

After testing the nucleophilicity of the terminal phosphido group (**A**) by reaction with dimethyl fumarate, Tejel and co-workers concluded that, though an outer-sphere mechanism for the hydrophosphination reaction was plausible, the possibility of an inner-

sphere mechanism could not be eliminated. Through independent reactions of $[Rh(Tp)(PMe_3)_2]$ (Tp = hydridotris(pyrazolyl)borate) with dimethyl fumarate, it was confirmed that complex **B** was formed cleanly and was also the only Rh-species observed at the end of the hydrophosphination catalysis. In addition, the dimethyl fumarate in complex **B** is replaced by $PHPh_2$ to regenerate complex **A**.

1.1.4 Palladium catalysts

Asymmetric hydrophosphination catalysed by palladium complexes with activated alkenes has been reported by Leung and Pullarkat *et al* (Scheme 4.9).[28–30]

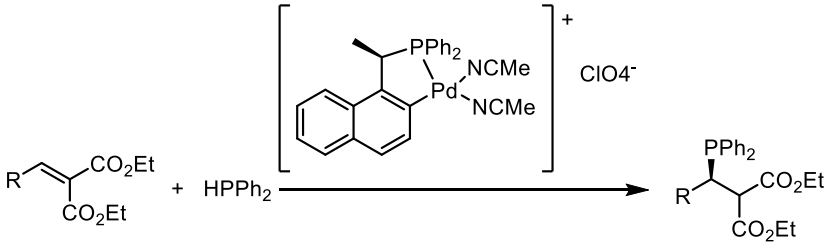

Scheme 4.9 Pd-catalysed asymmetric hydrophosphination.

More recently, Wang *et al.* have studied Pd-catalysed asymmetric hydrophosphination of substrates containing an unactivated double bond (Scheme 4.10). [31]

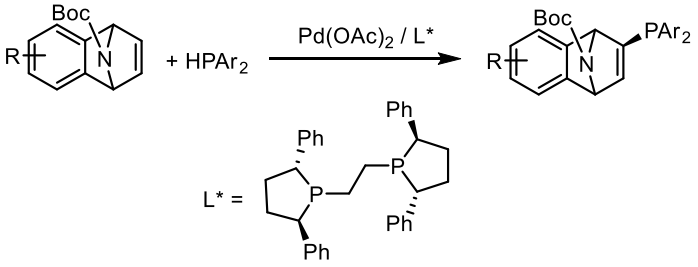

Scheme 4.10 Pd-catalysed asymmetric hydrophosphination of a non-activated double bond.

Tertiary phosphines were prepared in high yields (>99%) and enantioselectivities (>99%) with the products then employed as phosphine ligands for further metal-catalysed enantioselective transformations.

1.1.5 Nickel catalysts

Nickel complexes have been employed as hydrophosphination catalysts.[32–35] In 2004 Togni and co-workers developed an enantioselective Ni(II)-catalysed hydrophosphination of methacrylonitrile (Scheme 4.11).[36]

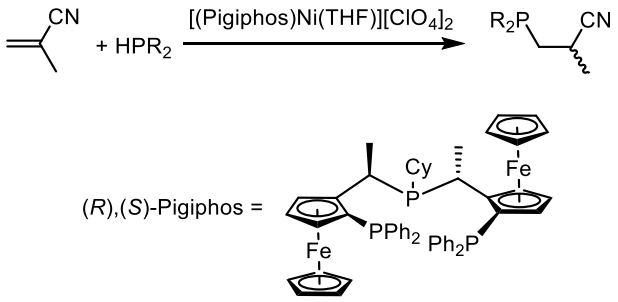

Scheme 4.11 Ni(II)-catalysed hydrophosphination of methacrylonitrile.

When methacrylonitrile is the solvent and 10 mol% of the Ni(II) catalyst is used, the reaction is complete in 5 h to give the anti-Markovnikov addition product. It was found that conversion and enantioselectivity were increased by use of bulky, nucleophilic phosphine substrates, suggesting that the mechanism of the reaction involves coordination of methacrylonitrile to Ni followed by nucleophilic attack by the secondary phosphine.

1.2 Electrophilic metal catalysts

Electrophilic metal complexes have proven to be effective hydrophosphination catalysts. The accepted mechanism for lanthanoid and alkaline earth metal catalysts is insertion followed by protonolysis as oppose to a Michael addition pathway (Scheme 4.3).[2] This inner-sphere reactivity may be because the phosphido ligands do not exhibit the transition metal gauche effect (dπ-pπ repulsions) which is present in ligands at electron-poor metals. In coordinatively saturated complexes where there is an approximately tetrahedral phosphorus that contains a non-bonding lone pair, the M-P bond is arranged in such a way to maximise the distance between the metal-based HOMO and non-bonding phosphido lone pair. This results in a longer M-P bond and a P lone pair with increased p character and greater nucleophilicity that can perform Michael type addition reactions (Figure 4.1).

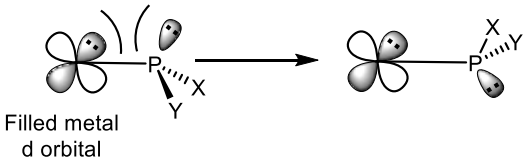

Figure 4.1 Transition metal gauche effect.

1.2.1 Organolanthanoid catalysts

Marks *et al.* reported the use of organolanthanoid compounds of the type $Cp^*_2Ln\{CH(TMS)_2\}$ (Ln = La, Sm, Y, Lu) for intramolecular hydrophosphinations to give cyclic phosphines and have studied the mechanism (Scheme 4.12).[37–39] Following initial protonolysis and activation of the lanthanocene precatalyst (step i), an alkene is inserted into the resulting lanthanide-phosphido bond (step ii). Subsequent Ln-C protonloysis forms the product with a new P-C bond and completes the cycle (step iii).

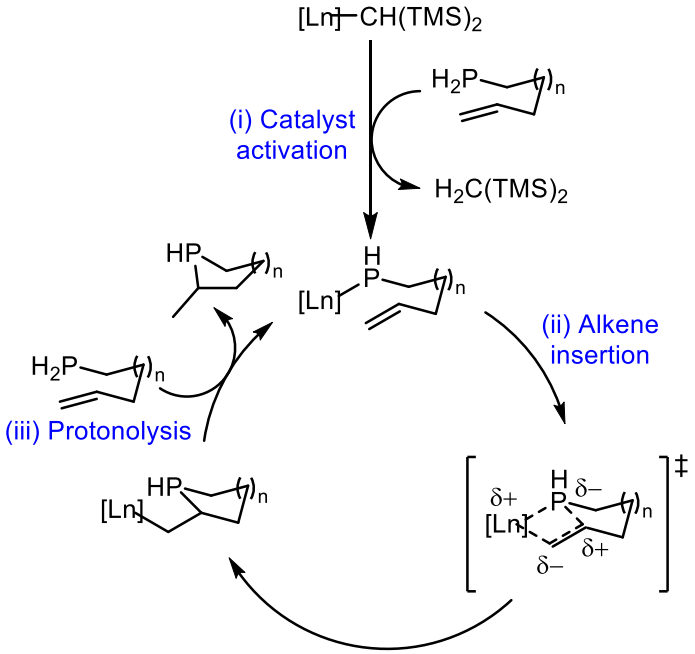

Scheme 4.12 Intramolecular hydrophosphination to give a cyclic phosphine.

It was determined that the insertion of the alkene into the Ln-P bond is the turnover-limiting step in the catalysis. It was also shown that medium-sized metal ions lead to a higher turnover frequency for phosphphinoalkenes and diastereoselectivity varied with substrate, lanthanide ion and ancillary ligands.

1.2.2 Calcium catalysts

Calcium(II) catalysts have attracted attention due to the low cost and low environmental impact of the element,[40] and have been successfully applied in hydroamination[41,42] and hydrosilylation[43] reactions. In 2007 Hill *et al.* reported the hydrophosphination of moderately activated alkenes, dienes and alkynes with diphenylphosphine catalysed by Ca(II) complex **C** (Scheme 4.13).

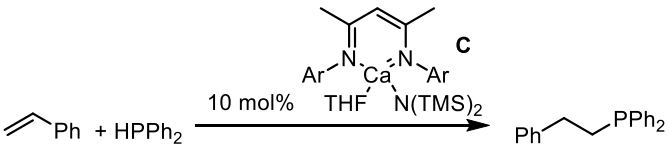

Scheme 4.13 Ca-catalysed hydrophosphination of styrene.

A small substrate scope was carried out with styrene, isoprene, 1,3-cyclohexadiene and diphenylacetylene and all gave anti-Markovnikov addition products, though more hindered substrates did not readily undergo hydrophosphination so required higher catalyst loadings.

1.2.3 Zirconium catalysts

Waterman *et al.* have studied triamidoamine-supported zirconium compounds such as **D**, as catalysts for the hydrophosphination of terminal alkynes, carbodiimides and unactivated alkenes (Scheme 4.14).[44–46]

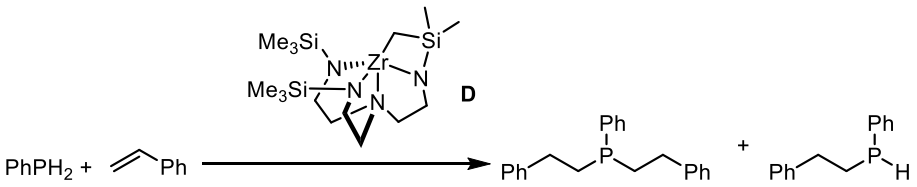

Scheme 4.14 Triamidoamine-supported zirconium catalysed hydrophosphination.

Using catalyst **D**, Waterman and co-workers have also shown that photolysis enhances catalytic activity.[47,48] Quantitative conversions of alkenes to secondary phosphines were achieved within 20 min under UV or visible irradiation with catalyst **D** and a wider range of unactivated alkene substrates were accessible under photolytic conditions compared to when the reaction is not irradiated. For example, the hydrophosphination of 1-hexene by diphenylphosphine catalysed by **D** at 60 °C gives 47% conversion after 4 days. Under photolysis at 253.7 nm at room temperature the reaction is performed in 1 day and gives almost 90% conversion. It was hypothesised that the improved catalytic

hydrophosphination was due to the photochemistry of a phosphido-Zr intermediate (**E**) which could be excited once irradiated (Figure 4.2).

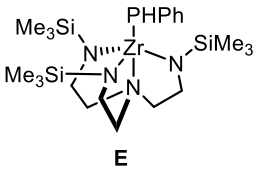

E

Figure 4.2 Phosphido-Zr intermediate **E**.

In collaboration with Higham, Waterman *et al.* have also studied zirconium-catalysed hydrophosphination using air-stable primary phosphines (Scheme 4.15).[49,50]

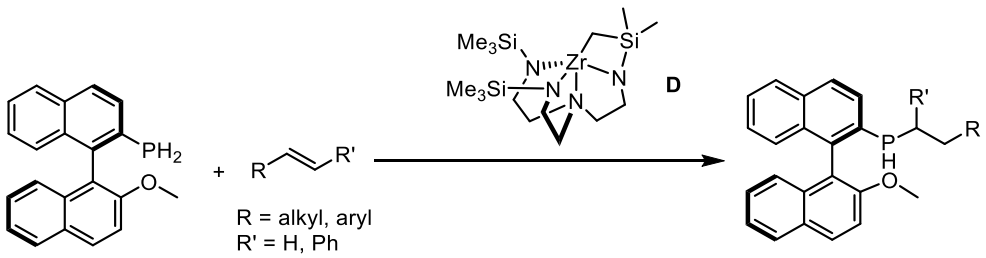

Scheme 4.15 Zr-catalysed hydrophosphination with an air stable primary phosphine.

A range of unsaturated substrates was tested including styrene, Michael acceptors and imines to give the anti-Markovnikov products as mixtures of diastereomers in modest yields. When the chiral phosphine shown in Scheme 4.15 was used, the turnover frequency was lower than when $PhPH_2$ was used which is possibly due to the larger steric bulk of the chiral substrate

1.2.4 Iron catalysts

The hydrophosphination of unactivated alkenes and alkynes using iron catalysts has been reported by Webster *et al.*[51–54] They have also investigated tuneable regioselectivity using an iron(II) β-diketiminate precatalyst to give Markovnikov or anti-Markovnikov products based on the reaction solvent (Scheme 4.16).[55]

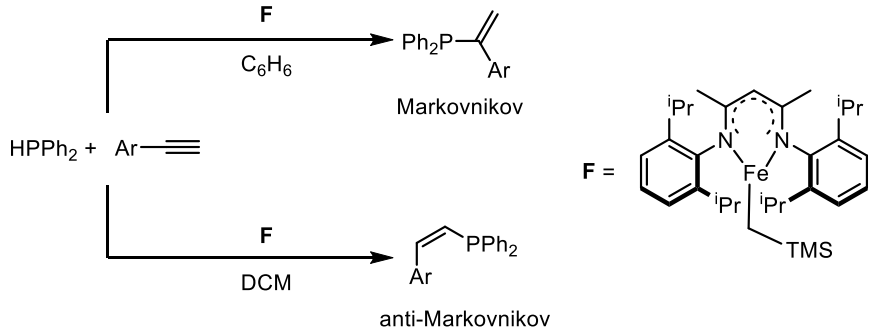

Scheme 4.16 Tuneable regioselectivity of Fe-catalysed hydrophosphination based on solvent choice.

Reaction of diphenylphosphine with phenyl acetylene in the presence of catalyst **F** in C_6H_6 (Scheme 4.16) led to a Markovnikov product selectively (9:1 Markovnikov:anti-Markovnikov). Conversely when the same reaction was performed in DCM the anti-Markovnikov product was observed, though more forcing conditions were required (3 h at 50 °C vs. 24 h at 70 °C). The reaction was applicable to a wide range of aryl alkynes with many obtained in high yields including alkynes with strongly electron donating as well as withdrawing groups. Remarkably, 4-aminophenyl acetylene generated product in high yield despite its free functionality available for further transformations. Substrates substituted at the ortho position were not suitable, for example for 2-amino-phenylactylenes and 2-chloro-phenylacetylenes no side reactions occurred therefore it was concluded that the lack of reaction was due to steric bulk and/or competing heteroatom coordination.

It was hypothesised that the divergent reactivity in different solvents is due to oxidation state and the presence of radicals. In the Markovnikov-selective reaction, Fe(II) is implicated and the reaction is quenched by the addition of a radical clock. For the reaction that yields anti-Markovnikov products performed in DCM, it is believed that halide abstraction from the reaction solvent occurs generating an Fe(III) centre. In this case, a radical clock had no effect suggesting that radicals are not involved in C-P bond formation.

1.3 Objectives

The aims of the projects described in part 2 of this thesis were to:

- synthesise novel diphosphine ligands via Pt(0)-catalysed hydrophosphination
  - investigate the substrate scope of the reaction including variation of the alkene and diphosphine reactants
  - investigate catalyst loading and the rate of the catalysis

- probe the mechanism of Pt(0)-catalysed hydrophosphination by a diphosphine by evaluating the Pt(0) coordination chemistry and utilising deuterium-labelling experiments in order to propose a catalytic cycle

1.4 References

1 L. Rosenberg, *ACS Catal.*, 2013, **3**, 2845–2855.

2 D. S. Glueck, in *Topics in Organometallic Chemistry*, Heidelberg: Springer, 2010, pp. 65–100.

3 A. C. Bange and R. Waterman, *Chem. Eur. J.*, 2016, **22**, 12598–12605.

4 B. A. Trofimov, S. N. Arbuzova and N. K. Gusarova, *Russ. Chem. Rev.*, 1999, **68**, 215–227.

5 S. N. Arbuzova, N. K. Gusarova and B. A. Trofimov, *ARKIVOC*, 2006, 12–36.

6 P. A. T. Hoye, J. W. Ellis, GB. Pat. GB2258654, 1993.

7 GE Healthcare Ltd., US. Pat. US5045302, 1989.

8 G. Fries, J. Wolf, K. Ilg, B. Walfort, D. Stalke and H. Werner, *Dalt. Trans.*, 2004, 1873–1881.

9 A. Baber, J. G. De Vries, A. G. Orpen, G. Pringle and K. Von Der Luehe, *Dalt. Trans.*, 2006, 4821–4828.

10 R. B. King and W. F. Masler, *J. Am. Chem. Soc.*, 1977, **99**, 4001–4008.

11 C. P. Casey, E. L. Paulsen, E. W. Beuttenmueller, B. R. Proft, B. A. Matter and D. R. Powell, *J. Am. Chem. Soc.*, 1999, **121**, 63–70.

12 N. Kapoor, D. D. Pathak, G. Gaur and M. Kutty, *J. Organomet. Chem.*, 1984, **276**, 167–170.

13 P. G. Pringle and M. B. Smith, *J. Chem. Soc. Chem. Commun.*, 1990, 1701–1702.

14 D. S. Glueck, *Dalt. Trans.*, 2008, 5276.

15 E. Costa, P. G. Pringle, B. Smith and K. Worboys, *J. Chem. Soc., Dalt. Trans.*, 1997, 4277–4282.

16 G. Clixby and L. Twyman, *Org. Biomol. Chem.*, 2016, **14**, 4170–4184.

17 K. Muñiz, *Adv. Synth. Catal.*, 2005, **347**, 275–281.

18 D. E. Bergbreiter, Y. Liu, S. Furyk and B. L. Case, *Teterahedron Lett.*, 1998, **39**, 8799–8802.

19 P. Thordarson, A. Marquis and M. J. Crossley, *Org. Biomol. Chem.*, 2003, **1**, 1216–1225.

20 D. K. Wicht, I. V. Kourkine, B. M. Lew, J. M. Nthenge and D. S. Glueck, *J. Am. Chem. Soc.*, 1997, **119**, 5039–5040.

21 D. K. Wicht, I. V. Kourkine, I. Kovacik, D. S. Glueck, T. E. Concolino, G. P. A. Yap, C. D. Incarvito and A. L. Rheingold, *Organometallics*, 1999, **18**, 5381–5394.

22 C. Scriban, I. Kovacik and D. S. Glueck, *Organometallics*, 2005, **24**, 4871–4874.

23 I. Kovacik, C. Scriban and D. S. Glueck, *Organometallics*, 2006, **25**, 536–539.

24 I. Kovacik, D. K. Wicht, N. S. Grewal, D. S. Glueck, C. D. Incarvito, I. A. Guzei and A. L. Rheingold, *Organometallics*, 2000, **19**, 950–953.

25 P. E. Sues, A. J. Lough and R. H. Morris, *J. Am. Chem. Soc.*, 2014, **136**, 4746–4760.

26 R. G. Belli, K. M. E. Burton, S. A. Rufh, R. McDonald and L. Rosenberg, *Organometallics*, 2015, **34**, 5637–5646.

27 A. M. Geer, Á. L. Serrano, B. De Bruin, M. A. Ciriano and C. Tejel, *Angew. Chemie - Int. Ed.*, 2015, **54**, 472–475.

28 C. Xu, G. Jun Hao Kennard, F. Hennersdorf, Y. Li, S. A. Pullarkat and P. H. Leung, *Organometallics*, 2012, **31**, 3022–3026.

29 X. Yang, Y. Jia, W. S. Tay, Y. Li, S. A. Pullarkat and P. Leung, *Dalt. Trans.*, 2016, 13449–13455.

30 S. A. Pullarkat, *Synth.*, 2016, **48**, 493–503.

31 Z. Lu, H. Zhang, Z. Yang, N. Ding, L. Meng and J. Wang, *ACS Catal.*, 2019, **9**, 1457–1463.

32 P. A. T. Hoye, P. G. Pringle, M. B. Smith and K. Worboys, *J. Chem. Soc. Dalt. Trans.*, 1993, 269–274.

33 Y. S. Ganushevich, V. A. Miluykov, F. M. Polyancev, S. K. Latypov, P. Lönnecke, E. Hey-Hawkins, D. G. Yakhvarov and O. G. Sinyashin, *Organometallics*, 2013, **32**, 3914–3919.

34 M. A. Kazankova, I. V Efimova, A. N. Kochetkov, V. V Afanas and I. P. Beletskaya, 2002, **38**, 1465–1474.

35 M. A. Kazankova, M. O. Shulyupin, A. A. Borisenko and I. P. Beletskaya, *Russ. J. Org. Chem.*, 2002, **38**, 1479–1484.

36 A. D. Sadow, I. Haller, L. Fadini and A. Togni, *J. Am. Chem. Soc.*, 2004, **126**, 14704–

14705.

37 M. R. Douglass and T. J. Marks, *J. Am. Chem. Soc.*, 2000, 1824–1825.

38 M. R. Douglass, C. L. Stern and T. J. Marks, *J. Am. Chem. Soc.*, 2001, **123**, 10221–10238.

39 A. Motta, I. L. Fragala, T. J. Marks and S. Chimiche, *Organometallics*, 2005, 4995–5003.

40 H. Hu and C. Cui, *Organometallics*, 2012, **31**, 1208–1211.

41 M. R. Crimmin, I. J. Casely and M. S. Hill, *J. Am. Chem. Soc.*, 2005, **127**, 2042–2043.

42 S. Datta, P. W. Roesky and S. Blechern, *Organometallics*, 2007, **26**, 4392–4394.

43 F. Buch, J. Brettar and S. Harder, *Angew. Chemie - Int. Ed.*, 2006, **45**, 2741–2745.

44 M. B. Ghebreab, C. A. Bange and R. Waterman, *J. Am. Chem. Soc.*, 2014, **136**, 9240–9243.

45 A. J. Roering, S. E. Leshinski, S. M. Chan, T. Shalumova, S. N. MacMillan, J. M. Tanski and R. Waterman, *Organometallics*, 2010, **29**, 2557–2565.

46 C. A. Bange and R. Waterman, *ACS Catal.*, 2016, **6**, 6413–6416.

47 B. T. Novas, C. A. Bange and R. Waterman, *Eur. J. Inorg. Chem.*, 2019, **2019**, 1640–1643.

48 C. A. Bange, M. A. Conger, B. T. Novas, E. R. Young, M. D. Liptak and R. Waterman, *ACS Catal.*, 2018, **8**, 6230–6238.

49 C. A. Bange, M. B. Ghebreab, A. Ficks, N. T. Mucha, L. J. Higham and R. Waterman, *Dalton Trans.*, 2016, **45**, 1863–1867.

50 C. Bange, N. Mucha, M. Cousins, A. Gehsmann, A. Singer, T. Truax, L. J. Higham and R. Waterman, *Inorganics*, 2016, **4**, 26.

51 M. Espinal-Viguri, A. K. King, J. P. Lowe, M. F. Mahon and R. L. Webster, *ACS Catal.*, 2016, **6**, 7892–7897.

52 K. J. Gallagher, M. Espinal-Viguri, M. F. Mahon and R. L. Webster, *Adv. Synth. Catal.*, 2016, **358**, 2460–2468.

53 K. J. Gallagher and R. L. Webster, *Chem. Commun.*, 2014, **50**, 12109–12111.

54 M. Espinal-viguri, M. F. Mahon, S. N. G. Tyler and R. L. Webster, *Tetrahedron*,

2017, **73**, 64–69.

55 A. K. King, K. J. Gallagher, M. F. Mahon and R. L. Webster, *Chem. - A Eur. J.*, 2017, **23**, 9039–9043.

Chapter 5

Self-replication of chelating diphosphines via Pt(0)-catalysed hydrophosphination

5.1 Introduction

5.1.1 Self-replication

Self-replication in biology, as demonstrated by DNA replication, is a vital process required for life. Complementary DNA strands are separated and then serve as templates for the formation of two copies of the original duplex. The idea that synthetic chemicals may form templates of their own production is attractive, in part to gain understanding of how self-replicating systems function, but also because examples of abiological self-replicating systems are unusual.[1]

The term autocatalysis is defined as a process in which the product itself is a catalyst for the reaction. As more catalyst is formed as the reaction proceeds, the rate of reaction accelerates until the starting material runs out. In a self-replicating reaction (a subset of autocatalysis), a molecule will *only* catalyse its own formation hence reducing the formation of side products.[1] Rebek was the first to report a synthetic, self-replicating molecule that consisted of complementary adenine and imide recognition building blocks involved in an aminolysis reaction followed by dimerization (Scheme 5.1).[2]

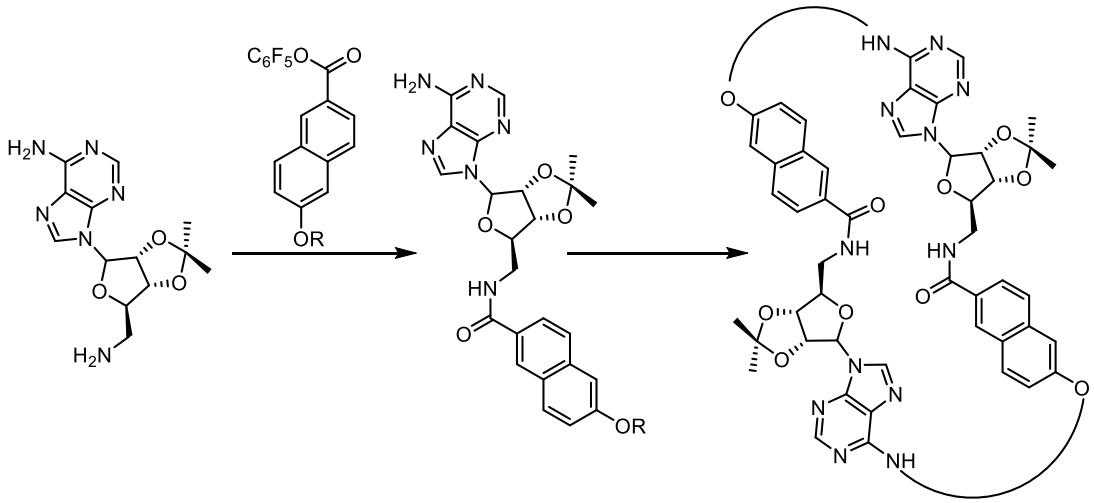

Scheme 5.1 Self-replicating system designed by Rebek *et al.*

The existence of self-replication in this reaction was debated and after exploration using various models it was concluded that several forms of catalysis, including self-replication were present in the Rebek system, signifying how complex it is to design a truly self-replicating system.[3–5]

In 2005, Muniz reported a self-replication process within the secondary cycle of Sharpless asymmetric aminohydroxylation of acrylic acid (Scheme 5.2).[6] Following *in situ* formation of azaglycol osmate ester **C** from enantiopure amino acid **A** and an osmium(VI) compound such as **B** there is an oxidation reaction to give catalyst **D**. A second oxidation, this time of an acrylate, results in the formation of complex **E**. Hydrolysis then gives free amino alcohol **A** and regenerates catalyst **D**. The isolation of intermediates was not possible but the agreement of mathematical rationalisations and the stereochemical outcome of the reaction led to the conclusion that the self-replication process proceeded as in Scheme 5.2.

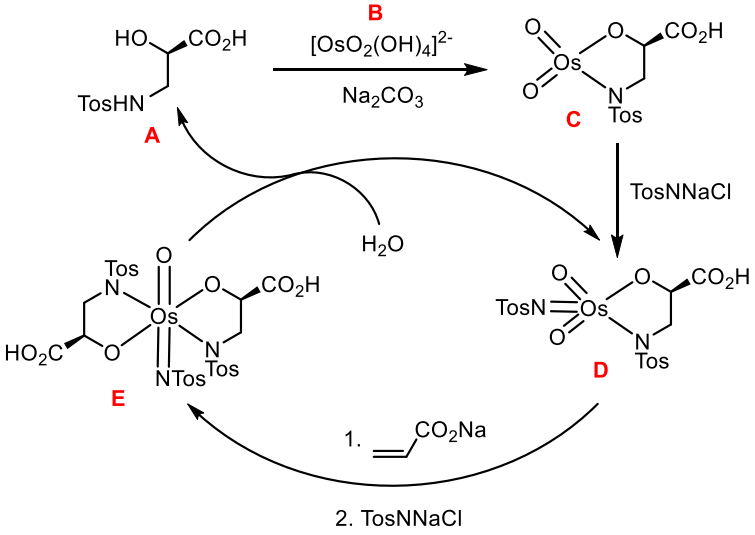

Scheme 5.2 Catalytic cycle for self-replication in asymmetric aminohydroxylation.

In this work, we discovered an example of a self-replicating system that produces useful, functionalised, chelating diphosphines via Pt(0)-catalysed hydrophosphination. Scheme 5.3 graphically represents the self-replicating nature of this process where the reaction of X with Y to produce L is mediated by Z which is a duplex of the product L.

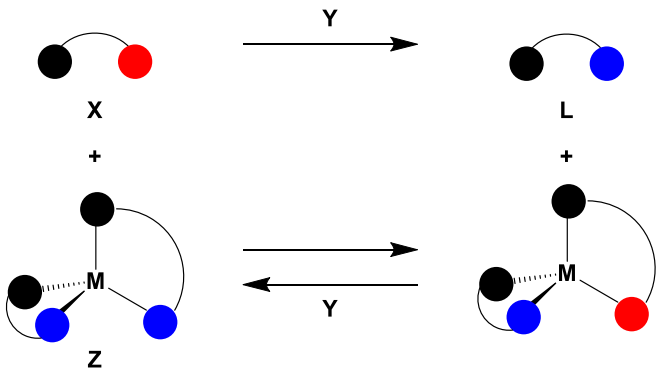

Scheme 5.3 Representation of the catalytic self-replication of diphosphines

5.1.2 Mechanistic studies of Pt(0)-catalysed hydrophosphination

Transition metal catalysed hydrophosphination was first reported by Pringle and Smith in 1990.[7] It was shown that Michael addition reactions were catalysed with high chemoselectivity by Pt(0) complexes in a self-replicating process where the phosphines coordinated to Pt(0) were also the product phosphines (Scheme 5.4).

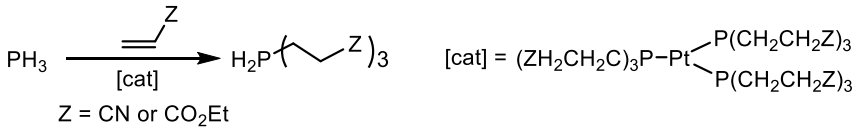

Scheme 5.4 Pt(0)-catalysed hydrophosphination with PH_3

A proposed mechanism for the final step of the hydrophosphination is shown in Scheme 5.5. The cycle involves coordination of the alkene to the Pt(0) centre followed by displacement of a tertiary phosphine ligand by a secondary phosphine. Oxidative addition of the P-H bond proceeds to give complex **1** before H-migration and coordination of another tertiary phosphine ligand. Reductive elimination of the functionalised product completes the cycle. It was suggested that **1** could be in equilibrium with dinuclear intermediates as **2** could be prepared independently. Subsequent work including kinetic measurements suggested a Michael-type attack of the coordinated PR_2 on complex **1** would give a metallacycle intermediate which upon reductive formation of the C-H bond would regenerate $[Pt(PR_3)_3]$.[8]

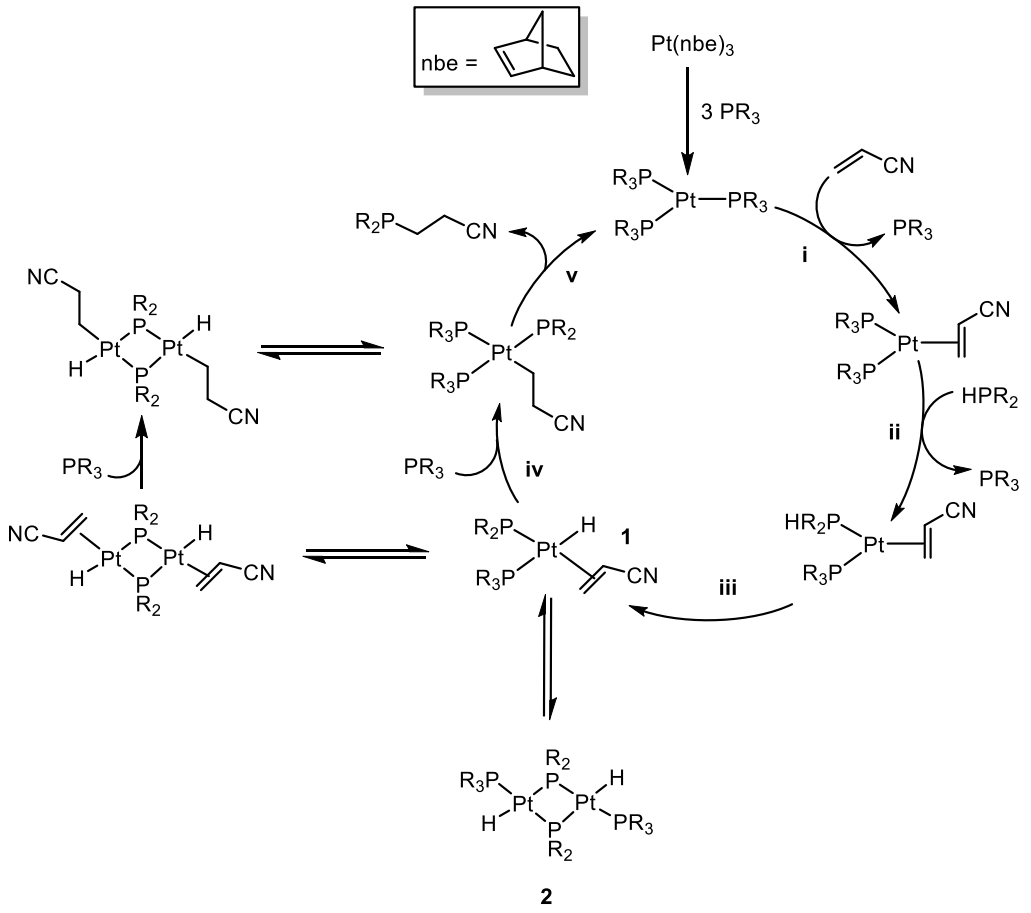

Scheme 5.5 First proposed mechanism for Pt(0)-catalysed hydrophosphination.

Following the work of Pringle *et al.*, in a series of publications, Glueck *et al.* investigated the mechanism of Pt(0)-catalysed hydrophosphination with monophosphine substrates and a [Pt((*R*,*R*)-Me-Duphos)(*trans*-stilbene)] catalyst.[9–12] Early work suggested that the reaction proceeds with a P-H oxidative addition then selective insertion of the alkene into the Pt-P bond rather than the Pt-H bond as suggested by Pringle *et al.* A subsequent revised mechanism shown in Scheme 5.6 proposed that P-C bond formation by Michael addition was more likely. The cycle starts with P-H oxidative addition followed by Michael addition to give a zwitterionic intermediate (**3**). This is followed by carbanion attack on the platinum hydride species and then displacement by another secondary phosphine to complete the cycle. An alternative pathway was also suggested where the stabilised carbanion attacks the electrophilic Pt centre forming a 5-coordinate intermediate (**4**) before Pt-P bond dissociation to give complex **5**. Product formation could then occur by C-H reductive elimination or by intramolecular proton transfer.

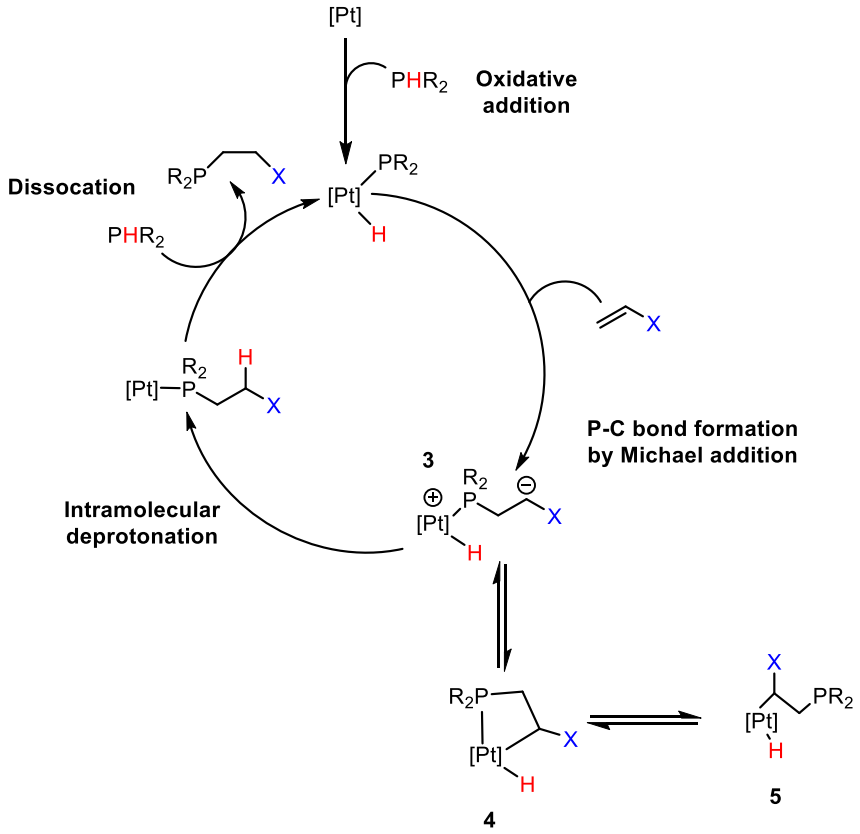

Scheme 5.6 Pt(0)-catalysed hydrophosphination mechanism proposed by Glueck.

In a trapping experiment to confirm the presence of zwitterion **3**, the reaction of **3** with an aldehyde followed by proton transfer was predicted to give phosphine **7** (Scheme 5.7). This reaction would compete with normal hydrophosphination and hence the product ratio of **6**/**7** would reflect the selectivity of zwitterion **3** for reaction with the internal Pt-H and external PhCHO electrophiles. It was found that secondary phosphines react very slowly with benzaldehyde in toluene even in the presence of a Pt(0) catalyst. Additionally, the reaction of PPh_2H and PhCHO seemed to be reversible, indicating a preference for reaction with the internal electrophile.[12]

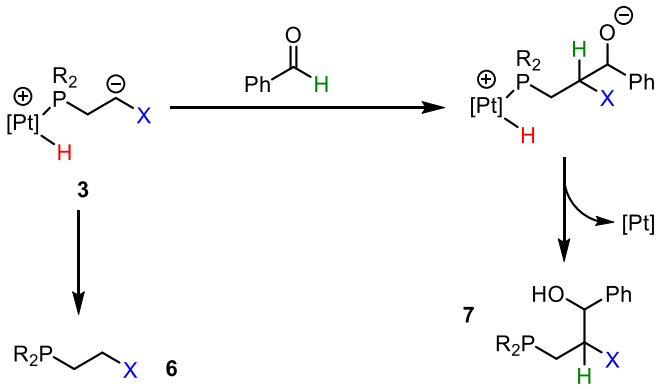

Scheme 5.7 Trapping of intermediate zwitterion with an electrophile.

It is important to note that all studies on the mechanism of Pt(0)-catalysed hydrophosphination conducted by Glueck *et al.* and Pringle *et al.* to date have been based on monophosphine substrates. Monodentate starting materials and/or products coordinate to the metal centre to form a coordinatively saturated complex that may reduce or inhibit further catalytic activity. This effect is thought to be further increased for bidentate ligands due to the chelate effect.

This Chapter will focus on the preparation of new functionalised diphosphine ligands via Pt(0)-catalysed hydrophosphination. The mechanism of the reaction as well as catalyst loading and investigations into the rate of reaction will be discussed.

5.3 Preparation of functionalised diphos 5.1

Diphos **P-PH$_2$** ($Ph_2PCH_2CH_2PH_2$) was prepared according to literature procedure (Scheme 5.8).[13] Diphenylphosphine was heated with diethyl vinylphosphonate and azoisobutylnitrile (AIBN), then the product treated with lithium aluminium hydride ($LiAlH_4$) to give precursor **P-PH$_2$**.

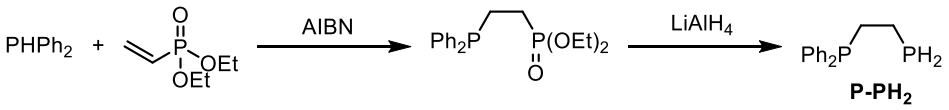

Scheme 5.8 Synthesis of precursor **P-PH$_2$**.

Reports of hydrophosphination as a route to unsymmetrical diphosphines in the literature have been mediated by alkyl lithium reagents,[14,15,16] base,[17,18] or radical initiators[19,20]. The hydrophosphination of **P-PH$_2$** was initially carried out in the presence of AIBN (10 mol%) to give novel ligand **5.1** (Scheme 5.9).

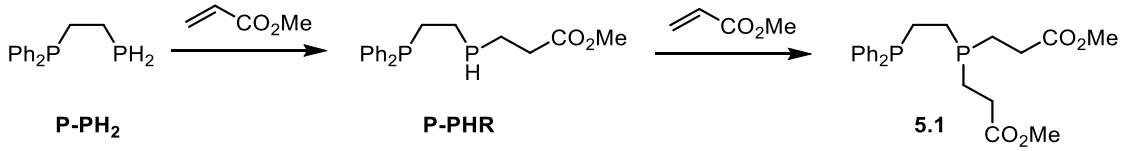

Scheme 5.9 Hydrophosphination by **P-PH$_2$** to give **5.1**.

When promoted by AIBN, after 6 h at 70 °C the product was a mixture of P-containing species with conversion to product **5.1** of approx. 75%, shown by *in situ* $^{31}P\{^1H\}$ NMR spectroscopy (Figure 5.1). When the reaction was carried out in the presence of the platinum complex [Pt(nbe)$_3$] (nbe = η^2-norbornene) (5 mol%) and 20 eq. ^{t}BuOH, after 1 h at ambient temperature, **5.1** was produced in quantitative yield shown by two doublets in the $^{31}P\{^1H\}$ NMR spectrum.

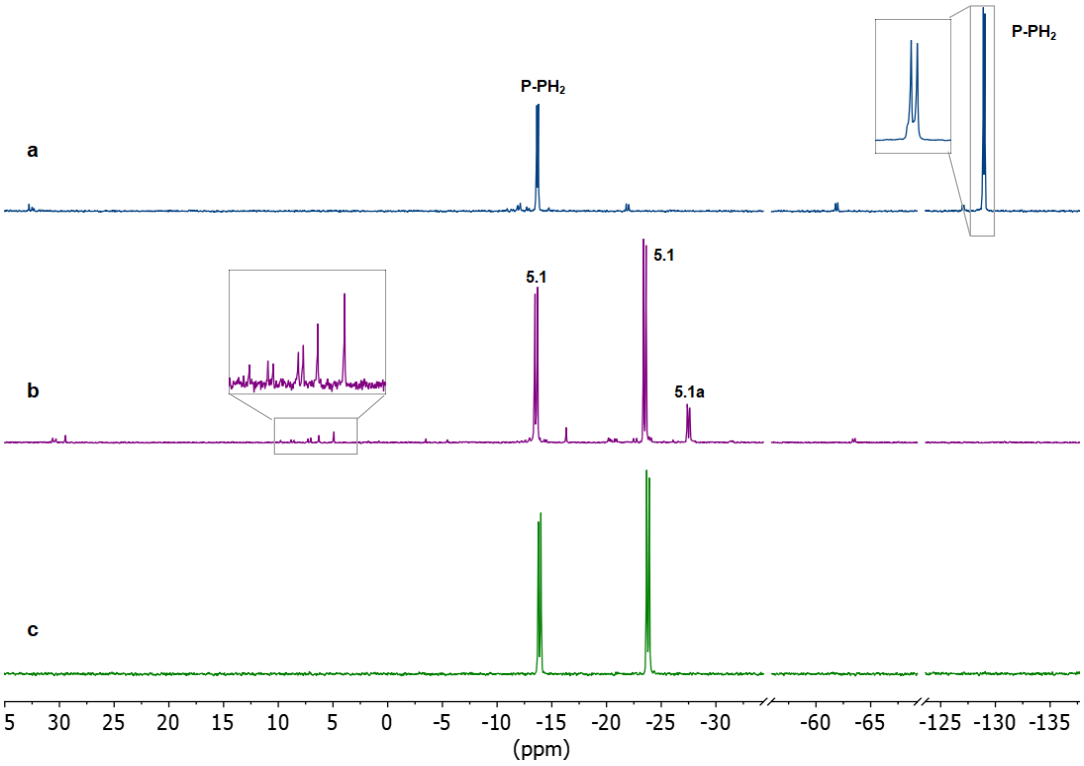

Figure 5.1 *In situ* $^{31}P\{^{1}H\}$ NMR spectra (121 Hz, MeCN) for the hydrophosphination reaction (Scheme 5.9) carried out under the following conditions: (a) no catalyst (after 6 h); (b) 10% AIBN (after 6 h); (c) 5 mol% $Pt(nbe)_3$, 20 eq. ^{t}BuOH (after 1 h).

The new functionalised diphosphine **5.1** has been isolated in 72% yield and fully characterised (see Chapter 6).

5.3.1 Suppression of telomer formation

The absence of ^{t}BuOH from the Pt(0)-catalysed hydrophosphination route to **5.1** results in the production of telomeric by-products e.g. **5.1a** (Scheme 5.10).

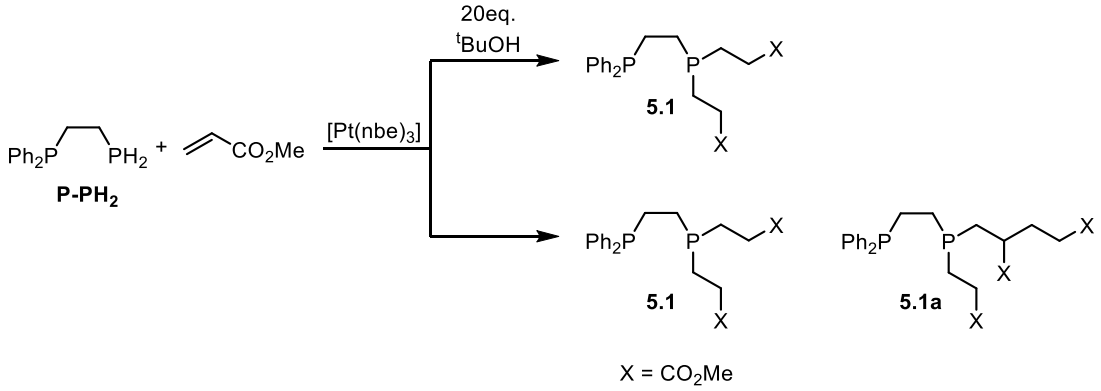

Scheme 5.10 Synthesis of **5.1** with and without ^{t}BuOH.

Previous work by Glueck *et al.* [11,12] on the hydrophosphination of monophosphine substrates suggests that formation of such contaminants is due to over-addition of the acrylate substrate to a zwitterionic intermediate in the catalytic cycle (pathway A, Scheme 5.11). The results also showed that addition of 20 eq. of a weak acid (^{t}BuOH) suppressed telomer formation as the protonation of the zwitterion was faster than the competing over-addition reaction (pathway B).

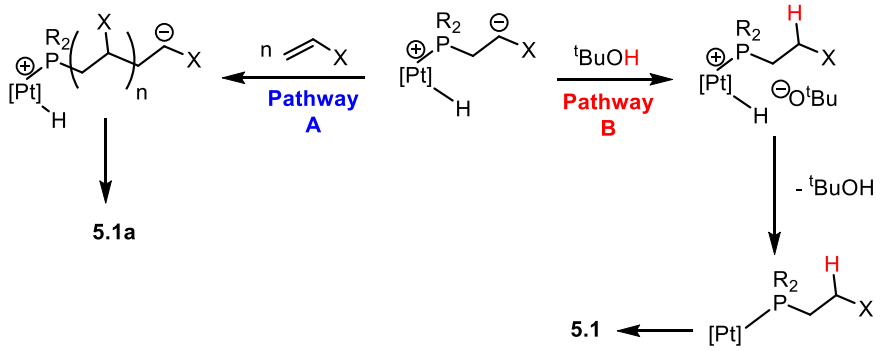

Scheme 5.11 Telomer formation and its suppression by ^{t}BuOH.

When an excess of methyl acrylate (10 eq.) was added to the reaction mixture in the absence of ^{t}BuOH, **5.1a** became the major product indicating that pathway A is favoured under these conditions (Figure 5.2).

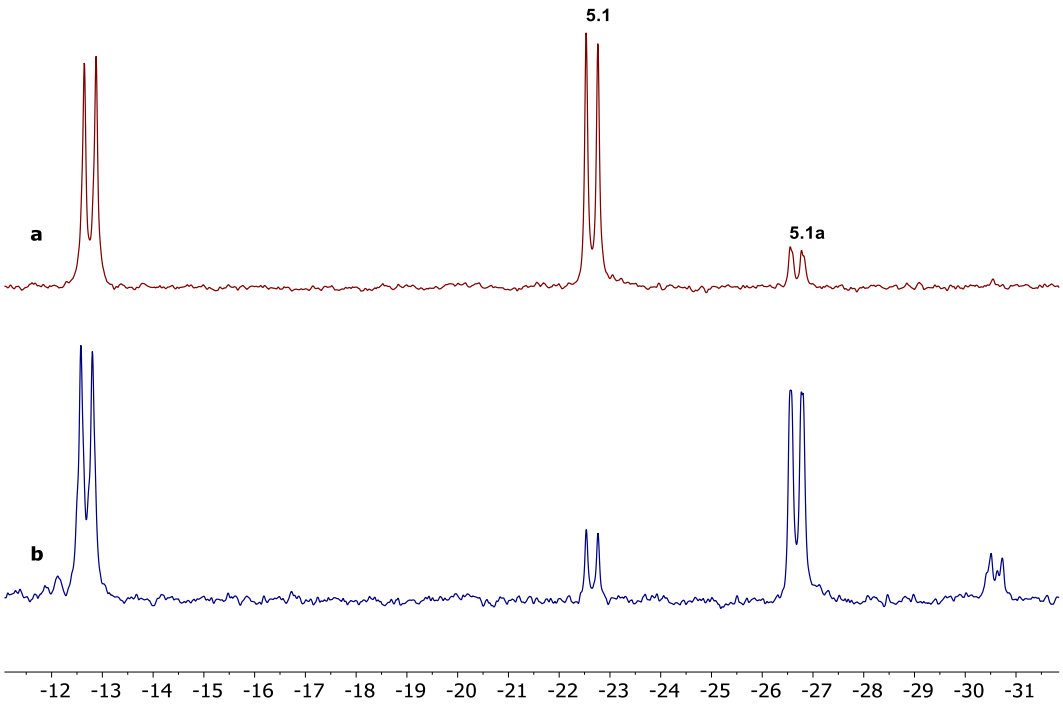

Figure 5.2 ^{31}P{^{1}H} NMR (121 MHz, MeCN) spectra for the synthesis of **5.1** with (a) 2 eq. methyl acrylate with no ^{t}BuOH added; (b) 10 eq. methyl acrylate with no ^{t}BuOH added.

Telomer formation was completely suppressed in the presence of 20 eq. ^{t}BuOH in the synthesis of diphos **5.1**.

5.3.2 Variation of alkene substrate

The Pt(0)-catalysed hydrophosphination conditions have been applied to acrylate, nitrile, amide and phosphonate substrates (Scheme 5.12).

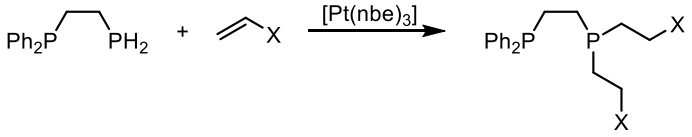

5.1 X = CO_2Me **5.5** X = $CONH_2$

5.2 X = CO_2Et **5.6** X = $CONMe_2$

5.3 X = $CO_2{}^{t}Bu$ **5.7** X = $PO(OEt)_2$

5.4 X = CN

Scheme 5.12 Preparation of diphosphines **5.1** – **5.7**.

Each of the new diphosphines **5.1**-**5.7** were formed at comparable rates with 5 mol% [Pt(nbe)$_3$] and each of the $^{31}P\{^{1}H\}$ NMR spectra comprised of two doublets with a $^{3}J_{PP}$ in a narrow range around 28 Hz. Compound **5.7** showed an additional triplet of doublets in the $^{31}P\{^{1}H\}$ NMR spectrum (δ -19.0 ppm, $^{3}J_{PP=O}$ = 49 Hz, $^{3}J_{PP}$ = 28 Hz), characteristic of the newly substituted phosphorus atom coupled with the two P(V) in the substituent. Each of the ligands **5.1**-**5.7** were isolated in good yields and fully characterised (see Chapter 6).

The effect of steric hindrance on the Pt(0)-catalysed hydrophosphination of acrylic esters was investigated using substituted acrylates (Scheme 5.13).

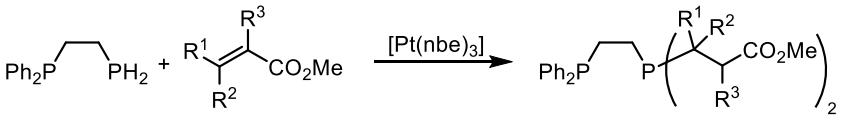

	R^1	R^2	R^3
5.8	H	H	Me
5.9	Me	H	H
5.10	Me	Me	H

Scheme 5.13 Synthesis of diphosphines **5.8**-**5.10**.

Increasing the steric bulk at the α-carbon did not significantly hinder the progress of the reaction; methyl methacrylate for example, was readily converted to give **5.8** as a mixture of *rac*/*meso* isomers (Figure 5.3) (Table 2.1).

Table 2.1 Reaction conditions for the synthesis of **5.8** to **5.10**.

Product	Time (h)	Temperature (°C)	Eq. acrylic ester	In situ yield[a]
5.1	1	25	2	>99%
5.8	2	25	2	95%
5.9	72	50	2.5	92%
5.10	-	50	3	0

[a]Determined by integration of *in situ* $^{31}P\{^{1}H\}$ NMR (122 MHz, MeCN) spectra

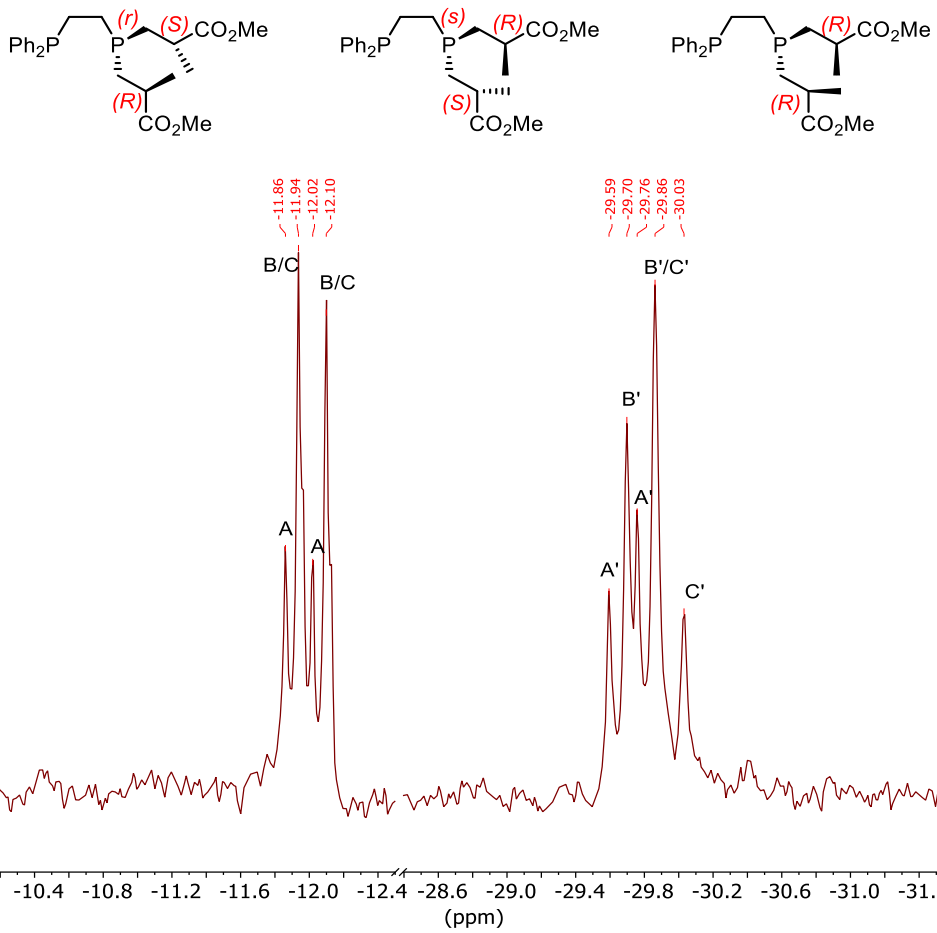

Figure 5.3 $^{31}P\{^{1}H\}$ NMR (162 MHz, $CDCl_3$) for **5.8** showing the 3 expected diastereoisomers formed: 2 meso isomers (Cs symmetry) and 1 rac isomer (C1 symmetry, only one of the enantiomers shown). The signals for two of the diastereoisomers labelled (A,A') and (B,B') are distinct. The evidence for the expected third diastereomer is the signal at the far right of the

spectrum labelled C' which is tentatively assigned as half of a doublet with the other half coincident with the B' signal, explaining the higher intensity of this signal. The other doublet is then assumed to be coincident with the signals labelled B/C.

Addition of groups at the β-carbon made more of an impact as methyl crotonate required more time, higher temperature and increased amounts of acrylic ester to give **5.9** as a mixture of *rac*/*meso* isomers (Figure 5.4).

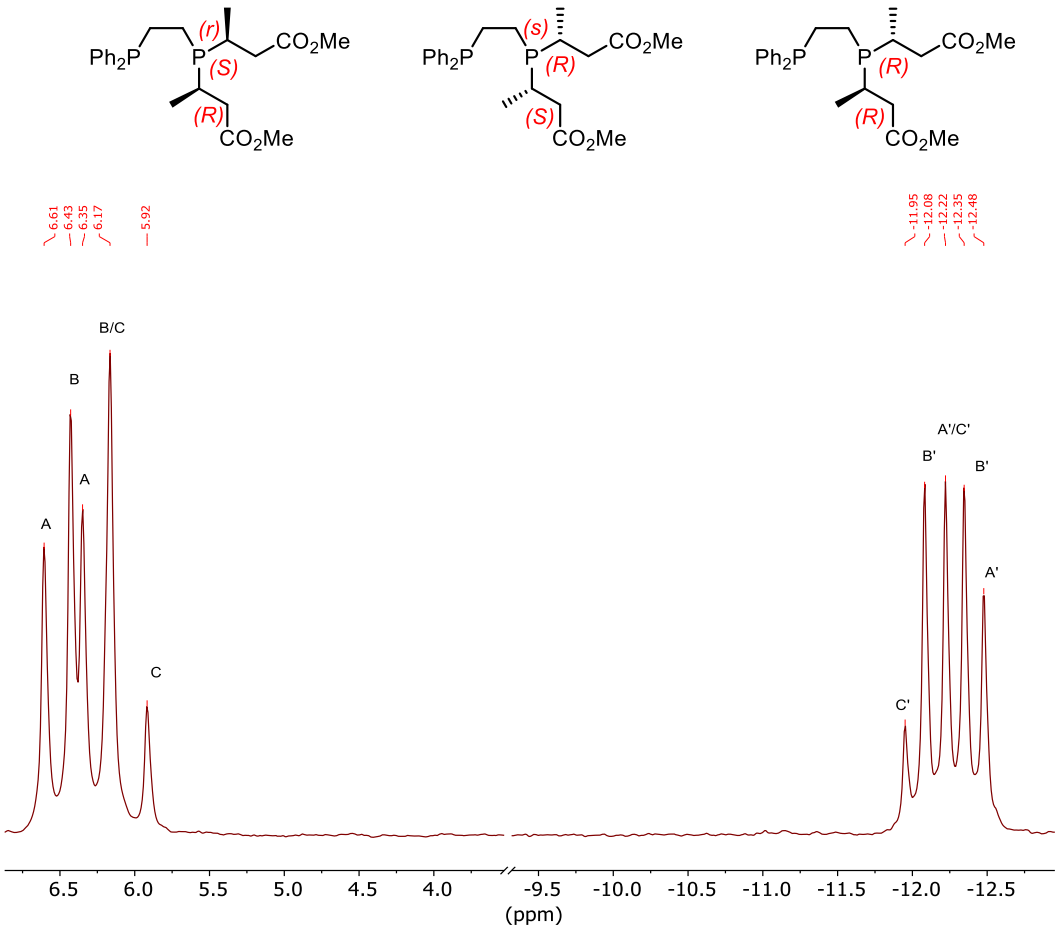

Figure 5.4 $^{31}P\{^{1}H\}$ NMR (122 MHz, MeCN) of **5.9** showing the 3 expected diastereoisomers formed: 2 *meso* isomers (C_s symmetry) and 1 *rac* isomer (C_1 symmetry, only one of the enantiomers shown). The signals for two of the diastereoisomers are labelled (A,A') and (B,B') are distinct; the third isomer is labelled (C,C') but has overlapping signals which are therefore tentatively assigned.

Substituting two groups at the β-position inhibited the reaction completely as methyl 3,3-dimethylacrylate did not undergo hydrophosphination to form **5.10** even after 3 days at 50 °C. This is consistent with the Pt(0)-hydrophosphination following a mechanism containing a Michael addition step.

5.3.3 Variation of diphos substrate

The diphos reactant for the Pt(0)-catalysed hydrophosphination previously described was varied to further uncover the scope of the reaction.

The disecondary diphosphine $PPh(H)CH_2CH_2PPh(H)$ was synthesised by dppe lithiation and subsequent protonation (see Chapter 6 for details); then, Pt(0)-catalysed hydrophosphination gave **5.11** as a mixture of diastereomers, isolated in 54% yield and fully characterised (Scheme 5.14).

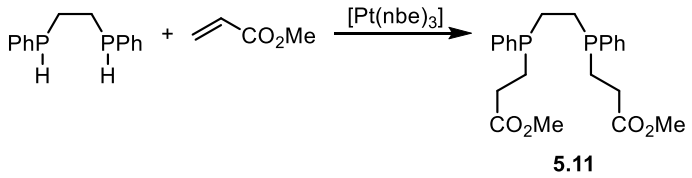

Scheme 5.14 Synthesis of **5.11.**

Tetra-substituted diphos **5.12** was synthesised from $PH_2CH_2CH_2PH_2$ in 2 h with 2 mol% $[Pt(nbe)_3]$ at ambient temperature (Scheme 5.15). The product proved to be very volatile and could not be isolated from the reaction solvent.

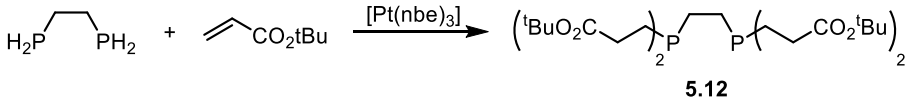

Scheme 5.15 Synthesis of **5.12**.

The Pt(II) complex of **5.12** was synthesised from $[PtCl_2(cod)]$ and fully characterised with crystals suitable for X-ray crystallography grown by vapour diffusion of hexane into a DCM solution (Figure 5.5).

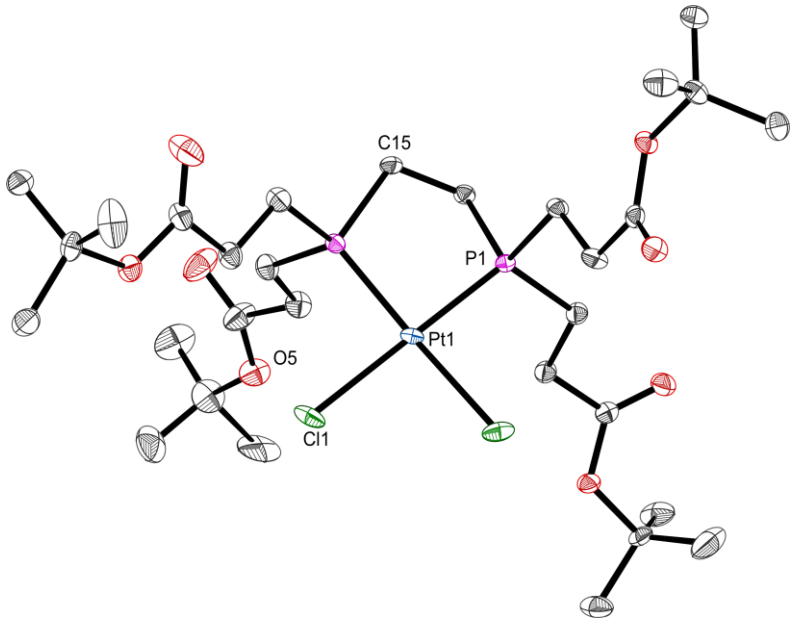

Figure 5.5 Crystal structure of [Pt(**5.12**)Cl_2]. Hydrogen atoms omitted for clarity. Selected bond lengths (Å) and bond angles (°): Pt(1)-P(1) 2.2121(6), Pt(1)-P(2) 2.2185(6), Pt(1)-Cl(1) 2.3547(6), Pt(1)-Cl(2) 2.3617(6), P(1)-C(15) 1.836(2), P(2)-C(16) 1.827(2), C(15)-C(16) 1.535(3), Cl(1)-Pt(1)-P(1) 91.90(2), Pt(1)-P(1)-C(15) 109.08(8), P(1)-C(15)-C(16) 110.41(16).

The bond lengths and angles reported above are comparable (within standard deviation) to [$PtCl_2$(dppe)].[21]

5.4 Catalyst loading

The catalyst loading of [Pt(nbe)$_3$] was varied in order to find the minimum concentration required for the hydrophosphination reaction shown in Scheme 5.16.

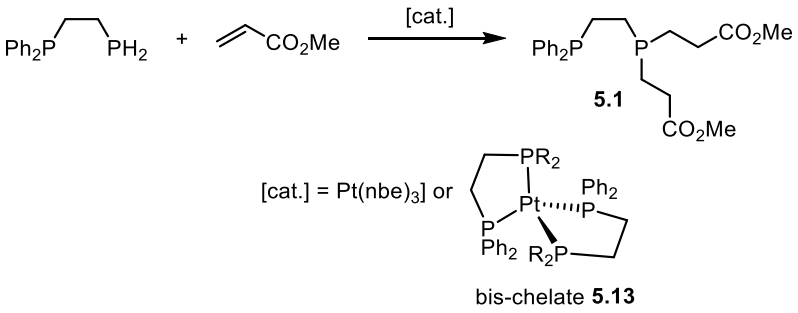

Scheme 5.16 Hydrophosphination investigated with varied catalyst loadings.

It was hypothesised that bis-chelate **5.13** must form early in the hydrophosphination reaction and may be an active catalyst, so loading of pre-formed **5.13** was also investigated.

The reaction time when using 5 mol% $[Pt(nbe)_3]$ for the reaction shown in Scheme 5.9 is approx. 1 h. In comparison, when the catalyst loading was decreased to 0.1 mol% $[Pt(nbe)_3]$ 22% product had formed after 3 h and 90% after 24 h (Figure 5.6). It can be seen from Figure 5.6 that when using pre-formed **5.13** at 0.1 mol% the reaction proceeds faster than when using $[Pt(nbe)_3]$. When the catalyst loading is decreased further to 0.01 mol% **5.13** is significantly faster than $[Pt(nbe)_3]$ with 66% product formed after 24 h compared to 16% respectively. At 0.01 mol% $[Pt(nbe)_3]$ the rate is comparable with that when no catalyst is used; 12% product is formed after 24 h.

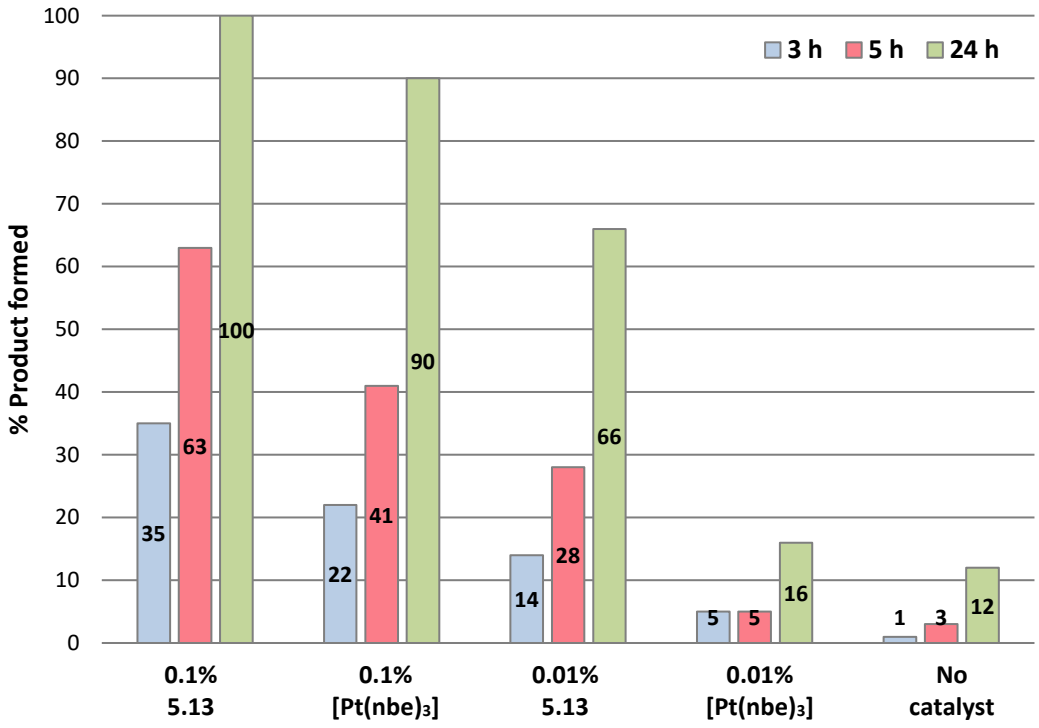

Figure 5.6 Catalyst loadings for reaction shown in Scheme 5.9. Product formation determined by *in situ* $^{31}P\{^1H\}$ NMR spectroscopy.

These results suggest that there is an induction period at the start of the reaction when $[Pt(nbe)_3]$ is the catalyst precursor. After enough **5.1** has formed, it becomes the ligand for its own catalysis and self-replication ensues. When the preformed **5.13** is the catalyst, no induction period is apparent, so the hydrophosphination is faster.

5.5 Rate monitoring reactions

To further illustrate that the rate of reaction is determined by the initial Pt(0) species present, hydrophosphination with 1.5 mol% [Pt(nbe)$_3$] or **5.13** was monitored over time and plotted in Figure 5.7.

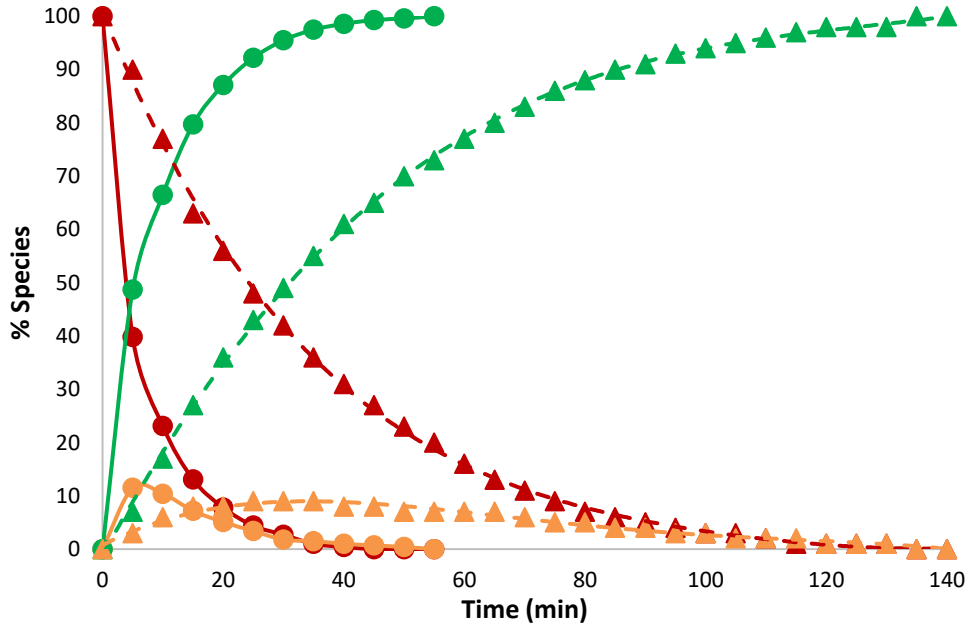

Figure 5.7 Plots of the variation of starting material **P-PH$_2$** (red), intermediate **P-PHR** (orange) and product **5.1** (green) as a function of time using [Pt(nbe)$_3$] (dotted lines) and complex **5.13** (solid lines) as catalyst precursors.

The two plots show the decrease in concentration of starting material **P-PH$_2$**, the increase in concentration of product **5.1** and the rise and fall in concentration of the intermediate secondary phosphine **P-PHR**. As shown in Section 5.4, when preformed **5.13** is used as the catalyst, the reaction is significantly faster with the reaction plotted in Figure 5.7 completed in 1 h compared to 100 min when using [Pt(nbe)$_3$]. This is consistent with there being an induction period associated with the *in situ* formation of **5.13** from [Pt(nbe)$_3$].

The catalysis involves two consecutive reactions catalysed by three of the available diphos ligands: conversion of **P-PH$_2$** to a secondary intermediate **P-PHR** then conversion of this to the product **5.1**. The kinetics are expected to be complicated and a function of many factors; therefore a detailed kinetic study was not attempted.

5.6 Deuterium-labelling experiments

In efforts to confirm a Michael-acceptor type mechanism over a coordination/insertion route (see Section 5.1.2) Glueck *et al.* performed deuterium labelling experiments.[11] Following treatment of a secondary phosphine with 20 eq. ^{t}BuOD in the presence of a Pt(0) catalyst, O-D/P-H exchange was observed by $^{31}P\{^1H\}$ NMR spectroscopy. When the alkene was added to the mixture, the extent of the deuterium incorporation was analysed (Scheme 5.17).

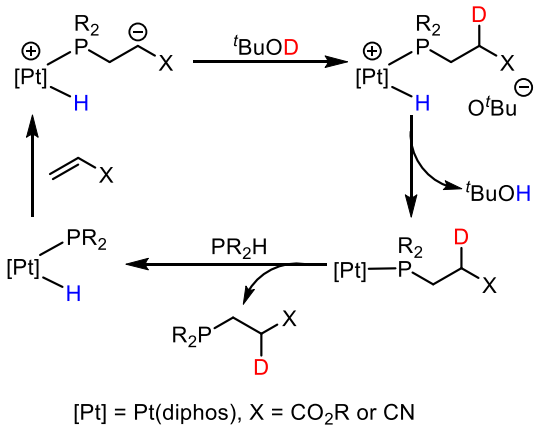

Scheme 5.17 Deuterium-labelling experiments performed by Glueck *et al.*

They predicted that if the reaction followed a mechanism with a zwitterionic intermediate, addition of ^{t}BuOD would lead to deuterium incorporation in the hydrophosphination product $R_2PCH_2CH(D)X$. Conversely, an unlabelled product would be formed if the reaction followed a coordination/insertion mechanism. The O-D/P-H exchange was too rapid in the presence of the Pt(0) catalyst for Glueck *et al.* to draw any useful conclusions concerning their mechanism.

Employing a similar strategy to Glueck, the mechanism of the diphos reaction was probed by carrying out a reaction with $PPh_2CH_2CH_2PD_2$ (**P-PD$_2$**) in the absence of ^{t}BuOH and in a second experiment, with **P-PH$_2$** and ^{t}BuOD (Scheme 5.18).

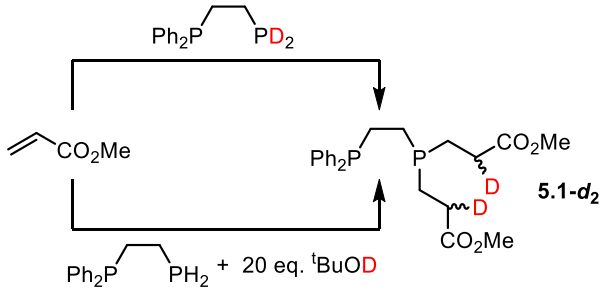

Scheme 5.18 Synthesis of deuterated **5.1** obtained using labelled reactants.

P-PD$_2$ was synthesised by stirring **P-PH$_2$** in D_2O and DCl (2.0 M in Et_2O) for 16 h. The resonances for **P-PD$_2$** and **P-PH$_2$** are clearly distinguishable by $^{31}P\{^1H\}$ NMR spectroscopy (Figure 5.8).

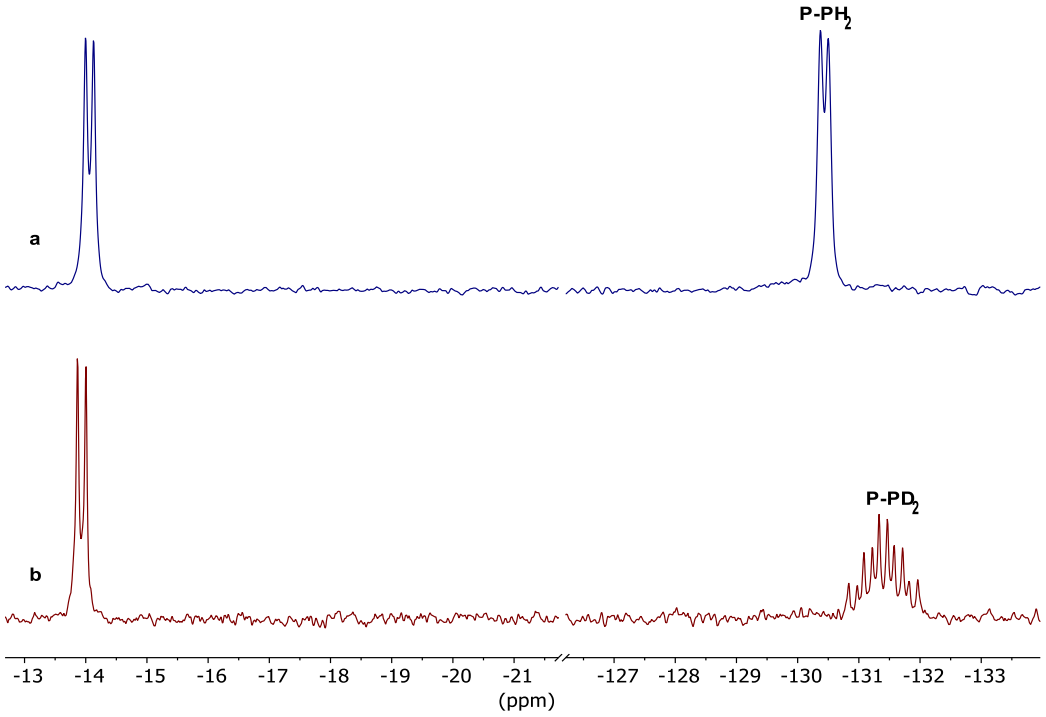

Figure 5.8 $^{31}P\{^1H\}$ NMR (122 MHz, CD_2Cl_2) spectra of (a) of **P-PH$_2$**; (b) **P-PD$_2$** showing a 1:2:3:2:1 quintet of doublets ($^3J_{PP}$ = 16.4 Hz, $^1J_{PD}$ = 29.9 Hz).

The location of the D-label at the α-carbon on **5.1-*d*$_2$** was analysed by ^1H NMR spectroscopy and showed that in both experiments the integration for the signal corresponding to the two α-CH_2 moieties was reduced overall by half, indicating incorporation of two deuterium atoms (Figure 5.9).

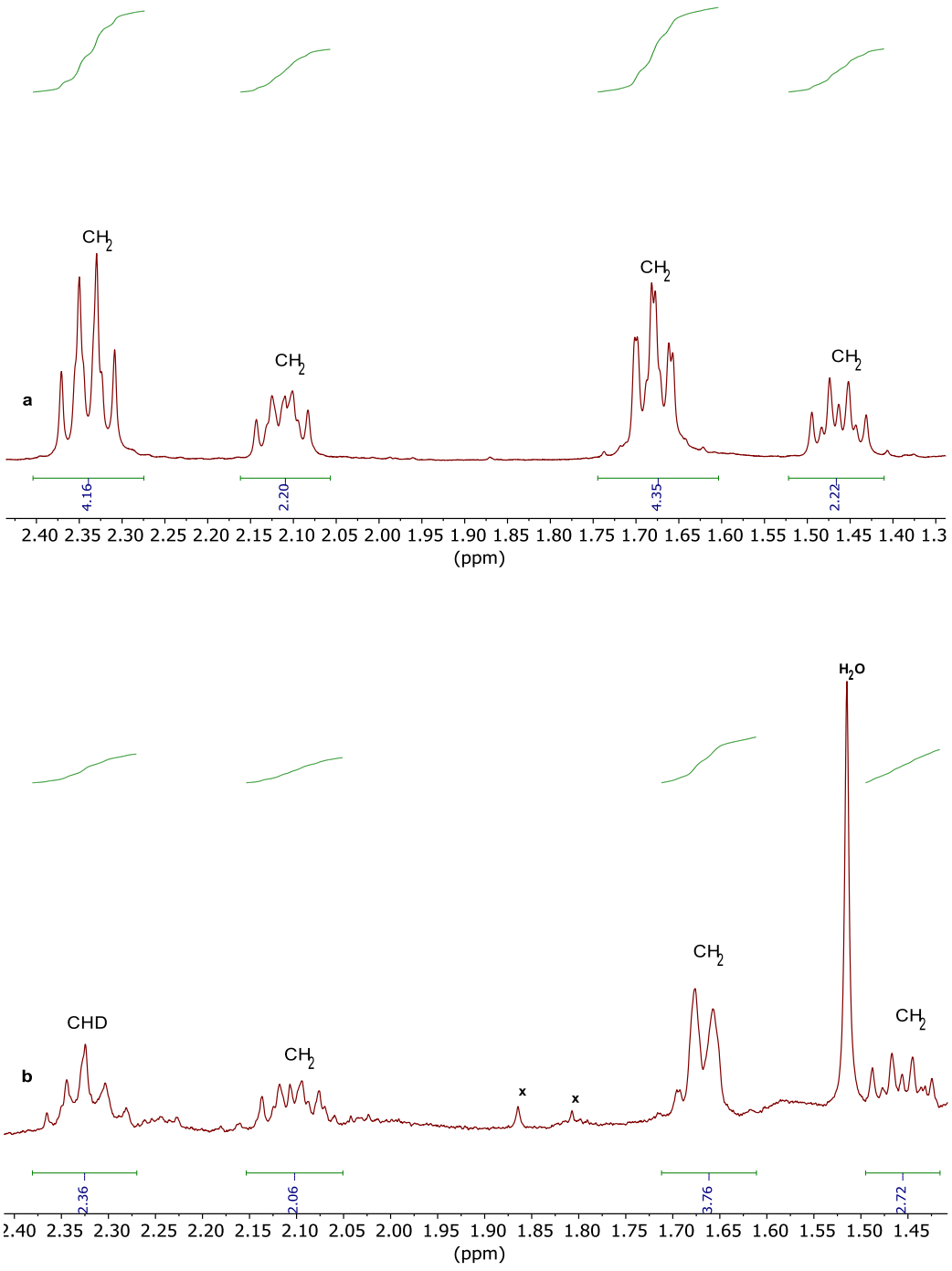

Figure 5.9 ^{1}H NMR (400 MHz, CD_2Cl_2) spectra of (a) **5.1-*d*$_2$** synthesised from **P-PD$_2$** and ^{t}BuOH (Scheme 5.18); (b) **5.1-*d*$_2$** synthesised from **P-PD$_2$** in the absence of ^{t}BuOH. x = unidentified impurities.

In addition, a diastereomeric mixture of the *rac*/*meso* isomers was observed in the ^{31}P{^{1}H} NMR spectrum (Figure 5.10). This pattern is consistent with both routes to protonation of the intermediate zwitterion are taking place.

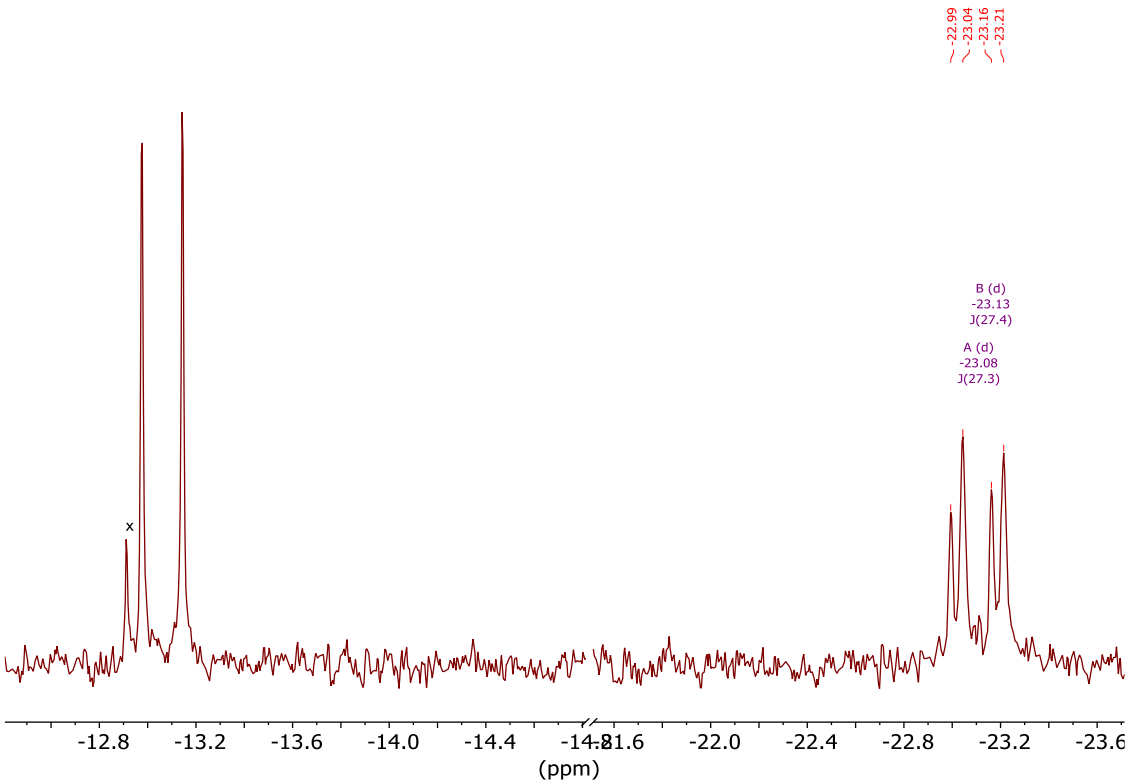

Figure 5.10 $^{31}P\{^{1}H\}$ NMR (162 MHz, CD_2Cl_2) spectrum when **5.1-*d*$_2$** is synthesised from **P-PD$_2$** in the absence of ^{t}BuOH. x = unidentified impurities. Three diastereoisomers are expected for **5.1-*d*$_2$**: 2 *meso* isomers (C_s symmetry) and 1 *rac* isomer (C_1 symmetry). It is clear that there is more than one compound present but that signals for three compounds are not resolved and there are very likely coincident signals.

In a competition reaction, a 1:1 mixture of **P-PH$_2$** and **P-PD$_2$** was treated with 1 mol eq. of methyl acrylate (Scheme 5.19).

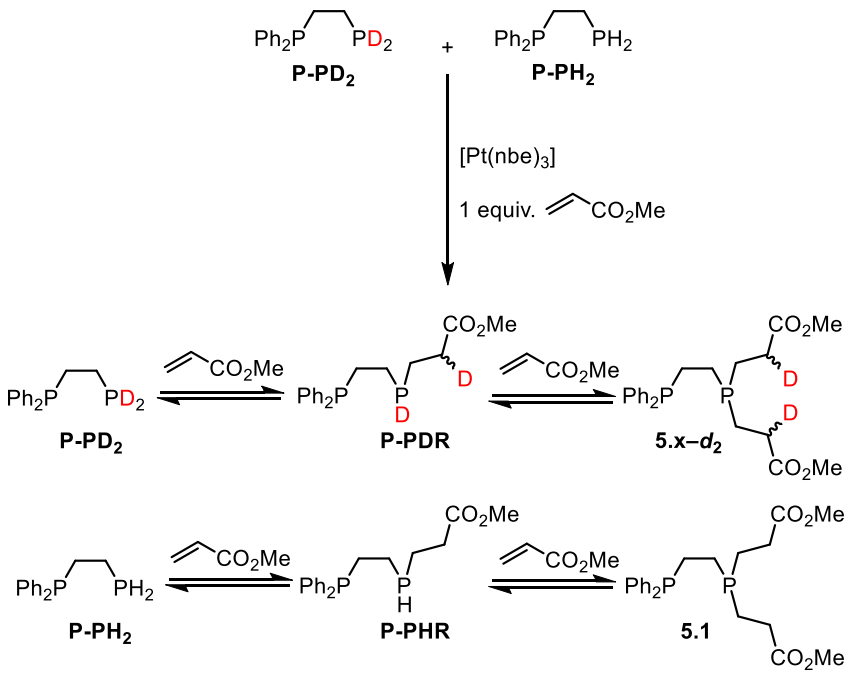

Scheme 5.19 Deuterium labelling studies.

The consumption of the primary phosphines was monitored by $^{31}P\{^{1}H\}$ NMR spectroscopy. Multiple P-containing species were observed, many of which overlapped but the primary phosphine resonances for **P-PH$_2$** and **P-PD$_2$** were easily distinguished (Figure 5.11).

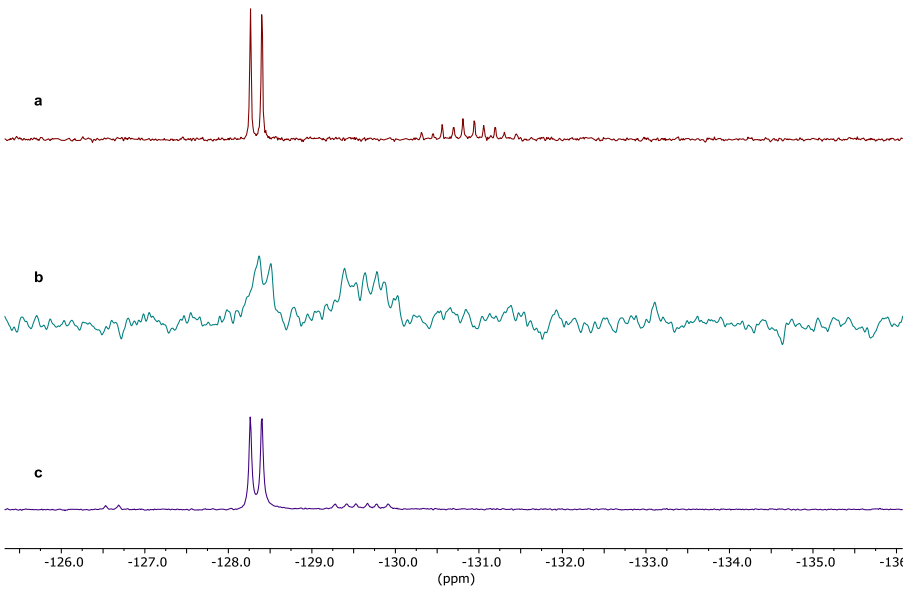

Figure 5.11 $^{31}P\{^{1}H\}$ NMR (122 MHz, CH_2Cl_2) spectra of a mixture of **P-PH$_2$** and **P-PD$_2$**; (a) 1:1 mixture; (b) 1:2 mixture after 10 min; (c) 5:1 mixture after 24 h.

After 10 min, the ratio of the signals for the primary phosphines had changed from 1:1 to 1:2 in favour of **P-PD$_2$**; apparently, the methyl acrylate preferentially reacts with the

weaker P-H bonds in **P-PH$_2$**. This kinetic isotope effect is evidence that P-H bond scission is involved in the turnover-limiting process. After 24 h, the ratio had inverted to 5:1 in favour of **P-PH$_2$** indicating that the reactions shown in Scheme 5.19 are reversible and a thermodynamic isotope effect is evident, as would be expected due to the C-D bonds formed in the products being stronger than the C-H bonds in the isotopologues.

5.7 Platinum(0) chemistry

The Pt(0) chemistry of **5.1** was investigated in order to probe the mechanism of Pt(0)-catalysed hydrophosphination of diphosphines further.

When 1 eq. of **5.1** was added to [Pt(nbe)$_3$], it was expected that the mono-chelate complex shown in Scheme 5.20 would form. However only bis-chelate **5.13** was observed as evidenced by a characteristic AA'XX' splitting pattern in the $^{31}P\{^1H\}$ NMR spectrum (Figure 5.12). The simulated spectrum is a good fit for the AA'XX' pattern.

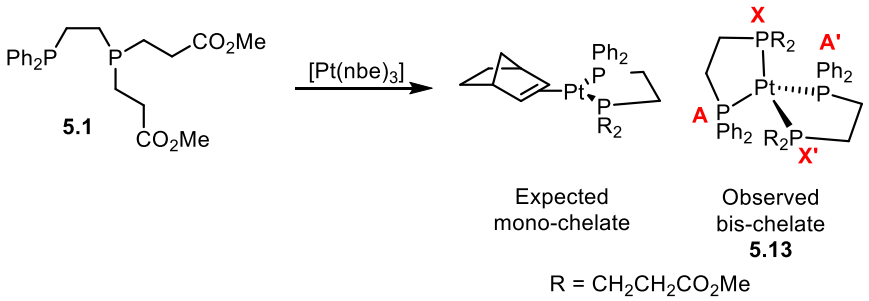

Scheme 5.20 Complexation of **5.1** to [Pt(nbe)$_3$].

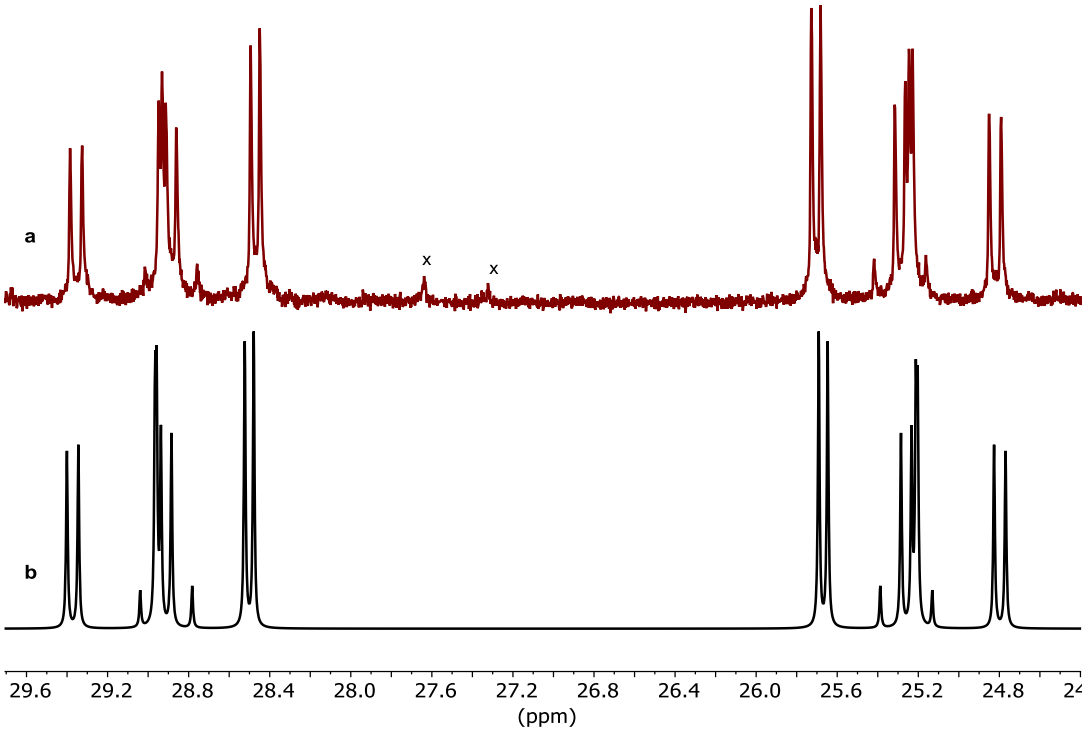

Figure 5.12 (a) Central peaks in the experimental $^{31}P\{^{1}H\}$ NMR (121 MHz, CH_2Cl_2) spectrum for **5.13**, (b) simulated spectrum for **5.13** with calculated coupling constants $J_{AA'}$ = 43.6 Hz, $J_{XX'}$ = 27.1 Hz, J_{AX} = 80.5 Hz and $J_{AX'}$ = 61.7 Hz. The ^{195}Pt satellites are omitted for clarity; x = unidentified impurity.

When another equivalent of **5.1** was added, the NMR spectrum did not change but became more resolved. Even when 0.1 eq. **5.1** was added to $[Pt(nbe)_3]$, the bis-chelate was the only species observed by $^{31}P\{^{1}H\}$ NMR spectroscopy; the presumed mono-chelate intermediate [Pt(nbe)(**5.1**)] has never been observed.

The formation of **5.13** is also supported by a triplet of triplets in the ^{135}Pt NMR spectrum (Figure 5.13).

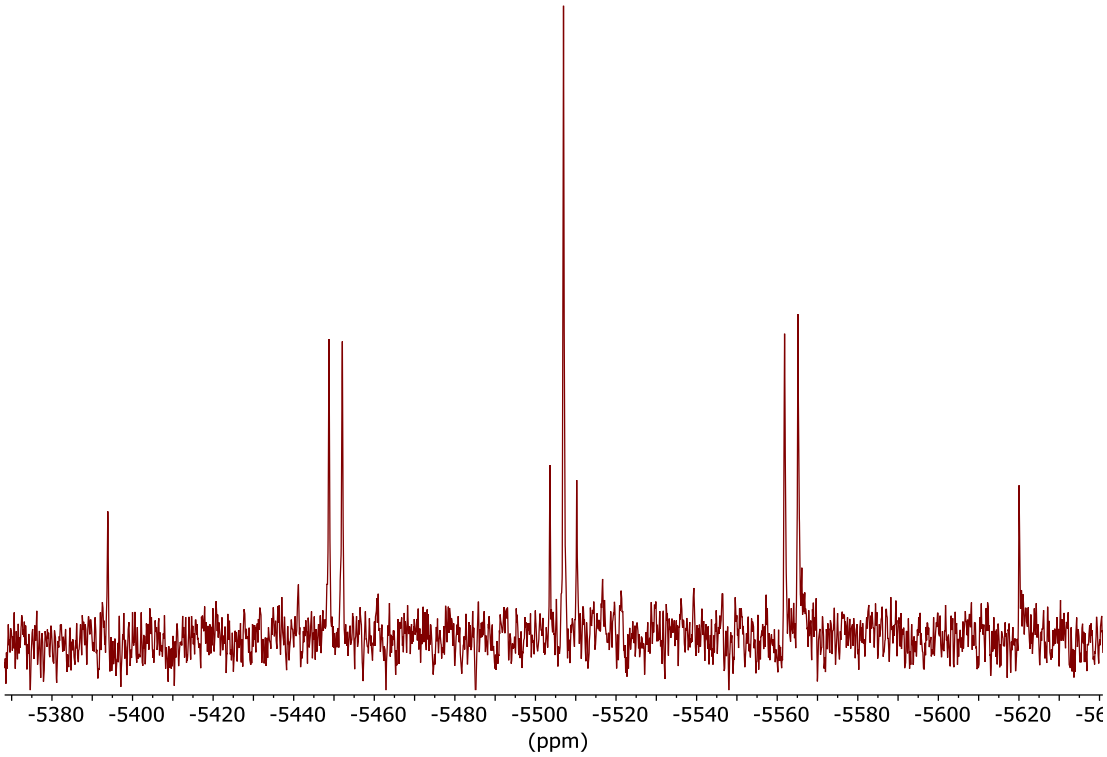

Figure 5.13 ^{195}Pt spectrum (65 MHz, CH_2Cl_2) of **5.13** ($^1J_{PtP}$ = 3758 Hz, 3557 Hz).

Attempts to grow crystals of platinum(0) complex **5.13** have been unsuccessful but from a solution of **5.13** in CH_2Cl_2, crystals of the platinum(II) complex [Pt(**5.1**)$_2$]Cl_2 suitable for X-ray crystallography slowly deposited over 2 d. The crystal structure of [Pt(**5.1**)$_2$]Cl_2 is shown in Figure 5.14 confirming the *cis* square planar geometry; this structure also confirms the identity of **5.1**. The same complex was prepared by treatment of [$PtCl_2$(cod)] with 2 eq. of **5.1** and has been fully characterised (see Chapter 6).

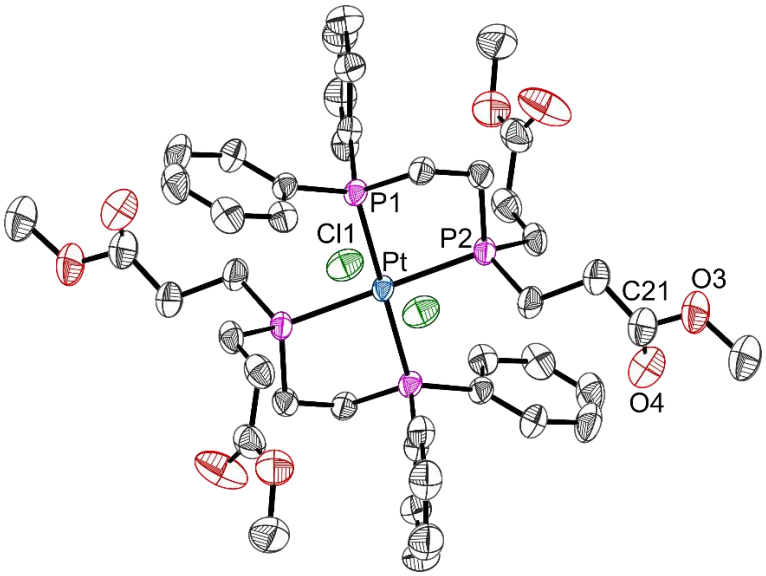

Figure 5.14 Crystal structure of the Pt(II) bis-chelate complex with two **5.1** ligands. Hydrogens omitted for clarity. Selected bond lengths (Å) and bond angles (°): Pt(1)-P(1) 2.3197, Pt(1)-P(2) 2.3262, P(1)-C(1) 1.818(8), P(1)-C(7) 1.811(2), P(1)-C(13) 1.824(3), P(2)-C(14) 1.834(2), P(2)-C(15) 1.828(3), C(13)-C(14) 1.552(4), P(2)-C(19) 1.809(2), P(1)-Pt(1)-P(1) 180.00, P(1)-Pt(1)-P(2) 83.16, P(1)-Pt(1)-P(2') 96.84.

5.7.1 Bis-chelate displacement studies

When bis-chelate **5.13** was treated with 100 eq. methyl acrylate in DCM or toluene, no change was observed to the AA'XX' pattern in the $^{31}P\{^{1}H\}$ NMR spectrum suggesting that the equilibrium depicted in Scheme 5.21 lies very strongly to the left. This contrasts with the analogous monophosphine systems reported by Pringle *et al.*[7,22] which, upon addition of CH_2=CHZ (Z = CO_2Et or CN) immediately forms [$Pt(PR_3)_2(\eta^2$-CH_2=CHZ)].

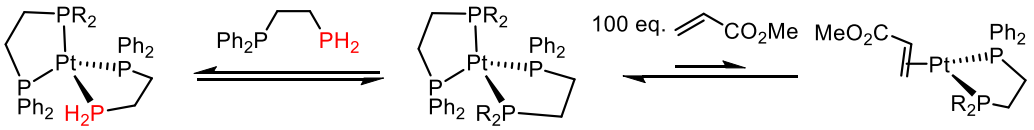

5.14 **5.13**

R = $CH_2CH_2CO_2Me$

Scheme 5.21 Displacement of **5.13** with methyl acrylate and **P-PH$_2$**.

The *in situ* $^{31}P\{^{1}H\}$ NMR spectrum after the addition of 1 eq. of **P-PH$_2$** to bis-chelate **5.13** shows displaced **P-PH$_2$** as well as **5.1**; the AA'XX' pattern corresponding to **5.13** is accompanied by other peaks which may be associated with the complex pattern expected for the ABCD spin system for the diphos-Pt complex **5.14** (Figure 5.15). This is consistent

with the equilibrium shown in Scheme 5.21. Subsequent addition of 1 eq. methyl acrylate led to a decrease in **P-PH$_2$** and formation of **5.1.**

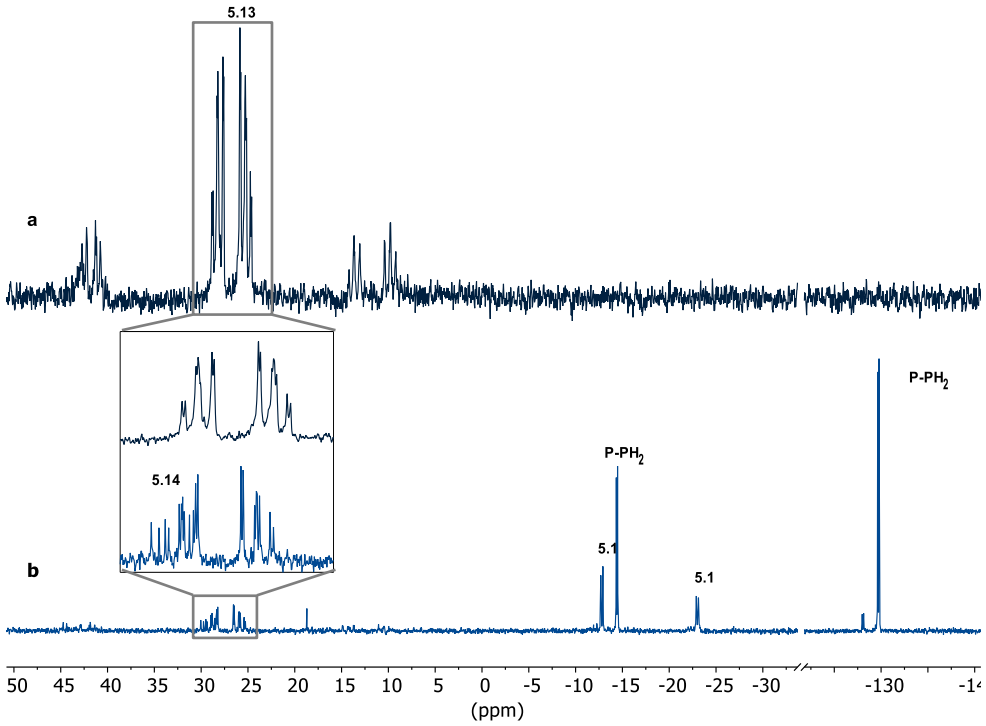

Figure 5.15 $^{31}P\{^{1}H\}$ NMR (122 MHz, d_8-toluene) spectra (a) bis-chelate **5.13**; (b) after addition of 1 eq. **P-PH$_2$**.

5.8 Mechanism proposal

Based on the observations discussed in this chapter, a mechanism is proposed for the hydrophosphination of **P-PH$_2$** and methyl acrylate to give secondary phosphine intermediate **P-PHR** (where R = $CH_2CH_2CO_2Me$) and then in the second cycle, the product **5.1**. The cycle consists of 16-electron complexes in equilibrium with 18-electron complexes (Scheme 5.22).

- Step i is the substitution of **5.1** from dissociated **5.13** by **P-PH$_2$** to give **5.14**, as observed stoichiometrically

- Step ii is the P-H oxidative addition to give the hydridoplatinum(II) complex **5.15a**

- Step iii is the nucleophilic attack of methyl acrylate by the terminal phosphide in **5.15a** to give the zwitterionic species **5.16a**

- Step iv is the intramolecular C–H formation to give **5.17a**

- The first cycle is completed by displacement of **P-PRH** to regenerate **5.14a**

Some additional features of note in the mechanism are:

1. It is likely that cycles A and B proceed via a $\kappa^1\kappa^2$-bis(diphos) species **5.13a**-**5.19a**;

2. The remarkable lack of significant inhibition by the product **5.1** implies some of the $\kappa^1\kappa^2$-bis(diphos) species are considerably more stable than their saturated $\kappa^1\kappa^2$-bis(diphos) isomers;

3. It is anticipated that 18-electron **5.13**-**5.19** are involved in the mechanism, at least as resting states;

4. **5.19a** also reacts with methyl acrylate to give telomers such as **5.1a** (see Scheme 5.10);

5. ^{t}BuOH prevents telomer formation by protonating the ylide **5.16a** and then the ^{t}BuO$^-$ generated would deprotonate the Pt–H to give **5.17a**.

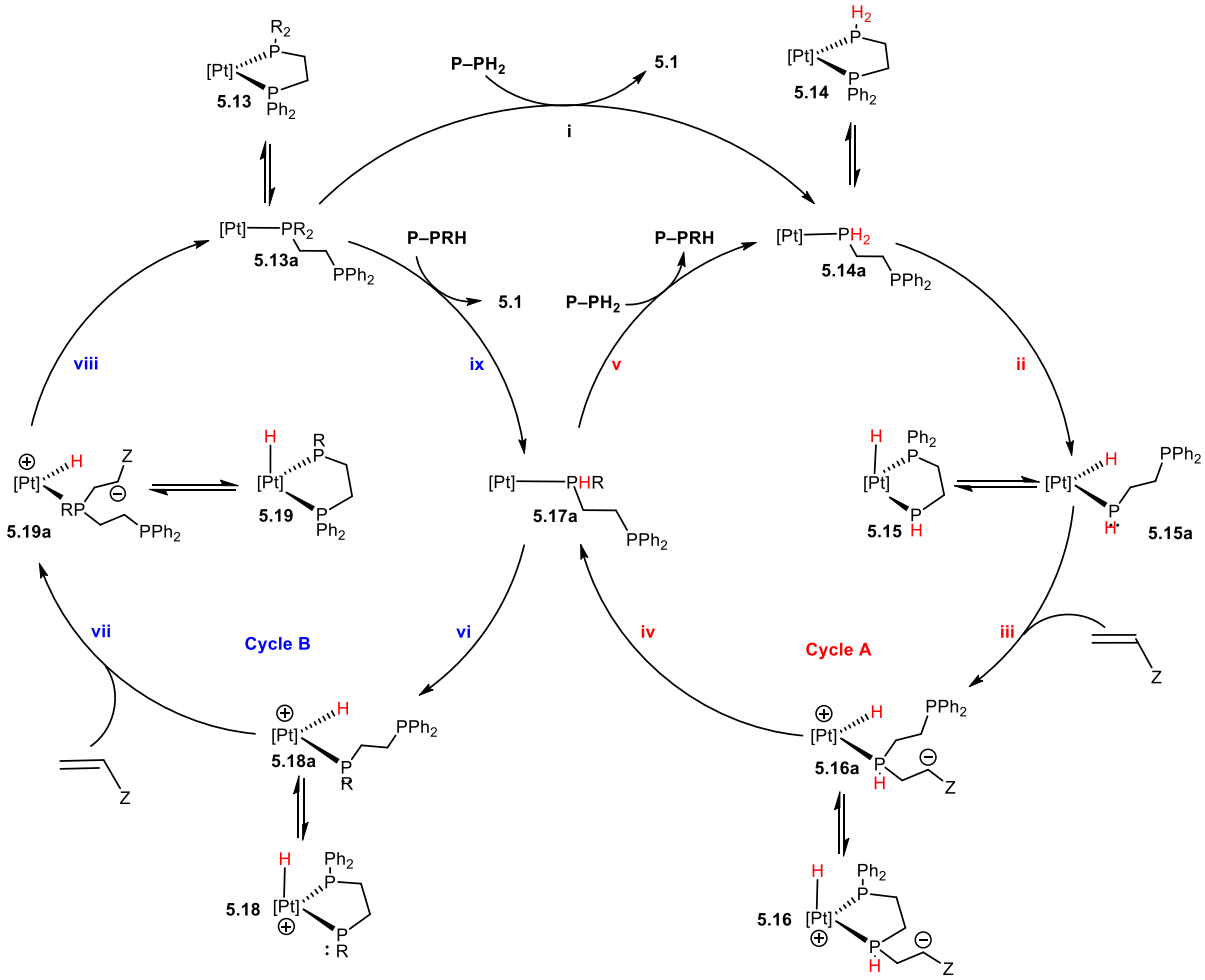

Scheme 5.22 Proposed mechanism for Pt(0)-catalysed hydrophosphination of methyl acrylate by **P-PH$_2$** to give intermediate **P-PHR** and final product **5.1** where R = $CH_2CH_2CO_2Me$.

5.9 Conclusions

It has been demonstrated that a range of functionalised bidentate phosphines such as **5.1** can be catalytically prepared from **P-PH$_2$** by a self-replication process in which a **5.1**-Pt unit acts as a template for the duplication of ligand **5.1**. The catalysis is remarkably efficient despite the expectation of inhibition of Pt(0) by chelating diphosphine products. This conundrum is addressed in the proposed mechanism for the reaction which involves ready interchange of 16- and 18-electron Pt(0) and Pt(II) species. This provides a rationale for labelling experiments which indicated the presence of a zwitterionic intermediate such as **5.1a**. The Pt(0) chemistry demonstrated the propensity to form bis-chelate **5.13** and the ability of substrate **P-PH$_2$** to displace it as shown by step i in the proposed mechanism. Kinetic observations indicate that it is likely there is an induction period at the start of the catalysis during which bis-chelate **5.13** is formed.

5.10 Future work

It would be of interest in future work to conduct more complex kinetic studies and to attempt to isolate proposed intermediates of the reactions, perhaps via stoichiometric reactions.

5.10.1 Investigation of the induction period

In preliminary studies the induction period of the catalysis has been investigated; 2 eq. **P-PH$_2$** was added to [Pt(nbe)$_3$] to form a bis-chelate of **P-PH$_2$** (Scheme 5.23).

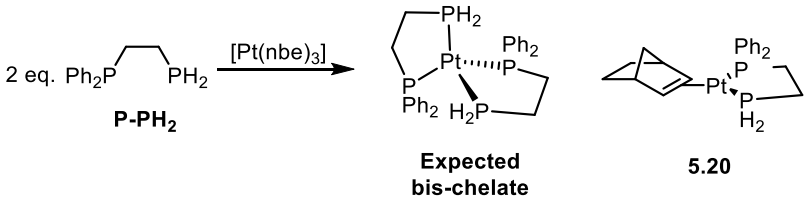

Scheme 5.23 Addition of **5.1** to [Pt(nbe)$_3$].

The *in situ* $^{31}P\{^1H\}$ NMR spectrum showed a broad signal (δ 40-65 ppm) and signals for **P-PH$_2$** (Figure 5.16). When another equivalent of [Pt(nbe)$_3$] was added the remaining ligand decreased suggesting mono-chelate complex **5.20** had formed.

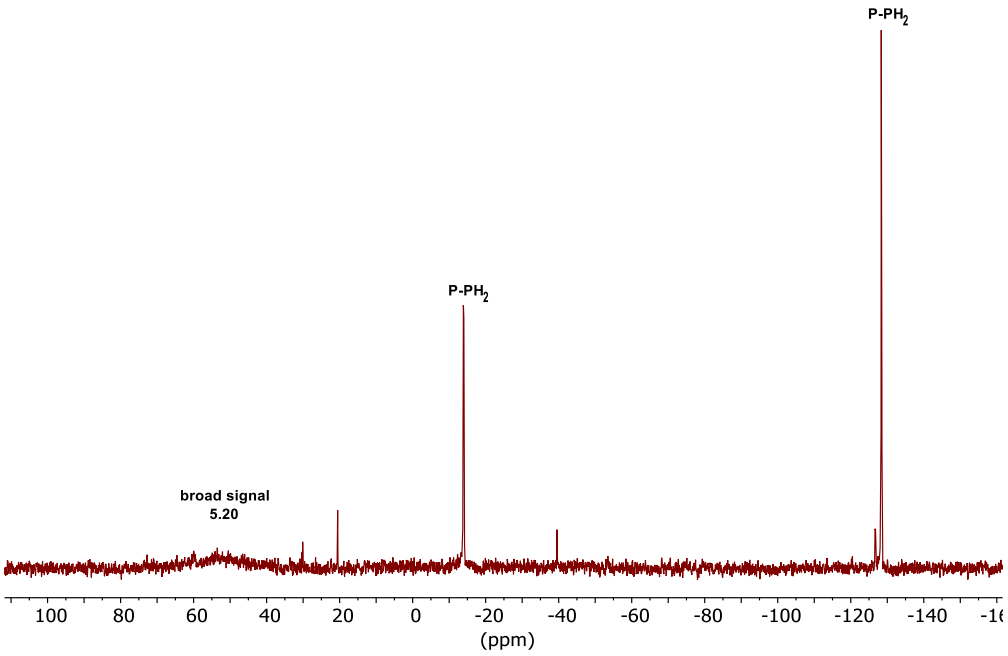

Figure 5.16 $^{31}P\{^1H\}$ NMR (122 MHz, MeCN) spectrum of the addition of **P-PH$_2$** to [Pt(nbe)$_3$].

Attempts to resolve the broad signal using low temperature NMR spectroscopy were unsuccessful. Addition of excess methyl acrylate did not change the $^{31}P\{^{1}H\}$ NMR spectrum, but additional peaks tentatively assigned to Pt(II) species were observed following the subsequent addition of 1 eq. **P-PH$_2$** (Figure 5.17).

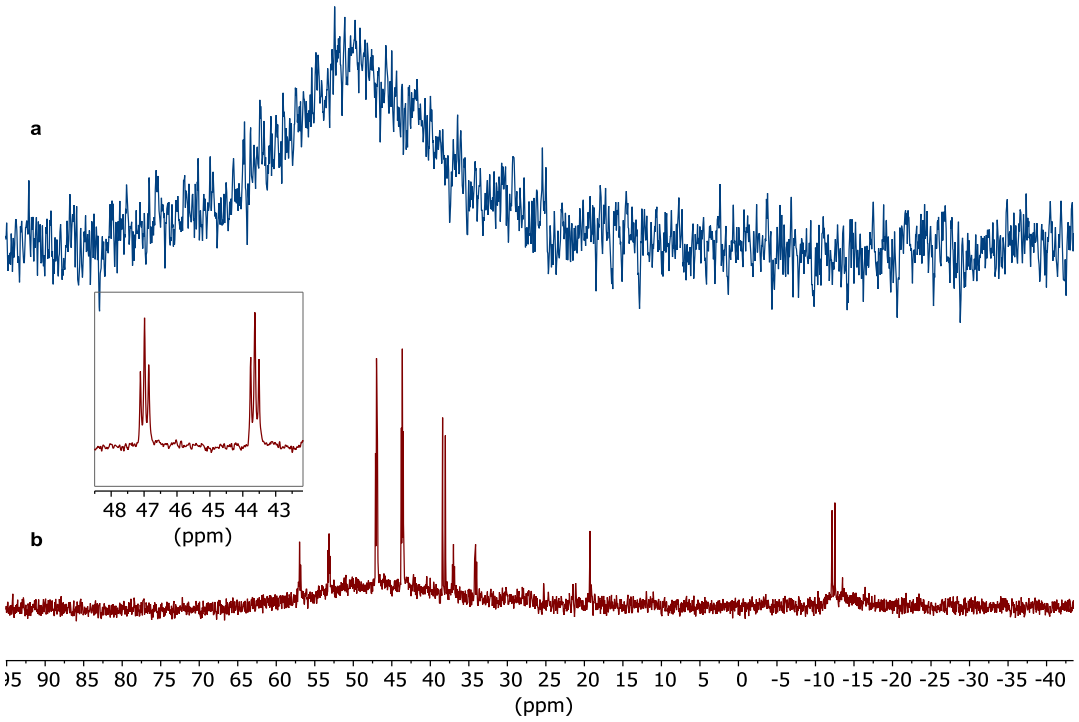

Figure 5.17 $^{31}P\{^{1}H\}$ NMR (122 MHz, MeCN) spectrum of (a) mono-chelate **5.20**; (b) the addition of **P-PH$_2$** to solution of mono-chelate **5.20** and methyl acrylate.

Further work should include full characterisation of proposed mono-chelate complex **5.20** as well as investigation into the formation of active catalyst **5.13**.

5.10.2 Computational studies

The mechanism of Pt(0)-catalysed hydrophosphination has not previously been studied computationally. It would be interesting to first probe the hydrophosphination mechanism proposed by Glueck *et al.* for monophosphine formation using a Pt(0)-stilbene catalyst precursor. The mechanism shown in Scheme 5.24 is supported by much empirical evidence and involves two pathways (a) and (b) which differ in the order of alkene coordination and P-H oxidative addition but coalesce at the isomeric intermediates **14-16**. Both reaction pathways could be studied by DFT calculations to give the relative energies of the species involved in order to decipher which pathway is more favourable. This work in in process in collaboration with Dr Natalie Fey.

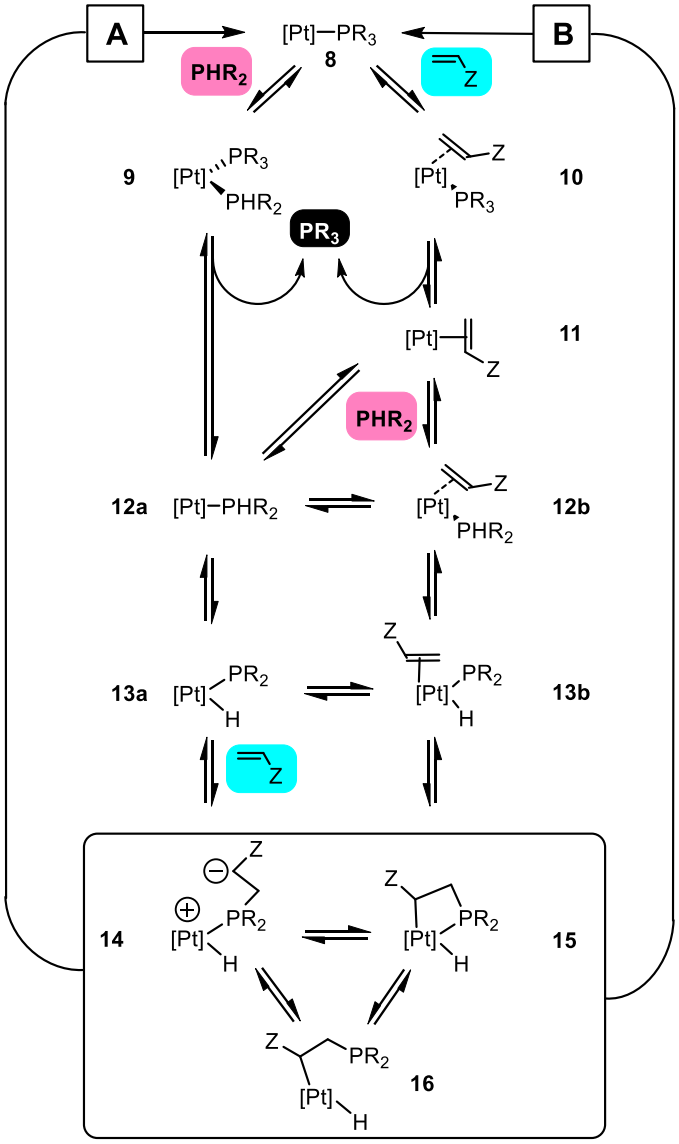

Scheme 5.24 Mechanism of Pt(0)-catalysed hydrophosphination of activated alkenes to give monophosphines. [Pt] = Pt(DuPhos); R = $CH_2CH_2CO_2Me$; Z = CO_2Me.

The mechanism for the diphosphine self-replication process shown in Scheme 5.22 (Section 5.8) is complicated by it being the product of two cycles but the proposed intermediates are related to those predicted for the monophosphine production. DFT calculations could be used to show which of the 16- and 18-electron isomers are more stable and the energy gaps between them in order to show if interchange between isomers is favourable at ambient temperatures.

5.10.3 Application of ligands to other catalysis

Ethylene bridged diphosphine ligands, including unsymmetrical diphos ligands have previously been used in a range of catalytic processes. Pringle *et al.* have shown that rhodium complexes of unsymmetrical ethylene diphos ligands are superior methanol carbonylation catalysts compared to dppe.[23] Diphosphines with a C_2-backbone have also been employed in enantioselective hydrogenation catalysis.[24] Rhodium complexes of (*S*,*S*)-Chiraphos were employed in asymmetric hydrogenation with great success by Bosnich *et al.* to obtain optically active amino acids.[25] Knowles revolutionised the commercial preparation of L-DOPA with the use of DiPAMP complexed to rhodium as a catalyst for asymmetric hydrogenation.[26,27] Additionally Burk *et al.* developed several rhodium complexes, including one based on a bidentate 2,5-disubstituted phospholane for use in enantioselective hydrogenation.[28]

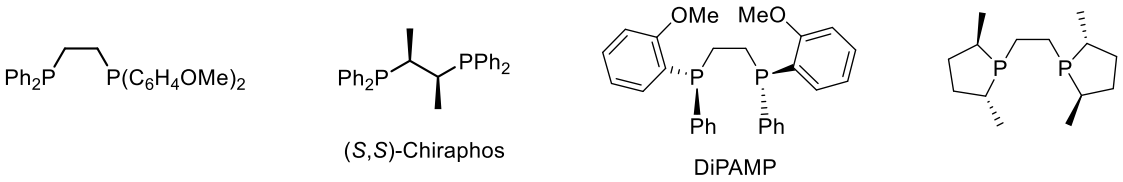

Nickel catalysed Suzuki-type cross-coupling of aryl meylates, tosylates, chlorides and bromides bearing electron-withdrawing and electron-donating substituents has been investigated using dppe as a ligand. Percec *et al.* showed that the dppe-containing catalyst exhibited high solvent-independent activity.[29]

It would be of interest to investigate the performance of the ligands synthesised in this chapter in catalytic processes e.g. asymmetric hydrogenation or carbonylation. Derivatives of such ligands by variation of the ethylene backbone or by introduction of chirality may make for an interesting comparison (examples below).

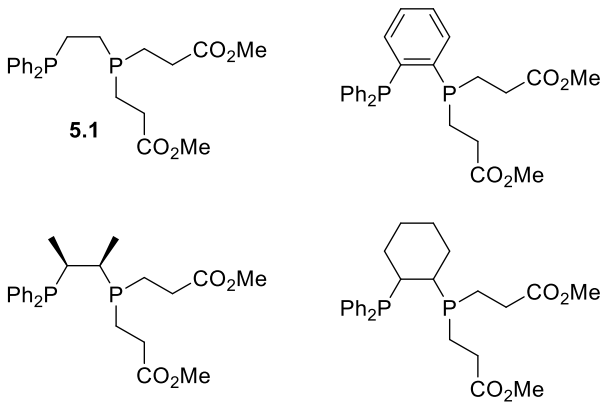

5.11 References

1 G. Clixby and L. Twyman, *Org. Biomol. Chem.*, 2016, **14**, 4170–4184.

2 T. Tjivikua, P. Ballester and J. Rebek, *J. Am. Chem. Soc.*, 1990, **112**, 1249–1250.

3 F. M. Menger, A. V Eliseev, N. A. Khanjin and M. J. Sherrod, *J. Org. Chem.*, 1995, **60**, 2870–2878.

4 E. A. Wintner, B. Tsao and J. Rebek, *J. Org. Chem.* 1995, 7997–8001.

5 D. N. Reinhoudt, D. M. Rudkevich and F. De Jong, *J. Am. Chem. Soc.*, 1996, **118**, 6880–6889.

6 K. Muñiz, *Adv. Synth. Catal.*, 2005, **347**, 275–281.

7 P. G. Pringle and M. B. Smith, *J. Chem. Soc. Chem. Commun.*, 1990, 1701–1702.

8 E. Costa, P. G. Pringle, B. Smith and K. Worboys, *J. Chem. Soc., Dalt. Trans.*, 1997, 4277–4282.

9 D. K. Wicht, I. V. Kourkine, B. M. Lew, J. M. Nthenge and D. S. Glueck, *J. Am. Chem. Soc.*, 1997, **119**, 5039–5040.

10 D. K. Wicht, I. V. Kourkine, I. Kovacik, D. S. Glueck, T. E. Concolino, G. P. A. Yap, C. D. Incarvito and A. L. Rheingold, *Organometallics*, 1999, **18**, 5381–5394.

11 C. Scriban, I. Kovacik and D. S. Glueck, *Organometallics*, 2005, **24**, 4871–4874.

12 C. Scriban, D. S. Glueck, L. N. Zakharov, W. S. Kassel, A. G. Dipasquale, J. A. Golen and A. L. Rheingold, *Organometallics*, 2006, **25**, 5757–5767.

13 E. S. Wiedner, J. A. S. Roberts, W. G. Dougherty, W. S. Kassel, D. L. Dubois and R. M. Bullock, *Inorg. Chem.*, 2013, **52**, 9975–9988.

14 G. Fries, J. Wolf, K. Ilg, B. Walfort, D. Stalke and H. Werner, *Dalt. Trans.*, 2004, 1873–1881.

15 A. Baber, J. G. de Vries, G. Orpen, P. G. Pringle and K. von der Luehe, *Dalton Trans.*, 2006, 4821–4828.

16 R. B. King and W. F. Masler, *J. Am. Chem. Soc.*, 1977, **99**, 4001–4008.

17 C. P. Casey, E. L. Paulsen, E. W. Beuttenmueller, B. R. Proft, B. A. Matter and D. R. Powell, *J. Am. Chem. Soc.*, 1999, **121**, 63–70.

18 N. Kapoor, D. D. Pathak, G. Gaur and M. Kutty, *J. Organomet. Chem.*, 1984, **276**, 167–170.

19 M. R. Eberhard, E. Carrington-Smith, E. E. Drent, P. S. Marsh, A. G. Orpen, H. Phetmung and G. Pringle, *Adv. Synth. Catal.*, 2005, **347**, 1345–1348.

20 T. J. Cunningham, M. R. J. Elsegood, P. F. Kelly, M. B. Smith and P. M. Staniland, *Eur. J. Inorg. Chem.*, 2008, 2326–2335.

21 D. H. Farrar and G. Ferguson, *J. Crystallogr. Spectrosc. Res.*, 1982, **12**, 465–471.

22 E. Costa, P. G. Pringle, B. Smith and K. Worboys, *J. Chem. Soc., Dalt. Trans.*, 1997, 4277.

23 C. A. Carraz, E. J. Ditzel, A. G. Orpen, D. D. Ellis, P. G. Pringle and G. J. Sunley, *Chem. Commun.*, 2000, **2**, 1277–1278.

24 I. D. Gridnev, M. Yasutake, N. Higashi and T. Imamoto, *J. Am. Chem. Soc.*, 2001, **123**, 5268–5276.

25 M. D. Fryzuk and B. Bosnich, *J. Am. Chem. Soc.*, 1977, **99**, 6262–6267.

26 B. D. Vineyard, W. S. Knowles, M. J. Sabacky, G. L. Bachman and D. J. Weinkauff, *J. Am. Chem. Soc.*, 1977, **99**, 5946–5952.

27 W. S. Knowles, *J. Chem. Educ.*, 2009, **63**, 222.

28 M. J. Burk, J. E. Feaster and R. L. Harlow, *Organometallics*, 1990, **9**, 2653–2655.

29 V. Percec, G. M. Golding, J. Smidrkal and O. Weichold, *J. Org. Chem.*, 2004, **69**, 3447–3452.

Chapter 6

Experimental

6.1 General

All reactions were carried out under a pre-purified nitrogen atmosphere, unless otherwise stated, using standard Schlenk line techniques. All air and moisture sensitive compounds were manipulated and stored in an Ar-atmosphere glovebox. CH_2Cl_2, toluene, THF, diethyl ether and MeCN were dried by Grubbs-type solvent purification system with activated alumina columns and deoxygenated by bubbling with N_2 for 20 min. Diphenylphosphine was distilled before use. All phosphines used were quenched using bleach. [Pt(nbe)$_3$] was synthesised according to literature methods and stored in an Ar-atmosphere glovebox.[1] Bottled CD_2Cl_2, *d*-MeCN and d_8-toluene were purchased from Sigma-Aldrich and stirred with calcium hydride overnight, distilled, deoxygenated by 3 freeze-pump-thaw cycles and stored over 3 Ångstrom molecular sieves. Technetium-99m and was provided by Guy's hospital radiopharmacy as pertechnetate. Copper-64 was also provided by Guy's hospital as an HCl solution. Cyclic-RGDfK peptide was purchased from Peptide Protein Research LTD. Balb/c mice (female, 71-77 days) were provided by Charles River, UK. Other commercial reagents and chemicals were used without further purification unless otherwise stated.

^{1}H, ^{13}C ^{31}P and ^{135}Pt NMR spectra were recorded on Jeol ECP(Eclipse) 300, Jeol ECS 300, Jeol ECS 400, Bruker AV400 or Bruker cryo500 spectrometers. Chemical shifts (δ) are reported in parts per million (ppm) and coupling constants (J) in Hz. Chemical shifts for ^{31}P NMR spectra are reported relative to 85% H_3PO_4 as an external standard. Mass spectra were obtained by the University of Bristol Mass Spectrometry Service using an EI (VG/Micromass Autospec) or ESI (Bruker Daltonics micrOTOF II) spectrometer. Mass spectra obtained from King's College London used an Advion Expression Compact Mass Spectrometer with an ESI probe. X-ray crystallography data were obtained using a Bruker Kappa Apex II diffractometer (see Section 6.5).

Semipreparative and Analytical HPLC purifications were performed using an Agilent 1200 series HPLC system with Laura software, UV detection at 220 nm, a Rheodyne sample loop (200 μL) and a LabLogic Flow-Count radiation detector. Solvent gradient and specifications are described below. Reverse-phase HPLC method 1 employed an Eclipse XDB-C18 5 μm 4.6 x 150 mm column with a flow rate of 3 mL min^{-1}. The gradient mobile phase started with 100% solvent A (0.1% trifluoroacetate in water) at 1 min to 100% solvent B (0.1% trifluoroacetate in acetonitrile) at 120 min. Method 2 employed an

Eclipse XDB-C18 5 μm 4.6 x 150 mm column with a flow rate of 1 mL min^{-1}. The gradient mobile phase started with 100% solvent A (0.1% trifluoroacetate in water) at 1 min to 100% solvent B (0.1% trifluoroacetate in acetonitrile) at 30 min.

6.2 Experimental procedures and characterising data for Chapter 2 – Synthesis, coordination and ^{99m}Tc-radiolabelling of tetrofosmin-like ligands

6.2.1 Synthesis of $PPh_2CH_2CH_2P(O)(OEt)_2$

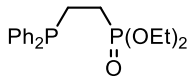

The synthesis of **P-P(O)(OEt)$_2$** was based on a method reported by Wiedner et al.[2]

^{31}P{^{1}H} NMR (162 MHz, $CDCl_3$): δ 31.7 (d, $^3J_{PP}$ = 63.1 Hz, *P*O(OEt)$_2$), -12.3 (d, $^3J_{PP}$ = 63.1 Hz, *P*Ph$_2$). **^{1}H NMR** (301 MHz, $CDCl_3$): δ 7.38-7.12 (m, 10H, Ar-*H*) 3.97-3.85 (m, 4H, CH_2), 2.21 – 2.06 (m, 2H, CH_2), 1.71 – 1.50 (m, 2H, CH_2), 1.14 (t, 6H, $^3J_{HH}$ = 7.1 Hz, CH_3).

6.2.2 Synthesis of $PPh_2CH_2CH_2PH_2$, P-PH_2

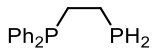

The synthesis of **P-PH$_2$** was based on a method reported by Wiedner et al.[2]

^{31}P{^{1}H} NMR (162 MHz, CD_2Cl_2): δ -14.8 (d, $^3J_{PP}$ = 15.0 Hz, *P*Ph$_2$), -131.3 (d, $^3J_{PP}$ = 15.0 Hz, *P*H$_2$). **^{1}H NMR** (CD_2Cl_2): δ 7.41 (m, 4H, Ar-H), 7.34 (m, 6H, Ar-H), 2.84 (dt, 2H, $^1J_{PH}$ = 194 Hz, $^3J_{HH}$ = 7.2 Hz, PH$_2$), 2.26 (m, 2H, CH_2), 1.58 (m, 2H, CH_2). **^{13}C{^{1}H} NMR** (100 MHz, CD_2Cl_2): δ 138.5 (d, $^2J_{PC}$ = 14 Hz, Ar-C), 132.7 (d, $^1J_{PC}$ = 19 Hz, PC), 128.7 (s, Ar-C), 128.5 (d, $^3J_{PC}$ = 6.4 Hz, Ar-C), 31.5 (dd, $^1J_{PC}$ =15 Hz, $^2J_{PC}$ = 3.1 Hz, CH_2), 10.5 (dd, $^1J_{PC}$ = 17 Hz, $^2J_{PC}$ = 9.8 Hz, CH_2).

6.2.3 Synthesis of $PPh_2CH_2CH_2P(CH_2CH_2CO_2Me)_2$, 2.2

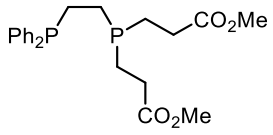

To a solution of $Ph_2PCH_2CH_2PH_2$ (**P-PH$_2$**) (100 mg, 0.41 mmol) in CH_2Cl_2 (2.00 mL) was added [Pt(nbe)$_3$] (9.00 mg, 0.0200 mmol) and stirred at room temperature for 10 min to afford a deep orange solution. *t*BuOH (8.10 mmol, 0.800 mL) was added, then methyl acrylate (0.073 mL, 0.81 mmol) was added dropwise and the mixture was left to stir for 2 h at room temperature. The reaction mixture was passed through a silica plug and the filtrate concentrated to dryness to give **L1** as a colourless oil (122 mg, 72%).

$^{31}P\{^{1}H\}$ NMR (162 MHz, CD_2Cl_2): δ -12.8 (d, $^{3}J_{PP}$ = 29.0 Hz, PPh$_2$), -20.7 (d, $^{3}J_{PP}$ = 28.0 Hz, P(CH$_2$CH$_2$CO$_2$Me)$_2$). **^{1}H NMR** (400 MHz, CD_2Cl_2): δ 7.44-7.38 (m, 4H, Ar-H), 7.38-7.30 (m, 6H, Ar-H), 3.63 (s, 6H, CO_2CH_3), 2.39-2.30 (m, 4H, CH_2), 2.16-2.08 (m, 2H, CH_2), 1.72-1.66 (m, 4H, CH_2), 1.51-1.43 (m, 2H, CH_2). **$^{13}C\{H\}$ NMR** (100 MHz, CD_2Cl_2): δ 173.4 (d, J = 11.7 Hz, CO_2Me), 138.5 (d, J = 14.4 Hz, Ar-C), 132.6 (d, J = 18.6 Hz, Ar-C), 128.7 (s, Ar-C), 128.4 (d, J = 6.6 Hz, Ar-C), 51.5 (s, CH_3) 30.3 (d, J = 16.6 Hz, CH_2), 23.5 (m, CH_2), 22.2 (t, J = 15.6 Hz, CH_2), 21.2 (d, J = 14.7 Hz, CH_2). **ESI+** m/z calcd. for $C_{22}H_{29}O_4P_2$([M + H]$^+$) = 419.1541; obs. = 419.1540.

6.2.4 Synthesis of PPh$_2$CH$_2$CH$_2$P(CH$_2$CH$_2$CO$_2$Na)$_2$, 2.3

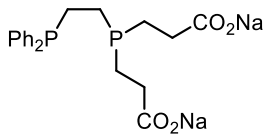

To a solution of Ph$_2$PCH$_2$CH$_2$P(CH$_2$CH$_2$CO$_2$Me) (849 mg, 2.03 mmol) in degassed MeOH/H$_2$O (10 mL/10 mL) was added sodium hydroxide (162 mg, 4.06 mmol) at room temperature and stirred for 16 h. The solvent was removed *in vacuo* to yield the title product as a white crystalline solid (700 mg, 79%).

$^{31}P\{^{1}H\}$ NMR (162 MHz, CD_3OD): δ -12.4 (d, $^{3}J_{PP}$ = 26.9 Hz), -22.5 (d, $^{3}J_{PP}$ = 26.9 Hz). **^{1}H NMR** (400 MHz, CD_3OD): δ 7.44-7.39 (m, 4H, Ar-H), 7.36-7.30 (m, 6H, Ar-H), 2.27-2.14 (m, 6H, CH_2), 1.77-1.68 (m, 4H, CH_2), 1.50-1.42 (m, 2H, CH_2). **^{13}C NMR** (162 MHz, CD_3OD): δ 182.2 (d, C=O), 139.9 (d, Ar-C), 133.8 (d, Ar-C), 129.6 (d, Ar-C), 35.1 (d, CH_2), 24.6 (t, CH_2), 24.4 (d, CH_2), 23.3 (t, CH_2). **ESI+** m/z calcd. for $C_{20}H_{22}O_4P_2Na_3$ ([M + Na]$^+$) = 457.1; obs. = 457.1.

6.2.5 Synthesis of Ph(H)PCH$_2$CH$_2$CH$_2$CH$_2$CH$_2$CO$_2$H, 2.4

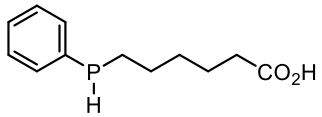

A mixture of phenylphosphine (300 mg, 2.73 mmol), AIBN (112 mg, 0.680 mmol) and hex-5-enoic acid (0.320 mL, 2.73 mmol) in toluene (2.00 mL) were stirred at 70 °C for 16 h. Volatiles were removed *in vacuo* and the resulting compound left under vacuum on the Schlenk line for 2 h. A crude mixture including the title compound was afforded as a

cloudy, viscous oil (306 mg, 50%) and taken through to the next step without further purification.

$^{31}P\{^{1}H\}$ NMR (162 MHz, C_6H_6): δ -51.9 (s) (title compound, 53% by integration), -25.7 (s) (bis-substituted product).

6.2.6 Synthesis of $Ph_2PCH_2CH_2P(Ph)(CH_2CH_2CH_2CH_2CH_2CO_2H)$, 2.5

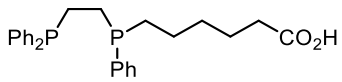

To a solution of crude 6-(phenylphosphaneyl)hexanoic acid (290 mg, 1.29 mmol), AIBN (53 mg, 0.32 mmol) in toluene (2 mL) was added diphenylvinylphosphine (0.260 mL, 1.29 mmol) dropwise at 70 °C. The mixture was stirred for 3h, cooled to rt and the volatiles removed *in vacuo*. The crude oil was purified by column chromatography (60/40 hexane/EtOAc) to afford the title product as a colourless oil (366 mg, 65%).

$^{31}P\{^{1}H\}$ NMR (162 MHz, C_6D_6): δ -12.3 (d, 28.2 Hz), -20.5 (d, 28.2 Hz). **^{1}H NMR** (301 MHz, CD_2Cl_2): δ 11.1 (s, 1H, CO_2H), 7.48-7.29 (m, 15H, Ar-H), 2.30 (t, 2H, CH_2), 2.15-1.95 (m, 2H, CH_2), 1.79-1.65 (m, 4H, CH_2), 1.63-1.54 (m, 2H, CH_2), 1.44-1.28 (m, 4H, CH_2). **ESI- *m/z*** calcd. For $C_{26}H_{30}O_2P_2$ ($[M - H]^-$) = 435.16; obs. = 435.2

6.2.7 Synthesis of $(CH_2CH_2CO_2{}^tBu)_2PCH_2CH_2P(CH_2CH_2CO_2{}^tBu)_2$, 2.6

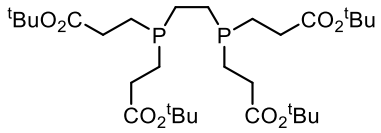

To a solution of $PH_2CH_2CH_2PH_2$ (200 mg, 0.640 mmol) in CH_2Cl_2 (10.0 mL) was added [Pt(nbe)$_3$] (20.0 mg, 0.0420 mmol) and was left to stir for 10 min to afford a deep orange solution. ^{t}BuOH (2.00 mL, 42.4 mmol,) was added and the solution was cooled in an ice bath. Tert-Butyl acrylate (1.20 mL, 8.48 mmol) was added dropwise and the mixture was left to stir at room temperature for 90 min. The solution was passed through a silica plug and the filtrate concentrated to dryness to give the title compound as a colourless oil. A yield could not be recorded as the product co-evaporated with the reaction solvent.

$^{31}P\{^{1}H\}$ NMR (162 MHz, CD_2Cl_2): δ -22.9 (s). **^{1}H NMR** (400 MHz, CD_2Cl_2): δ 2.31 (m, 8H, CH_2), 1.66 (m, 8H, CH_2), 1.48 (m, 4H, CH_2), 1.43 (s, 9H, OCH_3). **$^{13}C\{^{1}H\}$ NMR** (162

MHz, CD_2Cl_2): δ 172.8 (CO), 80.8 ($C(CH_3)_3$), 28.4 (CH_3), 32.27 (CH_2), 22.93 (CH_2), 22.2 (CH_2).

6.2.8 Synthesis of [Pt(2.6)Cl_2], 2.7

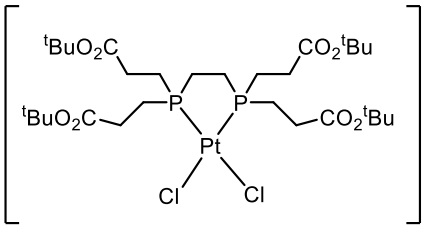

$Ph_2PCH_2CH_2P(CH_2CH_2CO_2{}^tBu)_2$ (40.0 mg, 0.066 mmol) and [Pt(cod)Cl_2] were stirred in DCM (1.00 mL) for 1h at room temperature. Hexane (2.00 mL) was added and the white precipitate washed with further hexane (2 x 2.00 mL) and dried to give the title compound. Crystals suitable for X-ray crystallography were obtained *via* vapour diffusion recrystallization from DCM and hexane.

$^{31}P\{^1H\}$ NMR (121 MHz, CH_2Cl_2): δ 51.6 (s, $^1J_{PtP}$ 3520 Hz).

6.2.9 Synthesis of [Re(O)$_2$(2.2)$_2$]I, 2.9 and 2.10

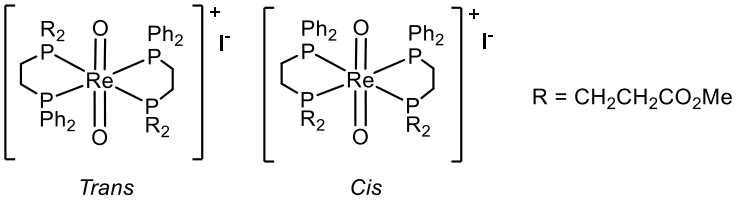

To a solution of [$ReIO_2(PPh_3)_2$] (25.0 mg, 0.0290 mmol) in CH_2Cl_2 (2.00 mL) was added **2.2** (24.0 mg, 0.0570 mmol). The solution turned from violet to dark orange and was left to stir for 10 min. The solution was concentrated to dryness and the resulting dark yellow precipitate was washed sequentially with pentane (3 x 1.00 mL) and toluene (3 x 1.00 mL). The product was obtained as mixture of *trans* and *cis* isomers. Yellow crystals of the *trans* complex suitable for X-ray crystallography were obtained *via* vapour diffusion recrystallization from methanol and pentane (0.0260 g, 85%).

$^{31}P\{^1H\}$ NMR (162 MHz, CD_2Cl_2): δ 11.6 (m, Re-PPh_2), 9.0 (m, Re-$P(CH_2CH_2CO_2Me)_2$). **^1H NMR** (400 MHz, CD_2Cl_2): δ 7.68 (m, 8H, Ar-H), 7.58 (m, 4H, Ar-H), 7.51 (m, 8H, Ar-H), 3.55 (s, 12H, CH_3), 2.73 (m, 4H, Ph_2PCH_2), 2.30 (m, 8H, $CH_2CH_2CO_2Me$), 2.01

(m, 8H, $CH_2CH_2CO_2Me$), 1.69 (m, 4H, $Ph_2PCH_2CH_2P$). **ESI+** ***m/z*** calcd. for $C_{44}H_{56}O_{10}P_4Re$ ($[M + H]^+$) = 1054.6; obs. = 1055.2.

6.2.10 Synthesis of $[Re(O)_2(2.3)_2]I$, 2.11 and 2.12

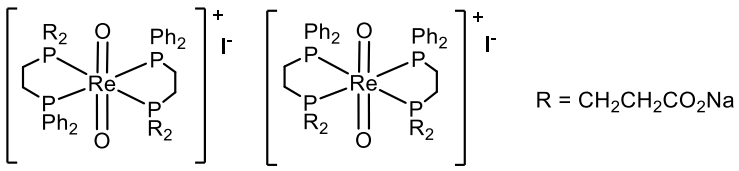

Trans **2.11** *Cis* **2.12**

To a solution of $[ReIO_2(PPh_3)_2]$ (52.0 mg, 0.0590 mmol) in CH_2Cl_2 (3.00 mL) was added **2.3** (50.0 mg, 0.12 mmol). The solution turned from violet to clear yellow and was left to stir for 2 h. The solution was concentrated to dryness and the resulting dark yellow precipitate was washed sequentially with diethyl ether (3 x 1.00 mL). The mixture of *trans* and *cis* isomers was separated by preparative HPLC and characterised separately.

Trans isomer, **2.11**

$^{31}P\{^1H\}$ NMR (121 MHz CD_3OD): δ 14.25 (d, $^3J_{PP}$ = 352 Hz), 9.70 (d, $^3J_{PP}$ = 352 Hz). **^1H NMR** (500 MHz CD_3OD): δ 7.41 (t, 4H, Ar-H), 7.25 (m, 16H, Ar-H), 2.88-2.73 (m, 8H, CH_2), 2.73-2.63 (m, 4H, CH_2), 2.62-2.46 (m, 8H, CH_2), 2.35-2.24 (m, 4H, CH_2). **$^{13}C\{^1H\}$ NMR** (125 MHz, CD_3OD): δ 174.9 (m, C=O), 133.1 (d, Ar-C), 131.3 (s, Ar-C), 128.5 (d, Ar-C), 2.8. (s, CH_2), 26.3 (s, CH_2), 22.2 (s, CH_2), 19.7 (s, CH_2). **ESI+** ***m/z*** calcd. for $C_{40}H_{44}O_{10}P_4ReINa_4$ ($[M + Na]^+$) 1236.9970; obs. = 1236.9942.

Cis isomer, **2.12**

$^{31}P\{^1H\}$ NMR (121 MHz CD_3OD): δ 11.2 (dt, $^3J_{PP}$ = 271.9 Hz). **^1H NMR** (500 MHz CD_3OD): δ 7.81-7.75 (m, 8H, Ar-H), 7.64-7.53 (m, 12H, Ar-H), 2.96-2.85 (m, 4H, CH2), 2.49-2.38 (4H, CH_2), 2.30-2.20 (m, 4H, CH_2), 2.18-2.04 (m, 8H, CH_2), 1.83-1.73 (m, 4H, CH_2). **$^{13}C\{^1H\}$ NMR** (125 MHz, CD_3OD): δ 175.0 (t, C=O), 134.5 (t, Ar-C), 133.5 (s, Ar-C), 130.7 (s, Ar-C), 130.5 (t, Ar-C), 31.5 (m, CH_2), 28.6 (s, CH_2), 22.1 (m, CH_2), 21.1 (t, CH_2). **ESI+** ***m/z*** calcd. for $C_{40}H_{44}O_{10}P_4ReINa_4$ ($[M + Na]^+$) 1236.9970; obs. = 1236.9942.

6.2.11 Synthesis of [Re(2.3)(CO)$_3$Br], 2.13

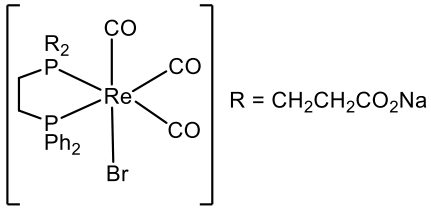

To a solution of **2.3** (20.0 mg, 0.0460 mmol) in MeOH (1.00 mL) was added [Re(CO)$_3$(H$_2$O)$_3$]Br (19.0 mg, 0.0460 mmol) and stirred at room temperature for 1 h. The solvent was removed in vacuo and the resultant white solid washed with pentane (2 x 1.00 mL) to give the title product as a white solid (23.0 mg, 64%).

^{31}P{^{1}H} NMR (121 MHz CH_3OH): δ 41.8 (d, $^3J_{PP}$ = 5.8 Hz), 37.49 (d, $^3J_{PP}$ = 5.8 Hz). **ESI+ *m/z*** calcd. for $C_{23}H_{23}BrNa_2O_7P_2Re$ ($[M + H]^+$) 784.95; obs. = 784.91.

6.2.12 Synthesis of Ph$_2$PCH$_2$CH$_2$P(CH$_2$CH$_2$CO$_2$NHS), 2.14

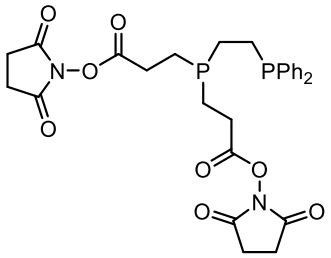

To a solution of **2.3** (30.0 mg, 0.0690 mmol) in DMF (2.50 mL) was added diisopropylcarbodiimide (0.120 mL, 0.690 mmol) and *N*-hydroxysuccinimide (80.0 mg, 0.690 mmol) and stirred for 48 h. The product was used without purification.

ESI+ *m/z* calcd. for $C_{22}H_{31}N_2O_8P_2$ ($[M + H]^+$) 585.1; obs. = 584.9.

6.2.13 Synthesis of $Ph_2PCH_2CH_2P(CH_2CH_2CO_2RGD)$, 2.15

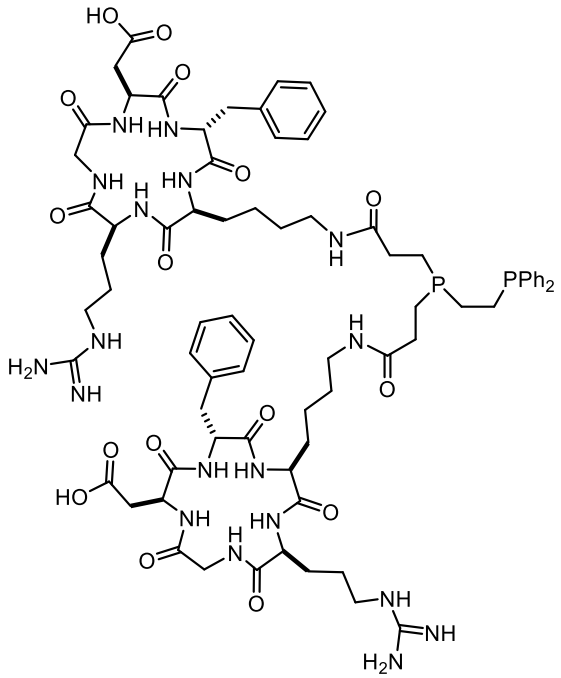

To a solution of **2.14** (3.00 mg, 0.00500 mmol) in DMF (1.00 mL) was added DIPEA (0.0200 mL, 0.0200 mmol) and cRGDfK peptide (12.0 mg, 0.0200 mmol) and stirred at room temperature for 16 h. The product was purified by HPLC; MeCN/H_2O (50/50) (0.2 mL) was added and the solution applied to a C18 semipreparative column and separated using reverse-phase HPLC column chromatography method 1. Fractions containing pure material were combined and freeze-dried. **2.15** eluted at 32 min.

ESI+ ***m/z*** calcd. for $C_{74}H_{103}N_{18}O_{16}P_2$ ($[M + H]^{2+}$) 781.9; obs. = 781.8.

6.2.14 Synthesis of ^{99m}Tc complexes

Kits for radiolabelling were prepared according to Tables 6.1-6.3 below. Kits were prepared with standard solutions of each kit component, dissolved in purified water or ethanol and freeze-dried immediately to yield colourless solids that were stored at -20 °C prior to use.

Formation of ^{99m}Tc complexes was achieved by radiolabelling a thawed kit with 300 μL [^{99m}Tc]pertechnetate saline solution (20-50 MBq) and ethanol (50:50). The reconstituted kit was incubated at 60 °C or room temperature for 30 min or 1 h. Sample aliquots were analysed by analytical HPLC (method 2, 10-30 μL).

Table 6.1 Kit preparation for diester ligand **2.2**.

Kit	Ligand (μmol)	Disodium sulphosalicylate (μmol)	Weak chelator (μmol)	Sodium hydrogen carbonate (μmol)	Stannous chloride dihydrate (μmol)	Final volume
EAC1	0.65	1.30	A - 4.60	20.7	0.26	1.0 mL
EAC2	0.65	0	A - 4.60	20.7	0.26	1.0 mL
EAC3	0.65	0	B - 3.60	20.7	0.26	1.0 mL
EAC4	0.27	0	A - 4.60	20.7	0.13	1.0 mL
EAC5	0.27	0	B - 3.60	20.7	0.13	1.0 mL

A = sodium d-gluconate, B = tartrate

Table 6.2 Kit preparation for dicarboxylate ligand **2.3**.

Kit	Ligand (μmol)	Disodium sulphosalicylate (μmol)	Weak chelator (μmol)	Sodium hydrogen carbonate (μmol)	Stannous chloride dihydrate (μmol)	Final volume
SAC1	0.65	1.30	A - 4.60	20.7	0.26	1.0 mL
SAC2	0.65	0	A - 4.60	20.7	0.26	1.0 mL
SAC3	0.65	0	B - 3.60	20.7	0.26	1.0 mL
SAC4	0.27	0	A - 4.60	20.7	0.13	1.0 mL
SAC5	0.27	0	B - 3.60	20.7	0.13	1.0 mL

A = sodium d-gluconate, B = tartrate

Table 6.3 Kit preparation for monocarboxylate ligand **2.5**.

Kit	Ligand (μmol)	Disodium sulphosalicylate (μmol)	Weak chelator (μmol)	Sodium hydrogen carbonate (μmol)	Stannous chloride dihydrate (μmol)	Final volume
LAC1	0.65	1.30	A - 4.60	20.7	0.26	1.0 mL
LAC2	0.65	1.30	B - 3.60	20.7	0.26	1.0 mL

A = sodium d-gluconate, B = tartrate

6.3 Experimental procedures and characterising data for Chapter 3 – Synthesis, coordination and ^{64}Cu-radiolabelling of anhydride diphos ligands

6.3.1 Synthesis of diphenylphosphino anhydride diphos, 3.1

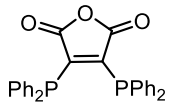

To a solution of diphenylphosphine (0.880 mL, 5.04 mmol) and triethylamine (0.700 mL, 5.04 mmol) in ditheyl ether (10.0 mL) was added 2,3-dichloromaleic anhydride (401 mg, 2.40 mmol) and stirred at room temperature for 2 h. Th yellow precipitate was filtered by Büchner filtration and washed 3 times with cold diethyl ether (3 x 5.00 mL). The solid was then passed through a silica plug with DCM and the solvent then removed *in vacuo* to give the title product as a yellow/orange solid (0.802 g, 76%).

^{31}P{^{1}H} NMR ($CDCl_3$, 162 MHz): δ -20.5 (s). **^{1}H NMR** ($CDCl_3$, 400 MHz): δ 7.4 – 7.25 (m).**^{13}C{^{1}H} NMR** ($CDCl_3$ 101 MHz): δ 162.6 (s, CO), 134.2 (t, C=C), 132.2 (s, Ar-C), 130.0 (s, Ar-C), 128.9 (t, Ar-C). **ESI+ *m/z*** calcd. for $[C_{28}H_{20}O_3P_2]^+$ = 467.09, obs. = 467.1.

6.3.2 Synthesis of dicyclohexylphosphino anhydride diphos, 3.2

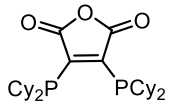

To a solution of dicyclohexylphosphine (0.550 mL, 2.52 mmol) and triethylamine (0.350 mL, 2.52 mmol) in THF (5.00 mL) was added 2,3-dichloromaleic anhydride (191 mg, 1.15 mmol) and stirred at room temperature for 2 h. The solution was filtered and distilled (150 ^{o}C, x 10^{-5} Torr) to afford the title product as an orange solid (500 mg, 89%). Orange crystals suitable for X-ray crystallography were grown from slow evaporation of a THF solution.

^{31}P{^{1}H} NMR (162 MHz, C_6H_6): δ -13.1 (s). **^{1}H NMR** (301 MHz, C_6H_6): δ 2.52 (m, 4H, CH), 1.89-1.00 (m, 40H, CH_2). **^{13}C{^{1}H} NMR** (101 MHz, d^8-THF): δ 164.5 (s, CO), 161.9 (s, C=C), 34.8 (t, CH_2), 31.9 (m, CH), 27.9 (m, CH_2), 27.2 (s, CH_2). **ESI+ *m/z*** calcd. for $C_{28}H_{44}O_3P_2$ ($[M + H]^+$) = 491.28; obs. = 491.28.

6.3.3 Synthesis of [Pt(3.2)Cl_2], 3.5

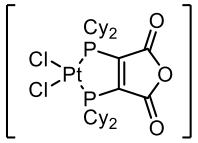

To a solution of dicyclohexylphosphino anhydride, **3.2** (20.0 mg, 0.0400 mmol) in DCM (1.00 mL) was added [Pt(cod)Cl_2] (11.0 mg, 0.0300 mmol) and stirred at room temperature for 2 h. The insoluble white precipitate was filtered to give the title product (15.0 mg, 66%).

$^{31}P\{^1H\}$ NMR (162 MHz, CH_2Cl_2): δ 110.6 (s, $^1J_{PtP}$ = 3953.3 Hz). **ESI+ *m/z*** calcd. for $C_{28}H_{44}Cl_2NaO_3P_2Pt$ ($[M + Na]^+$) = 778.17; obs. = 778.19.

6.3.4 Synthesis of diisobutylphosphino anhydride, 3.6

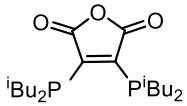

To a solution of diisobutylphosphine (0.200 mL, 1.33 mmol) and triethylamine (0.190 mL, 1.33 mmol) in THF (4.00 mL) was added 2,3-dichloromaleic anhydride (100 mg, 0.600 mmol) and stirred at room temperature for 2 h. The solution was filtered, and the solvent removed *in vacuo* to give an orange solid. No further purification was attempted.

$^{31}P\{^1H\}$ NMR (162 MHz, CH_2Cl_2): δ -43.4 (s). **ESI+ *m/z*** calcd. for $C_{20}H_{37}O_3P_2$ ($[M + Na]^+$) = 387.1; obs. = 387.0.

6.3.5 Synthesis of [Cu(3.2)$_2$]I, 3.7

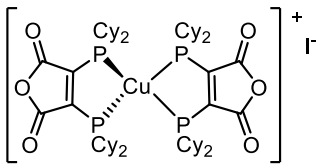

To a solution of **3.2** (20.0 mg, 0.0410 mmol) in MeCN (1.00 mL) was added [CuI] (12.0 mg, 0.0620) and stirred at room temperature for 1 h. The solution was filtered and the solid washed with MeCN and hexane to give the title product as a grey solid (11.0 mg,

23%). Blue crystals suitable for X-ray crystallography were grown from slow evaporation of a methanol solution.

$^{31}P\{^{1}H\}$ NMR (162 MHz, CH_2Cl_2): δ -16.9 (br. s). **ESI+ *m/z*** calcd. for $C_{56}H_{89}Cu_2I_2O_6P_4$ ($[M + H]^+$) = 1361.22; obs. = 1362.4.

6.3.6 Synthesis of [Ag(3.2)(H_2O)]Br, 3.13

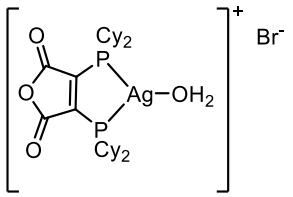

To a solution of **3.2** (30.0 mg, 0.0610 mmol) in MeCN (1.00 mL) was added [AgBr] (11.5 mg, 0.0610 mmol) and stirred at room temperature for 2 h. The suspension was filtered, and the solvent removed *in vacuo* to give the title product as an orange oil (32.0 mg, 77%).

$^{31}P\{^{1}H\}$ NMR (162 MHz, MeCN): δ 4.90 (d, $^{1}J(^{109}AgP)$ = 249.3 Hz, $^{1}J(^{107}AgP)$ = 218.0). **ESI+ *m/z*** calcd. for $C_{56}H_{89}AgO_6P_4$ ($[M - Br]^+$) = 1088.5; obs. = 1089.6.

6.3.7 Synthesis of [Au(3.2)$_2$]Cl, 3.17

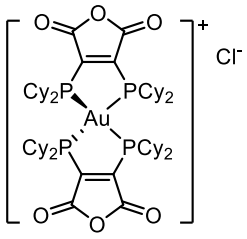

To a solution of **3.2** (30.0 mg, 0.0610 mmol) in DCM (1.00 mL) was added [AuCl(tht)] (20.0 mg, 0.0610 mmol) and stirred at room temperature for 30 min. Hexane (1.00 mL) was added and the precipitate washed with hexane (2 x 1 mL) to give the title product as a brown solid.

$^{31}P\{^{1}H\}$ NMR (162 MHz, CH_2Cl_2): δ 17.9 (s). **ESI+ *m/z*** calcd. for $C_{56}H_{88}AuO_6P_4$ ($[M - Cl]^+$) = 1177.5; obs. = 1177.7.

6.3.8 Synthesis of anhydride bioconjugate, 3.18

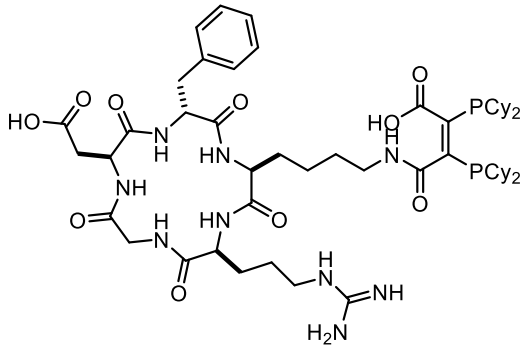

To a solution of cRGDfk peptide (8.50 mg, 0.0140 mmol) in DMF (1.00 mL) was added DIPEA (20.0 μL). The solution was degassed by freeze-pump-thaw before addition of 2,3-bis(dicyclohexylphosphino) maleic anhydride (5.00 mg, 0.0110 mmol) then stirred at 50 °C for 20 min. The resulting red/orange mixture was purified by preparative reverse-phase HPLC column chromatography (method 1).

^{31}P{^{1}H} NMR (162 MHz, C_3CN/D_2O): δ -8.8 (d, $^{3}J_{PP}$ = 163.8 Hz), -10.28 (d, $^{3}J_{PP}$ = 163.8 Hz). **^{1}H NMR** (400 MHz, C_3CN/D_2O): δ 7.36-7.18 (m, 5H, Ar-H), 4.77-4.72 (m, 1H, CH), 4.70-4.65 (m, 1H, CH), 4.32-4.26 (m, 1H, CH), 4.24-4.20 (m, 1H, CH), 4.06-40.1 (m, 1H, CH), 3.40-3.35 (m, 1H, CH), 3.20-3.10 (m, 3H, CH), 3.09-3.04 (m, 1H, CH), 3.02-2.95 (m, 1H, CH), 2.88-2.79 (m, 1H, CH), 2.63-2.56 (m, 1H, CH), 2.01-1.65 (m, 24H, CH_2), 1.64-1.45 (m, 6H, CH), 1.41-1.19 (m, 20H, CH_2).). **ESI+ *m/z*** calcd. for $C_{55}H_{86}N_9O_{10}P_2$ ($[M + H]^+$) 1094.59; obs. = 1094.50.

6.3.9 Synthesis of [^{64}Cu(3.18)$_2$]Cl, 3.19

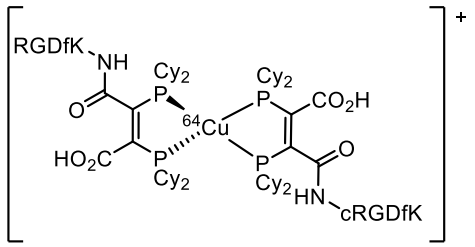

A solution of ^{64}CuCl in 0.100 M HCl (250 μL, 41.0 MBq) was evaporated to dryness. ^{64}CuCl was redissolved in ammonium acetate (170 μL) and pH adjusted to pH 6. To 150 μL of the ^{64}CuCl ammonium acetate solution was added a solution of **3.18** (100 μg) in EtOH/H_2O (50.0 μL). The solution was centrifuged at 1000 rpm for 1 min and the supernatant diluted with saline (450 μL) to give the title product as a saline solution.

6.3.10 Synthesis of $Et_2NP(CH_2CH_2CH_2OMe)_2$, 3.21

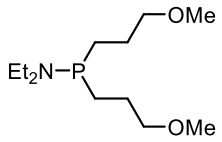

Magnesium turnings (525 mg, 21.6 mmol) were stirred in THF (12.0 mL) with a crystal of iodine for 30 min. To the mixture was added 1-bromo-3-methoxypropane (2.22 mL, 19.6 mL) and stirred at room temperature for 2 h. (3-methoxypropyl)magnesium bromide was used *in situ* and not isolated. The Grignard was added to a solution of dichloro(diethylamino)phosphine (1.32 mL, 9.00 mmol) in Et_2O (50.0 mL) at 0 °C, warmed to room temperature and stirred for 1 h. The mixture was filtered, and solvent removed *in vacuo* to give the title product as a colourless oil.

$^{31}P\{^1H\}$ NMR (162 MHz, $CDCl_3$): δ 54.4 (s). **^1H NMR** (400 MHz, $CDCl_3$): δ 3.23 (t, 4H, J = 6.4 Hz, CH_2OCH_3), 3.13 (s, 6H, OCH_3), 2.73 (q, 4H, J = 7.1 Hz, NCH_2), 1.55 – 1.36 (m, 6H, CH_2), 1.04 (m, 2H, CH_2), 0.83 (t, 6H, J = 7.1 Hz, NCH_2CH_3). **$^{13}C\{^1H\}$ NMR** (162 MHz, $CDCl_3$): δ 73.4 (CH_2OCH_3), 58.1 (OCH_3), 42.6 (NCH_2), 26.0 (CH_2), 25.5 (CH_2), 15.2 (NCH_2CH_3). **ESI+ *m/z*** calcd. For $C_{12}H_{28}NO_2P$ ($[M + H]^+$) = 250.1; obs. = 250.1

6.3.11 Synthesis of $ClP(CH_2CH_2CH_2OMe)_2$, 3.22

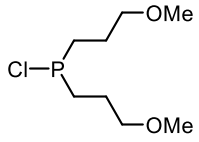

To a solution of N,N-diethyl-1,1-bis(3-methoxypropyl)phosphanamine (4.80 g, 19.6 mmol), in Et_2O (30.0 mL) was added 2.0 M HCl in Et_2O (12.0 mL) at 0 °C. The mixture was stirred at room temperature for 3 h, filtered and volatiles removed *in vacuo*. The crude yellow oil was taken to the next step without further purification.

$^{31}P\{^1H\}$ NMR (121 MHz): δ 112.8 (s).

6.3.12 Synthesis of $HP(CH_2CH_2CH_2OMe)_2$, 3.23

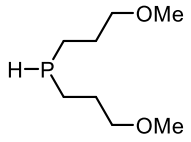

To a slurry of $LiAlH_4$ (2.20 g, 57.6 mmol) in Et_2O (40.0 mL) was added a solution of crude chlorobis(3-methoxypropyl)phosphine (4.00 g, 19.2 mmol) in Et_2O (10.0 mL) at 0 ^oC. The mixture was stirred at room temperature for 16 h then quenched with 4.00 mL degassed water, 4.00 M NaOH 4.00 mL, 4.00 mL degassed water. The solution was filtered, the salts washed with Et_2O (2 x 20.0 mL) and the volatiles removed *in vacuo* to give the title product as a colourless oil.

$^{31}P\{^1H\}$ NMR (162 MHz, CD_2Cl_2): δ -68.5 (s). **^1H NMR** (400 MHz, CD_2Cl_2): δ 3.37-3.33 (m, 4H, CH_2), 3.27 (s, 6H, OCH_3), 1.76-1.59 (m, 6H, CH_2), 1.55-1.43 (m, 2H, CH_2). **$^{13}C\{^1H\}$ NMR** (162 MHz, CD_2Cl_2): δ 73.6 (d, CH_2), 58.8 (s, OCH_3), 29.0 (d, CH_2), 17.4 (d, CH_2).

6.4 Experimental procedures and characterising data for Chapter 5 – Self-replication of chelating diphosphines via Pt(0)-catalysed hydrophosphination

6.4.1 Synthesis of $Ph_2PCH_2CH_2P(CH_2CH_2CO_2Me)_2$, 5.1

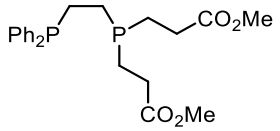

To a solution of $Ph_2PCH_2CH_2PH_2$ (100 mg, 0.410 mmol) in CH_2Cl_2 (2.00 mL) was added [Pt(nbe)$_3$] (9.00 mg, 0.0200 mmol) and stirred at room temperature for 10 min to afford a deep orange solution. ^{t}BuOH (0.800 mL, 8.10 mmol) was added, then methyl acrylate (0.0730 mL, 0.810 mmol) was added dropwise and the mixture was left to stir for 2 h at room temperature. The reaction mixture was then passed through a silica plug and the filtrate concentrated to dryness to give the title compound as a colourless oil (122 mg, 72 %).

$^{31}P\{^1H\}$ NMR (162 MHz, CD_2Cl_2): δ -12.8 (d, $^3J_{PP}$ = 29 Hz, *P*Ph$_2$), -20.7 (d, $^3J_{PP}$ = 28 Hz, *P*(CH$_2$CH$_2$CO$_2$Me)$_2$). **^{1}H NMR** (400 MHz, CD_2Cl_2): δ 7.44-7.38 (m, 4H, Ar-*H*), 7.38-7.30 (m, 6H, Ar-*H*), 3.63 (s, 6H, CO$_2$C*H*$_3$), 2.39-2.30 (m, 4H, CH$_2$), 2.16-2.08 (m, 2H, CH$_2$), 1.72-1.66 (m, 4H, CH$_2$), 1.51-1.43 (m, 2H, CH$_2$). **$^{13}C\{H\}$ NMR** (100 MHz, CD_2Cl_2): δ 173.4 (d, *J* = 11.7 Hz, *C*O$_2$Me), 138.5 (d, *J* = 14.4 Hz, Ar-C), 132.6 (d, *J* = 18.6 Hz, Ar-C), 128.7 (s, Ar-C), 128.4 (d, *J* = 6.6 Hz, Ar-C), 51.5 (s, CH$_3$) 30.3 (d, *J* = 16.6 Hz, CH$_2$), 23.5 (m, CH$_2$), 22.2 (t, *J* = 15.6 Hz, CH$_2$), 21.2 (d, *J* = 14.7 Hz, CH$_2$). **ESI+** *m*/*z* calcd. for $C_{22}H_{29}O_4P_2$([*M* + H]$^+$) = 419.1541; obs. = 419.1540.

6.4.2 Synthesis of $Ph_2PCH_2CH_2P(CH_2CH_2CO_2Et)_2$, 5.2

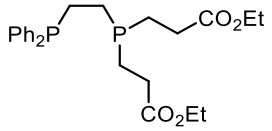

5.2 was synthesised according to procedure given for **5.1** but from ethyl acrylate (0.0880 mL, 0.810 mmol) to give the product as a colourless oil (172 mg, 95%).

$^{31}P\{^1H\}$ NMR (162 MHz, $CDCl_3$): δ -12.3 (d, $^3J_{PP}$ = 27.8 Hz, *P*Ph$_2$), -22.5 (d, $^3J_{PP}$ = 27.3 Hz, *P*(CH$_2$CH$_2$CO$_2$Et)$_2$). **^{1}H NMR** (400 MHz, CD_2Cl_2): δ 7.43-7.37 (m, 4H, Ar-*H*), 7.36-7.29 (m, 6H, Ar-*H*), 4.11 (q, 4H, J = 7.1, OCH$_2$), 2.38-2.29 (m, 4H, C*H*$_2$), 2.14-2.07 (m, 2H, C*H*$_2$), 1.73-1.66 (m, 4H, CH$_2$), 1.50-1.42 (m, 2H, C*H*$_2$) 1.23 (t, 6H, J = 7.2, CH$_3$).

^{13}C{H} NMR (101 MHz, $CDCl_3$): δ 173.2 (d, J = 12.2 Hz, CO_2Me), 138.2 (d, J = 13.7 Hz, Ar-C), 132.8 (d, J = 18.4 Hz, Ar-C), 128.8 (s, Ar-C), 128.6 (d, J = 6.6 Hz, Ar-C), 60.7 (s, OCH_2), 31.3 (s, CH_2), 30.7 (d, J = 16.3 Hz, CH_2), 23.7 (m, CH_2), 21.3 (d, J = 14.3 Hz, CH_2), 14.3 (s, CH_3). **ESI+** m/z calcd. for $C_{24}H_{33}O_4P_2$([M + H]$^+$) = 447.1854; obs. = 447.1861

6.4.3 Synthesis of $Ph_2PCH_2CH_2P(CH_2CH_2CO_2{}^tBu)_2$, 5.3

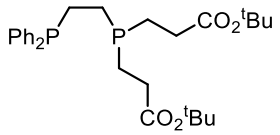

5.3 was synthesised according to the procedure given for **5.1** but from tert-butyl acrylate (0.120 mL, 0.810 mmol) to give the product as a colourless oil (186 mg, 91%).

^{31}P{^{1}H} NMR (162 MHz, $CDCl_3$): δ -13.7 (d, $^3J_{PP}$ = 27.8 Hz, PPh$_2$), -23.9 (d, $^3J_{PP}$ = 27.8 Hz, $P(CH_2CH_2CO_2{}^tBu)_2$). **^{1}H NMR** (400 MHz, CD_2Cl_2): δ 7.42-7.38 (m, 4H, Ar-H), 7.36-7.3 (m, 6H, Ar-H), 2.30-2.22 (m, 4H, CH_2), 2.15-2.08 (m, 2H, CH_2), 1.69-1.62 (m, 4H, CH_2), 1.50-1.46 (m, 2H, CH_2), 1.43 (s, 18H, ^{t}Bu). **^{13}C{H} NMR** (101 MHz, $CDCl_3$): δ 172.7 (d, $^3J_{PC}$ = 12.3 Hz, CO_2Me), 138.2 (d, J = 13.7 Hz, Ar-C), 133.0 (d, J = 18.5 Hz, Ar-C), 129.0 (s, Ar-C), 128.6 (d, J = 6.7 Hz, Ar-C), 80.7 (s, $C(CH_3)_3$), 31.9 (d, J = 16.1 Hz, CH_2), 28.2 (s, CH_3), 23.9 (m, CH_2), 22.4 (m, CH_2), 21.5 (d, $^2J_{PC}$ = 14.5 Hz, CH_2CO_2Me). **ESI+** m/z calcd. for $C_{28}H_{40}O_4P_2$([M + H]$^+$) = 503.2475; obs. = 503.2480.

6.4.4 Synthesis of $Ph_2PCH_2CH_2P(CH_2CH_2CN)_2$, 5.4

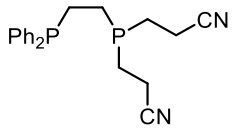

5.4 was synthesised according to the procedure given for **5.1** but from acrylonitrile (0.0540 mL, 0.810 mmol) to give the product as a colourless oil (138 mg, 95%).

^{31}P{^{1}H} NMR (162 MHz, $CDCl_3$): δ -12.9 (d, $^3J_{PP}$ = 28.8 Hz, PPh$_2$), -20.5 (d, $^3J_{PP}$ = 28.7 Hz, $P(CH_2CH_2CN)_2$). **^{1}H NMR** (400 MHz, $CDCl_3$): δ 7.44-7.39 (m, 4H, Ar-H), 7.38-7.34 (m, 6H, Ar-H), 2.44-2.36 (m, 4H, CH_2), 2.15-2.08 (m, 2H, CH_2), 1.81-1.74 (m, 4H, CH_2), 1.59-1.51 (m, 2H, CH_2). **^{13}C{H} NMR** (101 MHz, $CDCl_3$): δ 137.7 (d, J = 13.3 Hz, Ar-

C), 132.8 (d, J = 18.5 Hz, Ar-C), 129.2 (s, Ar-C), 128.8 (d, J = 6.7 Hz, Ar-C), 119.2 (d, J = 11.1 Hz, CN), 31.3 (s, CH_2), 23.7 (m, CH_2), 22.3 (m, CH_2), 14.4 (d, J = 21.9 Hz, CH_2). **ESI+** m/z calcd. for $C_{20}H_{23}N_2P_2([M + H]^+)$ = 353.1336; obs. = 353.1343.

6.4.5 Synthesis of $Ph_2PCH_2CH_2P(CH_2CH_2CONH_2)_2$, 5.5

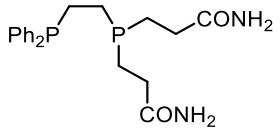

5.5 was synthesised according to the procedure given for **5.1** but from acrylamide (56.0 mg, 0.810 mmol) to give the product as a white solid (92 mg, 59%).

$^{31}P\{^1H\}$ NMR (162 MHz, CD_3OD): δ -12.6 (d, $^3J_{PP}$ = 28.8 Hz, PPh$_2$), -22.7 (d, $^3J_{PP}$ = 28.8 Hz, $P(CH_2CH_2CO_2NH_2)_2$). **^{1}H NMR** (400 MHz, CD_3OD): δ 7.46-7.40 (m, 4H, Ar-H), 7.38-7.31 (m, 6H, Ar-H), 2.30-2.22 (m, 4H, CH_2), 2.20-2.13 (m, 2H, CH_2), 1.73-1.66 (m, 4H, CH_2), 1.52-1.44 (m, 2H, CH_2). **$^{13}C\{H\}$ NMR** (101 MHz, CD_3OD): δ 177.2 (d, $^3J_{PC}$ = 12.8 Hz, CO$_2$NH$_2$), 138.5 (d, J = 13.2 Hz, Ar-C), 132.6 (d, J = 18.6 Hz, Ar-C), 129.0 (s, Ar-C), 128.3 (d, J = 6.6 Hz, Ar-C), 31.2 (d, J = 15.2 Hz, CH_2), 23.3 (m, CH_2), 22.0 (m, CH$_2$), 21.6 (d, $^2J_{PC}$ = 14.4 Hz, CH_2). **ESI+** m/z calcd. for $C_{20}H_{26}N_2O_2P_2([M + H]^+)$ = 389.1542; obs. = 389.1550.

6.4.6 Synthesis of $Ph_2PCH_2CH_2P(CH_2CH_2CONMe_2)_2$, 5.6

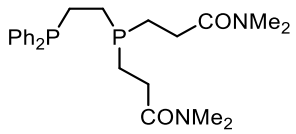

5.6 was synthesised according to the procedure given for **5.1** but from *N,N*-dimethylacrylamide (0.0840 mL, 0.810 mmol) to give the product as a colourless oil (128 mg, 71%).

$^{31}P\{^1H\}$ NMR (162 MHz, $CDCl_3$): δ -12.1 (d, $^3J_{PP}$ = 27.3 Hz, PPh$_2$), -22.4 (d, $^3J_{PP}$ = 27.3 Hz, $P(CH_2CH_2CO_2NMe_2)_2$). **^{1}H NMR** (400 MHz, $CDCl_3$): δ 7.41-7.36 (m, 4H, Ar-H), 7.34-7.28 (m, 6H, Ar-H), 2.92 (s, 6H, NCH_3), 2.91 (s, 6H, NCH_3), 2.39-2.28 (m, 4H, CH_2), 2.16-2.07 (m, 2H, CH_2), 1.78-1.67 (m, 4H, CH_2), 1.52-1.40 (m, 2H, CH_2). $^{13}C\{H\}$ NMR (101 MHz, CD_3OD): δ 172.4 (d, $^3J_{PC}$ = 11.5 Hz, CO$_2$NMe$_2$), 138.2 (d, J = 13.7 Hz, Ar-C),

132.8 (d, J = 18.3 Hz, Ar-C), 128.8 (s, Ar-C), 128.6 (d, J = 6.6 Hz, Ar-C), 37.2 (s, NCH_3), 35.6 (s, NCH_3), 29.5 (d, J = 16.6 Hz, CH_2), 23.6 (m, CH_2), 22.3 (m, CH_2), 21.2 (d, J = 12.9 Hz, CH_2). **ESI+** m/z calcd. for $C_{24}H_{34}N_2O_2P_2$ ($[M + H]^+$) = 445.2168; obs. = 445.2179

6.4.7 Synthesis of $Ph_2PCH_2CH_2P(CH_2CH_2PO(OEt)_2)_2$, 5.7

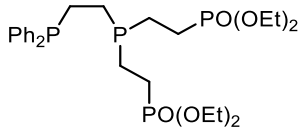

5.7 was synthesised according to the procedure given for **5.1** but from diethyl vinylphosphonate (2.50 mL, 0.830 mmol) to give the product as a colourless oil (145 mg, 63%).

$^{31}P\{^1H\}$ NMR (162 MHz, CD_2Cl_2): δ 31.2 (d, $^3J_{PP=O}$ = 49 Hz, $PO(OEt)_2$), -12.6 (d, $^3J_{PP}$ = 28 Hz, Ph_2P), -17.5 (td, $^3J_{PP=O}$ = 49 Hz, $^3J_{PP}$ = 28 Hz, $P(CH_2CH_2PO(OEt)_2)_2$). **^1H NMR** (400 MHz, CD_2Cl_2): δ 7.42 (m, 4H, Ar-H), 7.34 (m, 6H, Ar-H), 4.03 (m, 8H, OCH_2), 2.11 (m, 2H, $Ph_2PCH_2CH_2P$), 1.66 (m, 8H, $PCH_2CH_2P{=}O$), 1.47 (m, 2H, $Ph_2PCH_2CH_2P$), 1.28 (t, $^2J_{HH}$ = 7.1 Hz, 12H, CH_3). **$^{13}C\{H\}$ NMR** (100 MHz, CD_2Cl_2) δ 138.4 (d, $^2J_{PC}$ = 15 Hz, Ar-C), 132.7 (d, $^1J_{PC}$ = 18 Hz, PC), 128.7 (s, Ar-C), 128.5 (d, $^3J_{PC}$ = 6.3 Hz, Ar-C), 61.6 (d, $^2J_{PC}$ = 6.7 Hz, OCH_2), 16.3 (d, $^3J_{PC}$ = 5.7 Hz, CH_3). **ESI+** m/z 575.2 ($[M + H]^+$) calc. for $C_{22}H_{32}O_6P_4$ 574.48.

6.4.8 Synthesis of $P(Ph)(H)CH_2CH_2P(Ph)(H)$

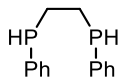

To a suspension of dppe (200 mg, 0.500 mmol) in THF (8.00 mL) was added lithium metal (20 mg, 2.00 mmol) and stirred at room temperature for 16 h. The yellow solution was filtered away from the excess lithium metal and H_2O added until the solution turned colourless. The solution was filtered again and the solvent removed *in vacuo* to give the title product as a yellow oil (120 mg, 98%).

$^{31}P\{^1H\}$ NMR (162 MHz, CD_2Cl_2): δ -46.4 (d, $^3J_{PP}$ = 25.7 Hz). **^1H NMR** (400 MHz, CD_2Cl_2): δ 7.71-7.19 (m, 10H, Ar-H), 2.10-1.74 (m, 4H, Ar-H).

6.4.9 Synthesis of P(Ph)($CH_2CH_2CO_2Me$)CH_2CH_2P(Ph)($CH_2CH_2CO_2Me$), 5.11

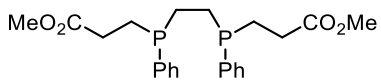

To a solution of $PhHPCH_2CH_2PHPh$ (100 mg, 0.407 mmol), tBuOH (0.800 mL, 8.14 mmol) and [Pt(nbe)$_3$] (4.00 mg, 8.14 x 10^{-3} mmol) in DCM (2 mL) was added methyl acrylate (0.0700 mL, 0.814 mmol) and stirred at room temperature for 16 h. The reaction mixture was passed through a silica plug and the solvent removed *in vacuo* to give the title product as a colourless oil (91.0 mg, 54%).

$^{31}P\{^1H\}$ NMR (162 MHz, CD_2Cl_2): δ_P -19.4 (s), -19.7 (s). **^1H NMR** (400 MHz, CD_2Cl_2): δ_H 7.47-7.28 (10H, m, Ar-H), 3.58 (6H, s, OCH_3), 2.35-2.13 (4H, m, CH_2), 1.96-1.89 (4H, m, CH_2), 1.80-1.59 (4H, m, CH_2). **$^{13}C\{^1H\}$ NMR** (162 MHz, CD_2Cl_2): δ_C 173.9 (C=O), 137.6 (Ar-C), 133.0 (Ar-C), 129.6 (Ar-C), 129.0 (Ar-C), 52.0 (OCH_3), 31.6 (CH_2), 30.8 (CH_2), 24.0 (CH_2). **ESI+ *m/z*** calcd. For $C_{22}H_{28}O_4P_2$ ($[M + H]^+$) = 419.1536; obs. = 419.1534

6.4.10 Synthesis of ($CH_2CH_2CO_2{}^tBu$)PCH_2CH_2P($CH_2CH_2CO_2{}^tBu$), 5.12

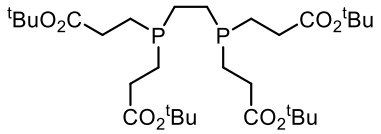

To a solution of $Ph_2PCH_2CH_2PH_2$ (200 mg, 0.640 mmol) in CH_2Cl_2 (10.0 mL) was added [Pt(nbe)$_3$] (20.0 mg, 0.0420 mmol) and was left to stir for 10 min to afford a deep orange solution. ^{t}BuOH (2.00 mL, 42.4 mmol,) was added and the solution was cooled in an ice bath. ^{t}Butyl acrylate (1.20 mL, 8.48 mmol) was added dropwise and the mixture was left to stir at room temperature for 90 min. The solution was passed through a silica plug and the filtrate concentrated to dryness to give the title compound as a colourless oil.

$^{31}P\{^1H\}$ NMR (162 MHz, CD_2Cl_2): δ -22.9 (s). **^1H NMR** (400 MHz, CD_2Cl_2): δ 2.31 (m, 8H, CH_2), 1.66 (m, 8H, CH_2), 1.48 (m, 4H, CH_2), 1.43 (s, 9H, OCH_3). **$^{13}C\{^1H\}$ NMR** (162 MHz, CD_2Cl_2): δ 172.8 (CO), 80.8 ($C(CH_3)_3$), 28.4 (CH_3), 32.27 (CH_2), 22.93 (CH_2), 22.2 (CH_2).

6.4.11 Synthesis of [Pt(5.12)Cl_2]

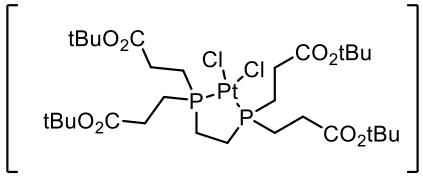

5.12 (40.0 mg, 0.0660 mmol) and [Pt(cod)Cl_2] were stirred in DCM (1.00 mL) for 1h at room temperature. Hexane (2.00 mL) was added and the white precipitate washed with further hexane (2 x 2.00 mL) and dried to give the title compound. Crystals suitable for X-ray crystallography were obtained *via* vapour diffusion recrystallization from DCM and hexane.

$^{31}P\{^1H\}$ NMR (121 MHz, CH_2Cl_2): δ_P 51.6 (s, $^1J_{PtP}$ 3520 Hz).

6.4.12 Synthesis of [Pt{κ^2-$Ph_2PCH_2CH_2P(CH_2CH_2CO_2Me)_2$}$_2$], 5.13

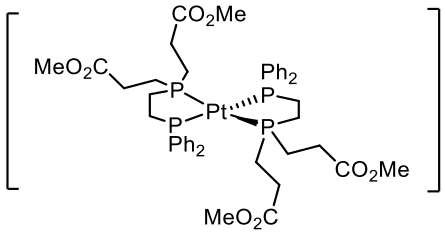

To [Pt(nbe)$_3$] (7.5 mg, 0.016 mmol) was added a solution of **5.1** (13.0 mg, 0.310) in toluene (0.500 mL) and stirred for 10 min at ambient temperature. The solvent was removed *in vacuo* at ambient temperature (n.b. heat causes decomposition of the complex) to give the product as an orange solid.

$^{31}P\{^1H\}$ NMR (122 MHz, CH_2Cl_2): δ 26.8 (AA'XX', $^1J_{PPt}$ = 3753 Hz, 3557 Hz, $J_{AA'}$ = 43.6 Hz, $J_{XX'}$ = 27.1 Hz, J_{AX} = 80.5 Hz and $J_{AX'}$ = 61.7 Hz). **^1H NMR** (400 MHz, C_6D_6): δ 7.72-7.65 (m, 4H, Ar-*H*), 7.63-7.56 (m, 4H, Ar-*H*), 7.30-7.23 (m, 6H, Ar-*H*), 7.12-7.00 (m, 6H, Ar-*H*), 3.62 (s, 6H, CO_2CH_3), 3.34 (s, 6H, CO_2CH_3), 2.80-2.66 (m, 2H, CH_2), 2.57-5.46 (m, 2H, CH_2), 2.33-2.18 (m, 2H. CH_2), 2.12-1.91 (m, 10H, CH_2), 1..85-1.58 (m, 6H, CH_2) 1.46-1.38 (m, 2H, CH_2). **$^{135}Pt\{^1H\}$ NMR** (65 MHz, CH_2Cl_2): δ -5507.0 (tt, $^1J_{PPt}$ = 3753Hz, 3557 Hz). **$^{13}C\{H\}$ NMR** (101 MHz, C_6D_6): δ 173.5 (t, J = 8.0 Hz, *C*O_2Me), 173.1 (t, J = 8.0 Hz, *C*O_2Me), 144.2 (m, Ar-C), 141.2 (m, Ar-C), 133.2 (t, J = 7.4 Hz), 131.9 (t, J = 7.3 Hz), 51.4 (s, CH_3), 50.9 (s, CH_3), 48.8 (s, CH_2), 43,0 (s, CH_2), 42.2 (s, CH_2), 39.8 (s, CH_2), 31.3 (m, CH_2), 29.3 (m, CH_2), 28.8 (s, CH_2), 28.1 (m, CH_2).

6.5 X-ray crystallography

The X-ray data presented in this thesis were collected by Dr Hazel Sparkes on a Bruker Apex II diffractometer at 100 K with a CCD area detector using Mo-Kα radiation (λ = 0.71073 Å) or on a Bruker Microstar rotating anode diffractometer using Cu-Kα radiation (λ = 1.54178 Å). Absorption corrections were preformed with the aid of SADABS.[3] Each structure was solved using either SHELXS or Superflip and refined against F2 using ShelXL[4] within Olex2.[5] Crystal structure refinement data are given in Table 6.4.

Table 6.4 Crystal data

Identification code	**2.7**	**2.9**
Empirical formula	$C_{30}H_{56}Cl_2O_8P_2Pt$	$C_{45}H_{60}IO_{11}P_4Re$
Formula weight	872.67	1213.91
Temperature/K	100(2)	100(2)
Crystal system	monoclinic	monoclinic
Space group	$P2_1/n$	$P2_1/n$
a/Å	12.0433(4)	9.6017(8)
b/Å	11.7338(4)	13.9749(19)
c/Å	26.8359(8)	18.5824(19)
α/°	90	90
β/°	98.546(2)	100.025(5)
γ/°	90	90
Volume/Å^3	3750.2(2)	2455.4(5)
Z	4	2
ϱ_{calc}g/cm^3	1.546	1.642
μ/mm^{-1}	4.012	3.289
F(000)	1768.0	1212.0
Crystal size/mm^3	0.434 × 0.322 × 0.31	0.254 × 0.132 × 0.132
Radiation	MoKα (λ = 0.71073)	MoKα (λ = 0.71073)
2Θ range for data collection/°	3.07 to 55.888	3.668 to 52.738
Index ranges	-15 ≤ h ≤ 15, -13 ≤ k ≤ 15, -35 ≤ l ≤ 35	-12 ≤ h ≤ 11, -17 ≤ k ≤ 16, -23 ≤ l ≤ 18
Reflections collected	33764	14576
Independent reflections	8991 [R_{int} = 0.0251, R_{sigma} = 0.0236]	5007 [R_{int} = 0.0718, R_{sigma} = 0.0831]
Data/restraints/parameters	8991/58/422	5007/398/378
Goodness-of-fit on F^2	1.024	0.998
Final R indexes [I>=2σ (I)]	R_1 = 0.0215, wR_2 = 0.0449	R_1 = 0.0426, wR_2 = 0.0755
Final R indexes [all data]	R_1 = 0.0252, wR_2 = 0.0460	R_1 = 0.0831, wR_2 = 0.0866
Largest diff. peak/hole / e Å^{-3}	1.21/-1.07	1.25/-1.06

Table 6.4 Crystal data (cont.)

Identification code	**3.2**	**3.10**
Empirical formula	$C_{30}H_{48}O_{3.5}P_2$	$C_{61.42}H_{109.68}Cu_2I_2O_{11.42}P_4$
Formula weight	526.62	1535.69
Temperature/K	100(2)	100(2)
Crystal system	triclinic	triclinic
Space group	P-1	P-1
a/Å	10.1470(2)	11.6844(10)
b/Å	11.9323(2)	12.9542(12)
c/Å	12.2150(2)	14.2682(13)
α/°	82.3770(10)	69.778(6)
β/°	83.9680(10)	83.023(6)
γ/°	82.2500(10)	64.885(6)
Volume/Å^3	1446.76(4)	1834.1(3)
Z	2	1
ϱ_{calc}g/cm^3	1.209	1.390
μ/mm^{-1}	0.181	1.560
F(000)	572.0	794.0
Crystal size/mm^3	0.539 × 0.438 × 0.31	0.282 × 0.207 × 0.188
Radiation	MoKα (λ = 0.71073)	MoKα (λ = 0.71073)
2Θ range for data collection/°	3.378 to 55.948	3.044 to 56.154
Index ranges	-13 ≤ h ≤ 13, -15 ≤ k ≤ 15, -15 ≤ l ≤ 16	-14 ≤ h ≤ 15, -17 ≤ k ≤ 17, -18 ≤ l ≤ 18
Reflections collected	26719	33898
Independent reflections	6948 [R_{int} = 0.0318, R_{sigma} = 0.0295]	8828 [R_{int} = 0.0603, R_{sigma} = 0.0587]
Data/restraints/parameters	6948/35/331	8828/106/461
Goodness-of-fit on F^2	1.032	1.019
Final R indexes [I>=2σ (I)]	R_1 = 0.0375, wR_2 = 0.0881	R_1 = 0.0390, wR_2 = 0.0893
Final R indexes [all data]	R_1 = 0.0468, wR_2 = 0.0936	R_1 = 0.0615, wR_2 = 0.0982
Largest diff. peak/hole / e Å^{-3}	0.80/-0.51	0.77/-0.58

Table 6.4 Crystal data (cont.)

Identification code	**3.16**	[Pt(**5.1**)$_2$]Cl$_2$
Empirical formula	$C_{56}H_{92}Ag_2Br_2O_6P_4$	$C_{44}H_{56}Cl_2O_8P_4Pt$
Formula weight	1360.73	1102.75
Temperature/K	100(2)	200(2)
Crystal system	triclinic	triclinic
Space group	P-1	P-1
a/Å	9.9493(2)	9.4489(3)
b/Å	13.0031(3)	12.0028(4)
c/Å	13.1836(4)	14.3968(6)
α/°	105.532(2)	109.395(2)
β/°	104.009(2)	93.927(2)
γ/°	108.479(2)	93.292(2)
Volume/Å^3	1455.40(7)	1530.93(10)
Z	1	1
ρ_{calc}g/cm^3	1.553	1.196
μ/mm^{-1}	2.203	2.521
F(000)	700.0	556.0
Crystal size/mm^3	0.218 × 0.181 × 0.133	0.602 × 0.246 × 0.182
Radiation	MoKα (λ = 0.71073)	MoKα (λ = 0.71073)
2Θ range for data collection/°	3.434 to 55.874	3.012 to 56.096
Index ranges	$-13 \leq h \leq 13$, $-17 \leq k \leq 16$, $-17 \leq l \leq 17$	$-11 \leq h \leq 12$, $-15 \leq k \leq 15$, $-19 \leq l \leq 18$
Reflections collected	26967	28427
Independent reflections	6963 [R_{int} = 0.0725, R_{sigma} = 0.0685]	7411 [R_{int} = 0.0375, R_{sigma} = 0.0355]
Data/restraints/parameters	6963/0/316	7411/140/304
Goodness-of-fit on F^2	1.008	1.008
Final R indexes [I>=2σ (I)]	R_1 = 0.0395, wR_2 = 0.0773	R_1 = 0.0249, wR_2 = 0.0560
Final R indexes [all data]	R_1 = 0.0644, wR_2 = 0.0851	R_1 = 0.0260, wR_2 = 0.0565
Largest diff. peak/hole / e Å^{-3}	0.60/-0.82	1.22/-0.57

6.6 References

1 R. J. Angelici, Ed., *Inorganic Syntheses: Reagents for transition metal complex and organometallic syntheses*, 1990, vol. 28.

2 E. S. Wiedner, J. A. S. Roberts, W. G. Dougherty, W. S. Kassel, D. L. Dubois and R. M. Bullock, *Inorg. Chem.*, 2013, **52**, 9975–9988.

3 G. M. Sheldrick, SADABS V2008/1.

4 G. M. Sheldrick, *Acta. Cryst.*, 2008, **A64**, 112–122.

5 O. V. Dolomanov, L. J. Bourhis, R. J. Gildea, J. A. K. Howards and H. J. Puschmann, *J. Appl. Crystallogr.*, 2009, **42**, 339–341.